University of Naples Federico II
Polytechnic and Basic Science School

Department of Chemical Sciences

Ph.D. in Chemical Sciences

New glycated eumelanin-based polymers for applications in organic bioelectronics

Emanuele Carrella

Advisor:
Prof. Alessandro Pezzella

Examiner:
Prof. Roberto Centore

XXXVII Cycle 2022 – 2025
Coordinator: prof. Angela Lombardi

Table of contents

Acknowledgements

This PhD project was made possible thanks to the financial support of Istituto Nazionale Previdenza Sociale (INPS) to whom I am sincerely grateful. Their funding has provided the means to undertake this study, and I acknowledge their commitment to supporting academic research.

Abstract

Nature-inspired products, such as biopolymers, have gained significant attention as functional materials in organic electronics, offering potential for both technological and biomedical applications. Among biomaterials, melanins are one of the most intriguing materials. The most studied type of melanin is eumelanin, a photoprotective pigment found in mammals, which arises from the oxidative polymerization of 5,6-dihydroxyindole (DHI) and 5,6-dihydroxyindole-2-carboxylic acid (DHICA). Eumelanin exhibits several valuable properties, such as: a) broad optical absorption across the UV-visible spectrum; b) effective UV dissipation mechanisms; c) photoconductivity in the solid state; and d) water-dependent conductivity. However, despite the growing interest in using synthetic eumelanin for organic electronics and bioelectronics, its practical use has been limited by several challenges, including its complete insolubility in all solvents, which makes it difficult to develop standardized, reproducible synthetic methods, low conductivity, and an incomplete understanding of the structure–property–function relationships.

The synthesis of functionalized eumelanin monomers to introduce new, significant properties into eumelanin units was demonstrated to be one of the most effective strategies to overcoming these material issues. In this context, this project aimed to create novel classes of synthetic melanin monomers that are functionalized to improve physical and chemical properties of the final material, such as solubility and conductivity.

The main activities of this project can be summarised as follows: a) to synthesize eumelanin-inspired monomers by designing new functionalization strategies; b) to characterize these new materials; c) starting from the latter, to create and characterize eumelanin-inspired materials for use as active layers in organic

electronic devices, aiming to improve some device performance. One key part of the project successfully developed a synthetic method to functionalize DHI and DHICA by introducing selenosugars at the C-3 position of *O*-acetylated DHI and DHICA, using easily accessible glycosyl diselenides as seleno-glycosylating agents. This method allows the incorporation of monosaccharides, disaccharides, and amino sugars, obtaining a class of new pro-soluble melanin monomers. Additionally, this strategy was extended to obtain the first amino acid-functionalized melanin monomer from a symmetrical N-protected selenocystine derivative. Other functionalizations explored were studied during my visiting period in Brazil in collaboration with Prof. Carlos De Oliveira Graeff and involved the incorporation of chalcogens into DHI monomer to investigate the impact of these heavy atoms on melanin's structure. The third part of the project aimed to better understand the already-known 3-thioglycosylated eumelanins to test the interaction of this polymers with natural molecules. In this regard, an especially interesting result of this research was the high affinity exhibited by synthetic thiolactosylated eumelanins towards galectins, a fundamental class of *β*-galactoside receptors with a profound impact in several key biological processes with therapeutical implications.

Chapter 1: Introduction on bioelectronics

1.1 Organic bioelectronics and bioinspired materials

Organic bioelectronics refers to the emerging field that merges biology, medicine, chemistry and materials science. It focuses on the study and the development of electronic devices capable of translating biological signals (which are mostly ionic) into electronic signals that can be processed by human-made artificial systems.[1–3]

These devices utilize organic polymers and small molecules, the so-called Organic Electronic Materials (OEMs), that possess both electronic and ionic conductivity. This unique property allows OEMs to effectively interface with biological systems, making them a crucial component of organic bioelectronics.

Over the past few decades, OEMs have demonstrated remarkable tunability in their mechanical, physical, and chemical properties. Their properties can be precisely controlled and modified through their synthetic and manufacturing protocols and are influenced by factors such as electronic structure, charge carrier density, and morphology. Since the birth of organic bioelectronics, most OEMs are synthetic while nowadays there is growing interest in exploring naturally occurring organic conductors and bio-inspired materials.

Generally, the term "bio-inspired" refers to the practice of using nature as a model to design and create new materials and devices. In organic bioelectronics, bio-inspired OEMs are referred to a class of synthetic materials that are biocompatible, biodegradable and have interesting biorecognition properties.

In the last decades, bioinspired materials have gained prominence in organic electronics due to the urgent need to address the global electronic waste (e-waste)

crisis.[4,5] In 2022, the world generated nearly 62 billion kg of e-waste, doubling the total amount in respect of the year 2010. Despite this significant growth in last years, only a small fraction (nearly 22%) of e-wastes were documented as being properly collected and recycled.[6] This means that tons of valuable materials were wasted, rather than being recovered and reused. In the perspective of reducing the gap between the production of wastes and the recycling rates, bioinspired materials would provide a compelling solution to reduce the growing volume of e-waste and its associated risks.[5–8]

Nowadays, the OEMs mostly used in organic electronics are conductive polymers (CPs). Briefly, CPs are a class of organic materials characterized by a highly π-conjugated system allowing the delocalization of the electrons over the polymer chain, which imparts semiconducting or metal-like electrical properties to the material. The most common CPs used in organic bioelectronics are shown in figure 1.1 and include polyacetylene (PA), polythiophene (PT), polypyrrole (PPy), poly(3,4-ethylenedioxythiophene) (PEDOT), polyaniline (PANI), and poly(3-hexylthiophene) (P3HT). These polymers are widely used in devices like sensors, organic field-effect transistor (OFET) and many other devices in organic electronics.

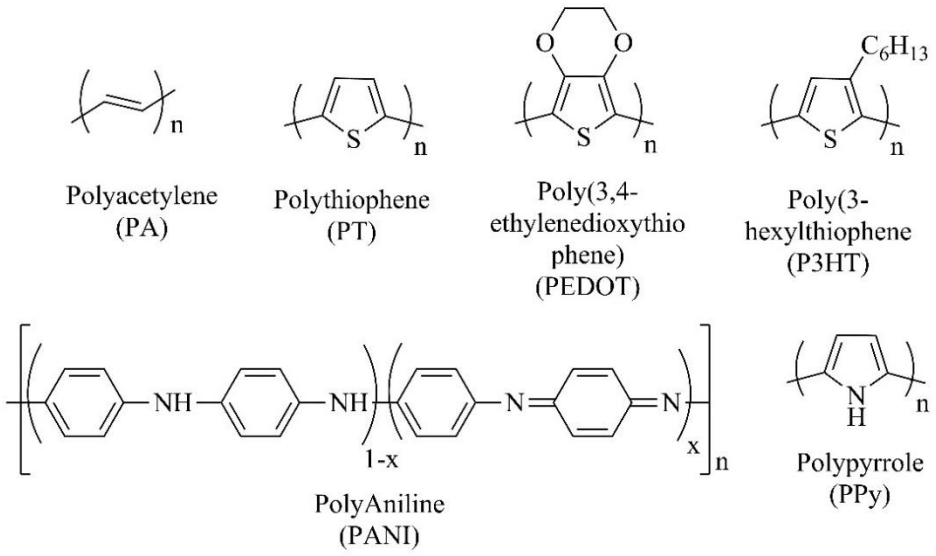

Figure 1.1: Common CPs utilized in organic bioelectronics: polyacetylene (PA), polythiophene (PT), poly (3,4-ethylenedioxythiophene) (PEDOT), poly(3-hexylthiophene) (P3HT) polyaniline (PANI) and polypyrrole (PPy).

To enhance the electrical conductivity of CPs, doping is essential. Unlike inorganic materials where a defect of crystalline structure is introduced to modify the band gap, doping in conjugated polymers mainly involves a modification in the polymer structure. In CPs, p-type doping can be achieved introducing holes (positive charge carriers) into the polymer by oxidizing the material. This oxidation results in the formation of polarons (positively charged species) that are delocalized along the conjugated polymer backbone. For example, PEDOT, when doped with poly(styrene sulfonate) (PSS), forms polarons that enhance conductivity (figure 1.2).[9]

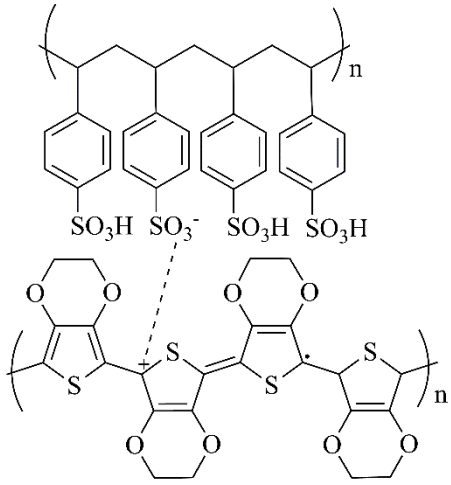

Figure 1.2: Polaron chemical structure formed by introducing poly(styrene sulfonate) (PSS) in poly(3,4-ethylenedioxythiophene) (PEDOT).

1.2 Bioelectronic devices and biosensors

Concerning organic bioelectronics, CPs offer multiple applications such as sensors, electrodes, and biointerfaces. Perhaps, the most interesting devices in this field are organic thin-film transistors (OTFTs) and organic electrochemical transistors (OECTs) that use different principles to amplify the detected signals. The architecture of a typical OTFT and OECT is displayed in detail in figure 1.3.

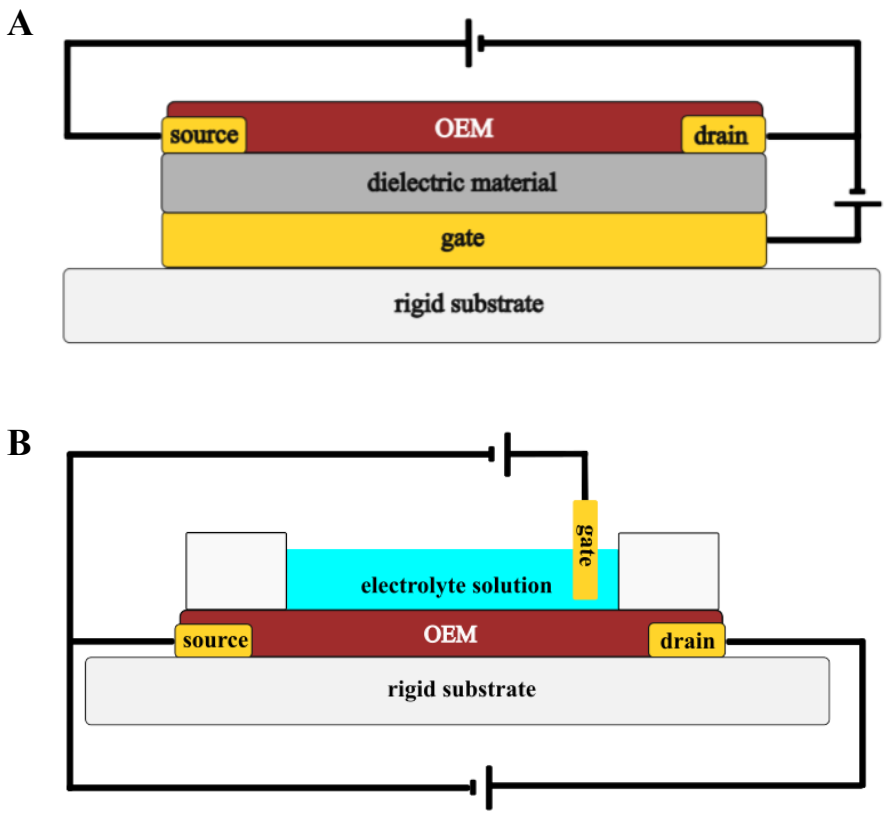

Figure 1.3: Device structures of organic thin-film transistors (OTFT) (A) and organic electrochemical transistors (OECTs) (B).

The principle of OTFTs relies on that of field effect transistors, where the flow of charges between the source and drain electrodes is modulated by an external field applied between the gate electrode and the active layer made out of CPs, placed between the source and the drain electrodes.

OECTs, on the other hand, are based on the electrochemical modulation of the organic semiconductor material in contact with an electrolyte solution. The working mechanism is based on the transport transduction that occurs at the interface between the electrolyte and the organic material in the channel of the transistor, made with a CP. This transduction allows the OECT to detect changes in ionic concentration and convert them into electrical signals. For example, in the case of PEDOT, the material undergoes through an electrochemical reversible reaction of doping and de-doping, modulating its conductivity based on ion flux.[10] PEDOT is probably one of the most common materials studied in OECT devices in the organic bioelectronics' community. Since its first application in 2002,[11] it has been used in combination with different receptors or membranes for the detection of many compounds such as acetylcholine, glutamate and ascorbic acid.[12,13]

When designing organic bioelectronic devices, natural materials can serve as valuable components for the active layers or components of multi-layered structures. Silk, a fiber-based biomaterial derived from the cocoon of *Bombyx mori*, is one of them. Due to its easy coating properties, silk was integrated into the structure of OECT as a component of the active layer, exploiting an imidazolium-based ionic liquid as electrolyte. This design achieved an ON/OFF switching ratio of about two orders of magnitude.[14]

Keratin, the major component of hair, nails, and feathers, is another biomaterial that has been utilized in the fabrication of transistors. Recent studies have taken advantage of keratin's dielectric properties and its insolubility in organic solvents. Particularly, this property allows the construction of the multilayer devices, as it

remains intact while is exposed to the solutions used for other layers. In one such approach, Singh et al. developed an OTFT using P3HT as the organic semiconductor and keratin as the dielectric gate. Notably, the biopolymer-based transistor demonstrated superior electrical performance such as improved switching voltage, carrier mobility, and threshold voltage compared to devices using SiO_2 as the dielectric layer.[15]

Among the multitude of materials found in nature, melanin, the natural pigment responsible for mammalian skin, hair and eye pigmentation is one of the most interesting natural substances.[16,17] The role and biological functions of melanin are still unclear, since melanin has not a defined structure and does not follow the typical structure-property function relationship, sparking greater scientific interest in this material.

Starting from this scenario, the research activity of my PhD project has been focused on the design, synthesis, and characterization of melanin-inspired materials with the aim of its potential application as an active layer in electronic devices. Before going into the details of the research activity described in chapters 3-5, the next chapter contains a presentation on melanin, with particular interest in the class of eumelanin.

1.3 References

(1) *Organic Bioelectronics: Bridging the Signaling Gap between Biology and Technology | Chemical Reviews*.

(2) Berggren, M.; Richter-Dahlfors, A. Organic Bioelectronics. *Advanced Materials* **2007**, *19* (20), 3201–3213.

(3) Rivnay, J.; Owens, R. M.; Malliaras, G. G. The Rise of Organic Bioelectronics. *Chem. Mater.* **2014**, *26* (1), 679–685.

(4) Perkins, D. N.; Brune Drisse, M.-N.; Nxele, T.; Sly, P. D. E-Waste: A Global Hazard. *Annals of Global Health* **2014**, *80* (4), 286–295.

(5) Wang, Z.; Zhang, B.; Guan, D. Take Responsibility for Electronic-Waste Disposal. *Nature* **2016**, *536* (7614), 23–25.

(6) Baldé, C. P.; Kuehr, R.; Yamamoto, T.; McDonald, R.; D'Angelo, E.; Althaf, S.; Bel, G.; Deubzer, O.; Fernandez-Cubillo, E.; Forti, V.; Gray, V.; Herat, S.; Honda, S.; Iattoni, G.; di Cortemiglia, V. L.; Lobuntsova, Y.; Nnorom, I.; Pralat, N.; Wagner, M. THE GLOBAL E WASTE MONITOR 2024. **2024**.

(7) Brown, M. S.; Somma, L.; Mendoza, M.; Noh, Y.; Mahler, G. J.; Koh, A. Upcycling Compact Discs for Flexible and Stretchable Bioelectronic Applications. *Nat Commun* **2022**, *13* (1), 3727.

(8) Lee, B.; Chung, S. Printed Carbon Electronics Get Recycled. *Nat Electron* **2021**, *4* (4), 241–242.

(9) Shi, H.; Liu, C.; Jiang, Q.; Xu, J. Effective Approaches to Improve the Electrical Conductivity of PEDOT:PSS: A Review. *Advanced Electronic Materials* **2015**, *1* (4), 1500017.

(10) Jimison, L. H.; Rivnay, J.; Owens, R. M. Conducting Polymers to Control and Monitor Cells. In *Organic Electronics*; John Wiley & Sons, Ltd, 2013; pp 27–67.

(11) Nilsson, D.; Chen, M.; Kugler, T.; Remonen, T.; Armgarth, M.; Berggren, M. Bi-Stable and Dynamic Current Modulation in Electrochemical Organic Transistors. *Advanced Materials* **2002**, *14* (1), 51–54.

(12) Gualandi, I.; Marzocchi, M.; Scavetta, E.; Calienni, M.; Bonfiglio, A.; Fraboni, B. A Simple All-PEDOT:PSS Electrochemical Transistor for Ascorbic Acid Sensing. *J. Mater. Chem. B* **2015**, *3* (33), 6753–6762.

(13) Kergoat, L.; Piro, B.; Simon, D. T.; Pham, M.-C.; Noël, V.; Berggren, M. Detection of Glutamate and Acetylcholine with Organic Electrochemical Transistors Based on Conducting Polymer/Platinum Nanoparticle Composites. *Advanced Materials* **2014**, *26* (32), 5658–5664.

(14) Müller, C.; Hamedi, M.; Karlsson, R.; Jansson, R.; Marcilla, R.; Hedhammar, M.; Inganäs, O. Woven Electrochemical Transistors on Silk Fibers. *Advanced Materials* **2011**, *23* (7), 898–901.

(15) Singh, R.; Lin, Y.-T.; Chuang, W.-L.; Ko, F.-H. A New Biodegradable Gate Dielectric Material Based on Keratin Protein for Organic Thin Film Transistors. *Organic Electronics* **2017**, *44*, 198–209.

(16) Mostert, A. B. Melanin, the What, the Why and the How: An Introductory Review for Materials Scientists Interested in Flexible and Versatile Polymers. *Polymers* **2021**, *13* (10), 1670.

(17) Paulin, J. V.; Graeff, C. F. O. From Nature to Organic (Bio)Electronics: A Review on Melanin-Inspired Materials. *J. Mater. Chem. C* **2021**, *9* (41), 14514–14531..

Chapter 2: Eumelanin

2.1 Introduction on melanin

The term "melanin" (Greek μέλας, mèlas = black) was coined by Berzelius in 1840,[1] and was first referred to a group of dark pigments found across a wide range of species, from animals to plants and microorganisms. Since then, it was used to describe all black or dark brown pigments without specifying structural, biogenetic, or functional aspects. One of the most common classifications of melanin was proposed by Nicolaus in 1969,[2] that divided melanins into three categories:

- Eumelanins: eumelanin is the most widely studied of all melanins since it is the primary pigment found in human hair and skin and it is also the main component of squid ink.[3] It is known that “Eu” is the Greek prefix meaning “good”; eumelanin arises from the oxidative polymerization of L-dopa via intermediates such as 5,6-dihydroxyindole (DHI) and 5,6-dihydroxyindole-2-carboxylic acid (DHICA) and is black to brown in colour;[4]
- Pheomelanins: pheomelanin is yellow-to-reddish-brown, alkali-soluble, sulphur-containing pigments derived from the oxidation of cysteinyldopa (5-CysDOPA), with intermediates including benzothiazine and benzothiazole. Pheomelanin oligomeric structure incorporates L-cysteine units, unlike eumelanin. Pheomelanin is also found in human skin and hair and is characterized by a colour ranging from red to yellow.[5,6] Although pheomelanin makes up approximately 25% of total melanin, its

exact structure is not yet understood, as pure pheomelanin is rare to find in nature;[7,8]

- Allomelanins: unlike the first three classes of melanin, allomelanin (the prefix "allo" in Greek means “heterogeneous” or “different”) is a heterogeneous group of biopolymers that can be found in fungi, bacteria, and plants.[9] For example, *Pseudomonas* and *Aspergillus fumigatus* can produce eumelanin-like pigments from tyrosine, while fungi like *Cryptococcus neoformans* produce similar pigments via alternative pathways. Depending on the precursor molecules, allomelanin is further divided into numerous subtypes of melanins united by the presence of hydroxylated aromatic units.

In addition to these categories, other classes of melanins have been more recently introduced such as pyomelanins and neuromelanins. The latter are dark pigments produced in neurons by the oxidation of dopamine and other catecholamine precursors,[9] with the *substantia nigra* melanin being a prominent example. Pyomelanins are a melanin subclass produced by microorganisms, typically through the oxidation of homogentisic acid.

Given the wide variety of dark phenolic pigments in microorganisms and plants, a more inclusive classification is often maintained, distinguishing between natural pigments that should keep the natural source in their name (hair melanin, sepia melanin) and synthetic pigments that should keep the precursor in their name (dopamine melanin, dihydroxyindole melanin). The latter could be synthesized via chemical or enzymatic processes from natural precursors and are shown in figure 2.1.

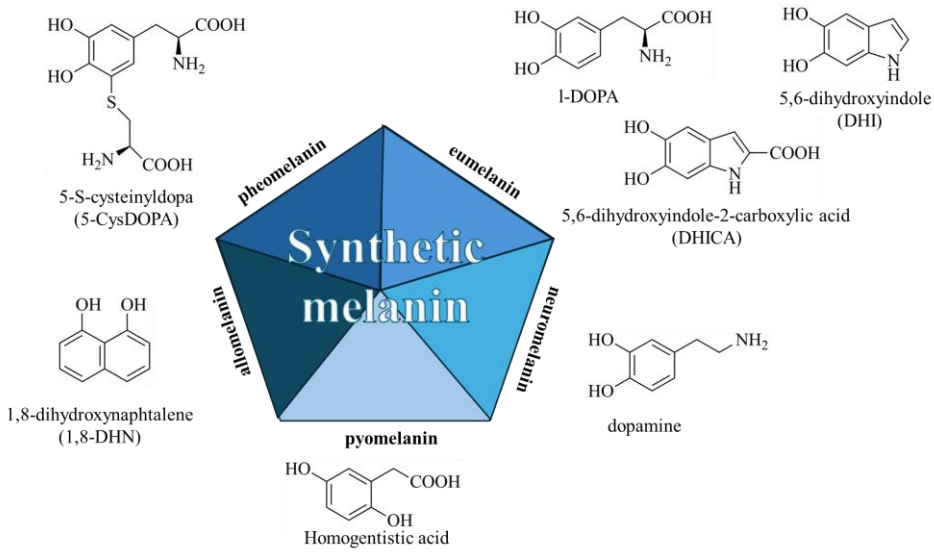

Figure 2.1: Synthetic melanin classification. For each synthetic melanin the main precursor(s) is (are) shown.

2.2 Interest in melanin

Melanocytes, the cells responsible for producing melanin. have distinctive and fascinating characteristics that make them attractive for innovative approaches to solve important biomedical and technological challenges. The uniqueness of pigment cells largely stems from melanin, the pigment itself, which has attracted the interest of chemist and medicine scientists for many years. The study of melanin and melanogenesis has gained wider recognition, opening new research avenues in fields like biomedicine, dermocosmetics, nanotechnology, and materials science.

Melanin is found throughout the human body, including the eyes,[10] hair,[11–13] skin inner ear[14] and, brain stem.[15] Eumelanin is crucial for human health, as it protects the skin from the harmful effects of UV radiation by dissipating it into heat[16] neutralizing reactive oxygen and nitrogen species (ROS/RNS) produced by radiation exposure,[17] thus reducing the risk of DNA damage and sunburn. Although melanin acts as a photo protectant, the ROS/RNS it absorbs can alter melanin and cause DNA damage in cells, potentially contributing to malignant melanoma, although the link is still not fully understood.[18,19] Skin cancers, particularly melanoma, are some of the most common and increasingly prevalent cancers worldwide.[20] Cutaneous melanoma (CM) is a condition marked by the malignant transformation of melanocytes. Although it has a lower incidence than other types of skin cancer, CM is more aggressive and accounts for the majority of skin cancer-related deaths.[21] Moreover, melanin plays a significant role in the CM progression. Although skin with higher melanin content is more resistant to carcinogenesis compared to skin with lower melanin,[20] some studies suggest that pheomelanin may increase DNA damage in cells exposed to UV light[22] and may function as a photosensitizer.[23] This makes it crucial to understand melanin's biological role, especially in regions with high solar radiation. Melanin is also

related to various pigmentation disorders,[24] such as albinism and vitiligo, which result from genetic mutations affecting melanin biosynthesis and melanosomal proteins.[25] A deeper understanding of melanin's functions can aid in developing treatments for these disorders.

Moreover, melanin has been associated with diseases unrelated to its photoprotective role, such as Parkinson's disease,[15] suggesting that its function may extend beyond protection against UV radiation. Although melanin is most connected to the skin, its presence in other tissues has suggested alternative theories regarding its primary function. These hypotheses include melanin's potential involvement in immune response,[26] its ability to protect against transition metal ion toxicity,[15] its contribution to camouflage pigmentation,[27] and its regulation of metal ions.[28]

The structural complexity of melanin makes it difficult to fully understand its functions. Unlike most biological materials, melanin lacks a defined structure, which make it impossible to establish the usual structure-property-function relationship.

Melanin's molecular structure is intricate and disordered, which makes it an intriguing model for studying the role of disorder in biological systems. To date, one of the most difficult challenges in determining melanin's precise chemical structure is represented by its insolubility and heterogeneous nature.[24] The large-scale amorphous nature of melanin also makes it challenging to study using conventional structural analysis methods.[29] These challenges make melanin a promising system for developing innovative methods that could have broader applications across various biosystems.[30,31]

Apart from the biological interest, melanin's unique physical and chemical properties are highly relevant for materials scientists working on flexible materials for device and sensing applications. Melanin is recognized for its radical scavenging ability,[2,33] broad UV-Vis absorption with non-radiative relaxation of

excited states,[32] metal-ion chelation capacity,[34,35] drug uptake potential,[36,37] thermal regulation, redox activities, and energy transduction.[38]

A deep understanding of melanin's properties, along with its natural biocompatibility, has led to novel opportunities for the use of various forms of melanin and their precursors in cosmetic and healthcare industries[39] and in the development of organic electronic devices. On a technological level, eumelanin has been the subject of significant research within organic electronics and material sciences.[40,41] Some potential applications include the creation of active layers in electrochemical energy storage systems like supercapacitors,[42] highly sensitive humidity sensors (which take advantage of eumelanin's sensitivity to hydration in solid-state conductivity)[43] and optoelectronic devices, such as organic photovoltaic cells[44] and solar cells.[45,46] Despite the rising interest in utilizing both natural and synthetic eumelanin for organic electronics and bioelectronics, the widespread adoption of eumelanin-based technologies has faced obstacles, because of its insolubility in water and typical organic solvents. At the same time, a major focus of organic electronics research has been on developing multicomponent materials that combine diverse features in hybrid systems, allowing for the emergence of additional properties from the interaction of these components.[47,48]

2.3 Synthesis of melanin

As noted before, eumelanin is the most studied pigment among the various melanin types, primarily because of its abundance and distinctive characteristics.[49] Investigating eumelanin biosynthesis, or melanogenesis, is particularly difficult due to the extreme stability and insolubility of the final product[3]and the high instability of the intermediates. In humans, melanin is produced in melanocytes and follows the well-established Raper-Mason pathway (Scheme 2.1),[50–52] which covers much of the early stages of melanogenesis. In the beginning, the amino acid L-tyrosine is oxidized by oxygen in a reaction catalysed by the enzyme tyrosinase to produce 3,4-dihydroxyphenylalanine (L-DOPA). The latter is then oxidized to form dopaquinone, a precursor common to both eumelanin and pheomelanin. Dopaquinone is a highly reactive key intermediate that can follow different pathways. In the absence of cysteine, dopaquinone undergoes cyclization to form cyclodopa, which then reacts with dopaquinone in a redox-exchange reaction to produce dopachrome, a red-orange intermediate.[50,51] Dopachrome can spontaneously rearrange to 5,6-dihydroxyindole (DHI) in vitro at neutral pH. However, in vivo, the enzyme dopachrome-tautomerase guides the rearrangement towards the formation of 5,6-dihydroxyindole-2-carboxylic acid (DHICA). Finally, eumelanin is produced through the oxidative polymerization of DHI and DHICA.

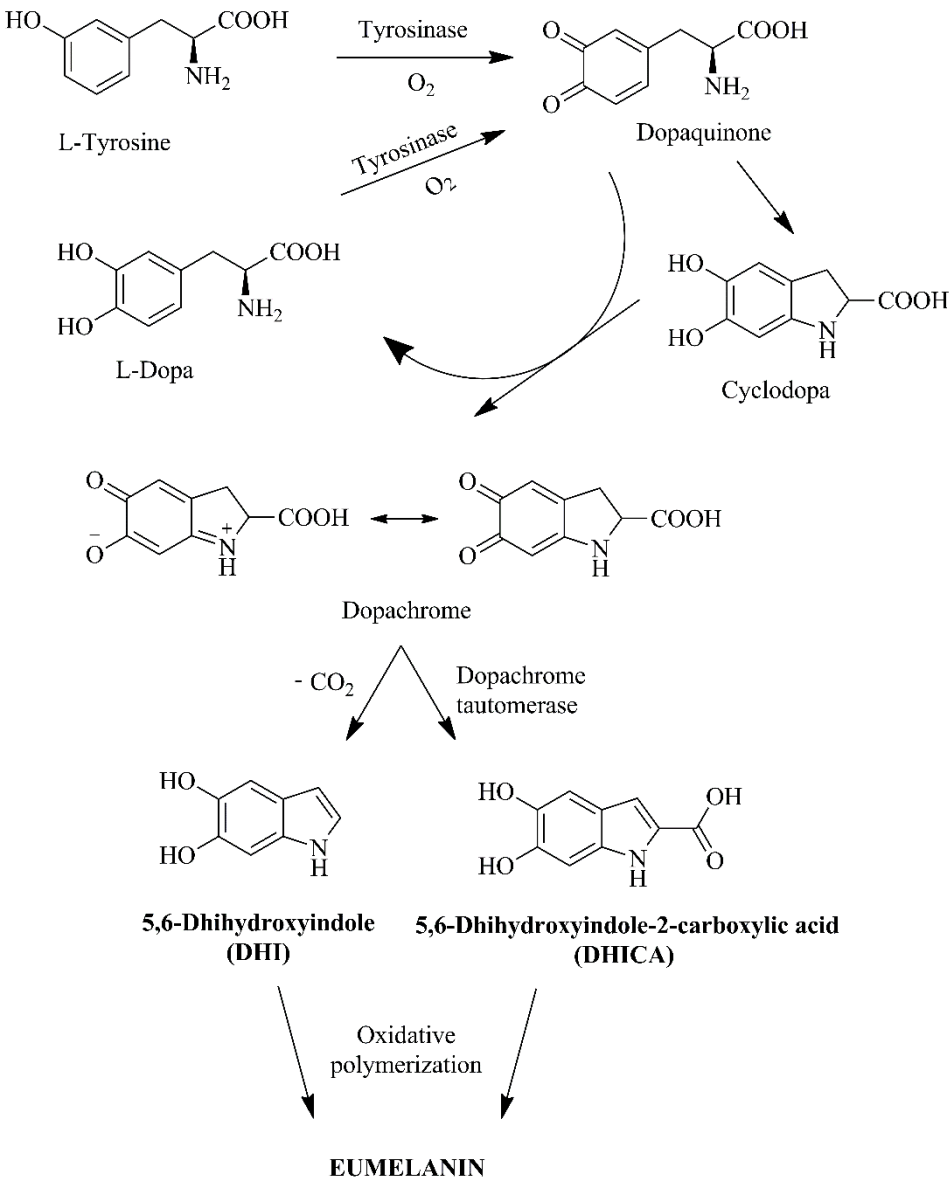

Scheme 2.1: eumelanin synthesis from Tyrosine or L-Dopa proposed by Raper and Mason.[50,51]

Current understanding of melanin formation from DHI and DHICA is still unclear, though some progress has been made. DHI quinone and DHICA quinone can dimerize with DHI, DHICA, or both, forming homodimers and heterodimers.

Several oligomers, ranging up to tetramers, have been isolated and characterized as acetylated derivatives for DHI or as non-derivatives for DHICA.[39] These oligomers likely form through free radical polymerization, although the exact mechanism remains debated,[53] contributing to melanin's supramolecular structure.

It's also important to note that melanogenesis, as discussed, primarily considers eumelanin formation, but in vivo, eumelanin synthesis is always accompanied by pheomelanin formation in a process called mixed melanogenesis.[54]

The spontaneous reactions involved in eumelanin synthesis are influenced by several factors, including the presence of thiols, pH, specific ions (like zinc and copper),[55] and oxygen. The ratio of the two dihydroxyindoles is also affected by other environmental conditions, such as the availability of the enzyme dopachrome tautomerase.[56]

Various approaches have been developed to obtain melanin for the investigation of its unique properties. Eumelanin isolation still represents a challenge due to its limited solubility and the presence of associated biomolecules like proteins and metal cations that influence the structural aggregation and physical properties.[57]

Current isolation strategies include extracting eumelanin from human hair, from the ink sac of cuttlefish *Sepia Officinalis*, and bird feathers. These approaches have proven effective in removing cellular components and proteins without altering the physicochemical properties of eumelanin.[2,58,59] However, a wide variety of synthetic methods and procedures have been described, involving different conditions that do not always meet the requirements of biological relevance.

A comprehensive review about synthetic melanins and laboratory methodologies was provided by D'Ischia et al. in 2013.[58] This work showed the most common

synthetic routes to obtain melanin precursors and, starting from the latter, how to obtain the corresponding synthetic melanins.

The structural features and properties of synthetic melanin in the reported cases are determined by the choice of starting materials, reaction conditions, and post-synthetic procedures. Therefore, comparing pigments produced under different conditions can be deceptive, even if they come from the same substrate. For instance, to obtain synthetic eumelanin, oxidative polymerization of its main key precursors DHI and DHICA can be performed under various conditions, including:

- Peroxidase/H_2O_2 system: this enzyme system, at biomimetic pH, is faster and yields higher amounts of eumelanin compared to the tyrosinase-based approach. A synthetic eumelanin produced by oxidizing tyrosine with persulfate or peroxidase is commercially available;[3]
- Chemical oxidation: potassium ferricyanide and sodium periodate can be used in varying amounts relative to the substrate, depending on their electronic properties (one- or two-electron oxidation);
- Biomimetic conditions: oxidation of DHI is catalysed by the enzyme tyrosinase in an aqueous buffer at neutral pH. This approach mimics the biological pathway, making it seem ideal. However, eumelanin synthesis proceeds slowly under these conditions, especially when enzyme concentrations are high.[60] Additionally, reproducibility is low due to challenges in measuring and controlling tyrosinase activity during the reaction.[4] Alternatively, L-DOPA and tyrosine can be used as substrates for enzymatic preparations;
- Autoxidative conditions: often involving metal ions such as copper, these conditions exploit the tendency of DHI and DHICA to oxidize in air under mildly alkaline conditions.[61]

Other synthetic approaches for the synthesis of synthetic melanin were adopted, especially in the field of material science. The latter were achieved through:

1. Biomimetic conditions: this method usually uses DL-Dopa, or other starting materials dissolved in water and allowed to oxidize while air is bubbled through the solution. The obtained melanin is dominated by DHI (with around 10% DHICA).[56,58,62] This approach is simple and cost-effective, ideal for material scientists to start working with melanin;

2. Electrochemical Methods: these often involves electropolymerization on conductive substrates such Indium Tin Oxide (ITO), using an electric current passed through a solution of the substrate. An important example was reported using DL-DOPA;[63]

3. Ammonia-Induced Solid-State Polymerization (AISSP): this method involves the deposition of DHI monomer onto a substrate, to anneal it and exposing it to ammonia vapours, for an accelerated polymerization;[64]

4. Solvent-Based Methods: in contrast to typical water-based methods, the Graeff group demonstrated melanin synthesis in solvents like DMSO and DMF, yielding spin-coated films with smooth surfaces (~0.3 nm roughness).[65] These materials have the advantage of better solubility, spin-coating compatibility, and stability on hydrophobic substrates. The synthesized melanin also contains additional sulfonated groups, making it distinct from traditional melanin but still resembling its functional properties.[66,67] The Graeff group has also worked on improving reaction rates by synthesizing melanin under O_2 pressure, enhancing carboxyl content and solubility in water.[68,69]

These methodologies are crucial for material and polymer scientists, as they facilitate the creation of melanin-like films and materials for various applications.

While these approaches differ in terms of synthesis times and material properties, they all provide pathways for integrating melanin into functional materials for further research.

Since synthetic eumelanin is produced under controlled conditions and contains known monomer units, it is easier to analyse compared to melanin isolated from natural sources, which is more complex. Synthetic eumelanin serves as a useful model system for testing new approaches or theories in the study of this complex biopolymer.

2.4 Structure of melanin

As aforementioned, natural eumelanin is a complex, amorphous polymer made up of DHI and DHICA units. The ratio of these two primary precursors depends on the activity of the enzyme dopachrome tautomerase. Dopachrome spontaneously decarboxylates to DHI in vitro, but in vivo, the enzyme dopachrome tautomerase facilitates the production of DHICA. As a result, natural eumelanin contains more than 50% DHICA.[62] The distinct bonding patterns between DHI and DHICA contribute to the pigment's inherent disorder, which manifests at multiple structural levels. The various bonding patterns between DHI and DHICA contribute to the pigment's structural disorder, which occurs at multiple levels.[49] In particular, it has been recognized that melanin polymers exhibit a complex array of chemical disorders that contribute to their diverse properties. These classified disorders each one is influencing and contributing to the structure and behaviour of the polymer. These degrees of disorder include at molecular level the chemical diversity of the structural units (i.e. polymerization with coupling between different starting monomers), molecular size disorder, configurational and redox disorder.

Finally, supramolecular disorder shows how oligomers organize as they aggregate into larger structures. The extent of this disorder depends on the ratio of planar to twisted structural segments, which is influenced by factors like inter-unit double bonds and the flexibility of the units. Additionally, the effectiveness of intermolecular interactions such as π-π stacking, cation-π interactions, and hydrogen bonding plays a key role in the aggregation of these oligomers.

Early structural models proposed that eumelanin was a high-molecular-weight heteropolymer, formed through random regiochemistry between DHI and DHICA units in different oxidation states. However, in the mid-1990s, an alternative supramolecular architecture for eumelanin particles was suggested.[70] This model

suggested that eumelanin was not a large, extended heteropolymer, but rather a mixture of stacked oligomeric "protomolecules," each consisting of three or four planar layers, with no more than five or six indole units, measuring about 15–20 Å in size. Despite extensive research, the structure of eumelanin remains elusive, primarily due to its amorphous nature and insolubility.

A dual approach combining biomimetic synthesis of oligomeric intermediates[46,71] and post-synthetic oxidative degradation has led to the identification of active polymerization positions in eumelanin: 2, 3, 4, and 7,[28,30,72] specifically:

- DHI polymerizes by forming oligomers through C-C coupling at positions 2, 4, and 7;
- DHICA polymerizes by forming oligomers through C-C coupling at positions 4 and 7. The carboxyl group at position 2 blocks position 2 for DHICA, and position 3 is mostly inactivated due to the electron-withdrawing effect of the carboxyl group at position 2.[73]

DHI oligomers tend to adopt a planar, branched structure, while DHICA oligomers form a non-planar, linear backbone with hindered biphenyl-type bonds and exhibit atropoisomerism. The twisted backbones in DHICA oligomers prevent π-stacking, unlike the planar DHI oligomers, and lead to rod-like assemblies with weak intermolecular interactions.[59,74,75]

2.5 Eumelanin physical and chemical properties

Melanin's UV-visible absorption spectrum is broad and lacks a distinct peak, which is uncommon for organic chromophores. This characteristic arises from the overlap of multiple peaks throughout the UV-Vis spectrum,[33] a consequence of the pigment's chemical disorder and heterogeneity,[76] The observed monotonic trend can be attributed to the superposition of absorption profiles from oligomers of different sizes and structures, further complicated by the coexistence of oxidized and reduced monomer units within the eumelanin polymer.[76,77] Furthermore, melanin's emission spectrum has a quantum yield of less than 0.1%, meaning more than 99% of the absorbed UV-Vis energy is converted into heat[78] highlighting its effectiveness as a photo-protectant. Melanin's photostability can vary based on conditions such as its source (natural or synthetic), hydration, pH, and the presence of redox-active metal ions.[79–81] As for solvent stability, melanin is typically stable in most solvents, though its long-term stability is affected by factors like oxygen concentration, pH (it is less stable at high pH), and the presence of redox-active metal ions, which also influence its photobleaching characteristics.[32] Eumelanin is also known to possess a stable free radical detectable by electron paramagnetic resonance, characterized by a single, slightly asymmetric line. It was one of the first biomaterials to have its free radical signal reported.[82] The presence of a long-lived organic radical in a material is thought to have a protective function such as radical scavenging and antioxidant activity. DHICA eumelanin, compared to DHI eumelanin, demonstrates greater homogeneity of free radical components and exhibits more potent free radical scavenging properties, likely due to weaker aggregation and enhanced accessibility to free radicals. DHICA eumelanin also acts as a scavenger of hydroxyl (OH) and nitric oxide (NO) radicals and functions as an H donor.[17]

Since the 1970s, melanin has been considered an example of an amorphous semiconductor due to several factors: its broad optical absorbance profile indicating localized states in the gap,[83] the free radical signal suggesting available electrons at the Fermi level for conduction and semiconductor-like conductivity behaviour depending on temperature.[84,85] McGinnes explained this phenomenon using the amorphous organic semiconductor model, proposing that absorbed water is distributed throughout the polymer, lowering the energy barrier for charge transport.[83] This model, however, is inconsistent with experimental observations such as the broad UV-vis spectrum, indicative of chemical disorder,[76] and the presence of ionizable groups within the eumelanin structure. The aforementioned incompatibility with the amorphous semiconductor model, have led to an alternative charge transport model for melanin's conductivity.[86,40] This model suggests that melanin's conductivity is governed by a comproportionation reaction (scheme 2.2).

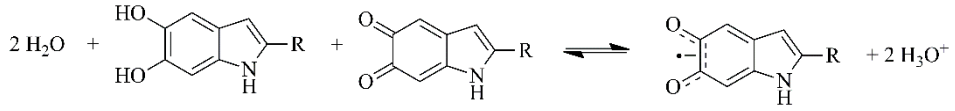

R = H,COOH

Scheme 2.2: DHI / DHICA comproportionation reaction.

The addition of water moves the equilibrium towards the production of radicals and protons, making melanin a mixed electronic-ionic conductor. This model explains various properties of melanin, including its absorbance spectra, the radical presence, photoconductivity behaviour with hydration-dependent changes observed[87] and temperature dependence is explained by this equilibrium, showing semiconducting-like behaviour.[88]

Support for this model comes from kinetic isotope experiments using D_2O hydration, photo-induced semiquinone production studies,[89] and demonstrations of proton conductivity,[90] with protons being the dominant charge carrier when hydrated.[91] However, there are differences between natural and synthetic melanin, and while many researchers support the idea of proton involvement in conductivity, some still combine the mixed proton-electronic model with the amorphous semiconductor model.

2.6 References

(1) Borovanský, J.; Riley, P. A. Physiological and Pathological Functions of Melanosomes. In *Melanins and Melanosomes*; John Wiley & Sons, Ltd, 2011; pp 343–381.

(2) Nicolaus, R. A.; Piattelli, M.; Fattorusso, E. The Structure of Melanins and Melanogenesis—IV: On Some Natural Melanins. *Tetrahedron* **1964**, *20* (5), 1163–1172.

(3) Kollias, N.; Sayre, R. M.; Zeise, L.; Chedekel, M. R. New Trends in Photobiology: Photoprotection by Melanin. *Journal of Photochemistry and Photobiology B: Biology* **1991**, *9* (2), 135–160.

(4) Prota, G. CHAPTER 5 - EUMELANINS. In *Melanins and Melanogenesis*; Prota, G., Ed.; Academic Press: San Diego, 1992; pp 88–118.

(5) Hearing, V. J. Biochemical Control of Melanogenesis and Melanosomal Organization. *Journal of Investigative Dermatology Symposium Proceedings* **1999**, *4* (1), 24–28.

(6) Hearing, V. J. The Regulation of Melanin Formation. In *The Pigmentary System*; John Wiley & Sons, Ltd, 2006; pp 191–212.

(7) Solano, F. Photoprotection versus Photodamage: Updating an Old but Still Unsolved Controversy about Melanin. *Polymer International* **2016**, *65* (11), 1276–1287.

(8) Simon, J. D.; Peles, D. N. The Red and the Black. *Acc. Chem. Res.* **2010**, *43* (11), 1452–1460.

(9) Cao, W.; Zhou, X.; McCallum, N. C.; Hu, Z.; Ni, Q. Z.; Kapoor, U.; Heil, C. M.; Cay, K. S.; Zand, T.; Mantanona, A. J.; Jayaraman, A.; Dhinojwala, A.; Deheyn, D. D.; Shawkey, M. D.; Burkart, M. D.; Rinehart, J. D.; Gianneschi, N. C. Unraveling the Structure and Function of Melanin through Synthesis. *J. Am. Chem. Soc.* **2021**, *143* (7), 2622–2637.

(10) Wielgus, A. R.; Sarna, T. Melanin in Human Irides of Different Color and Age of Donors. *Pigment Cell Research* **2005**, *18* (6), 454–464.

(11) Ito, S.; Jimbow, K. Quantitative Analysis of Eumelanin and Pheomelanin in Hair and Melanomas. *Journal of Investigative Dermatology* **1983**, *80* (4), 268–272.

(12) Itou, T.; Ito, S.; Wakamatsu, K. Effects of Aging on Hair Color, Melanosomes, and Melanin Composition in Japanese Males and Their Sex Differences. *International Journal of Molecular Sciences* **2022**, *23* (22), 14459.

(13) Itou, T.; Ito, S.; Wakamatsu, K. Effects of Aging on Hair Color, Melanosome Morphology, and Melanin Composition in Japanese Females. *International Journal of Molecular Sciences* **2019**, *20* (15), 3739.

(14) Gottesberge, A. M. M. zum. Physiology and Pathophysiology of Inner Ear Melanin. *Pigment Cell Research* **1988**, *1* (4), 238–249.

(15) Zucca, F. A.; Giaveri, G.; Gallorini, M.; Albertini, A.; Toscani, M.; Pezzoli, G.; Lucius, R.; Wilms, H.; Sulzer, D.; Ito, S.; Wakamatsu, K.; Zecca, L. The Neuromelanin of Human Substantia Nigra: Physiological and Pathogenic Aspects. *Pigment Cell Research* **2004**, *17* (6), 610–617.

(16) Pezzella, A.; Wünsche, J. Eumelanin: An Old Natural Pigment and a New Material for Organic Electronics – Chemical, Physical, and Structural Properties in Relation to Potential Applications. In *Organic Electronics*; John Wiley & Sons, Ltd, 2013; pp 113–137.

(17) Jiang, S.; Liu, X.-M.; Dai, X.; Zhou, Q.; Lei, T.-C.; Beermann, F.; Wakamatsu, K.; Xu, S.-Z. Regulation of DHICA-Mediated Antioxidation by Dopachrome Tautomerase: Implication for Skin Photoprotection against UVA Radiation. *Free Radical Biology and Medicine* **2010**, *48* (9), 1144–1151.

(18) Nofsinger, J. B.; Forest, S. E.; Simon, J. D. Explanation for the Disparity among Absorption and Action Spectra of Eumelanin. *J. Phys. Chem. B* **1999**, *103* (51), 11428–11432.

(19) Menon, I. A.; Haberman, H. F. MECHANISMS OF ACTION OF MELANINS. *British Journal of Dermatology* **1977**, *97* (1), 109–112.

(20) Lin, J. Y.; Fisher, D. E. Melanocyte Biology and Skin Pigmentation. *Nature* **2007**, *445* (7130), 843–850.

(21) Cabaço, L. C.; Tomás, A.; Pojo, M.; Barral, D. C. The Dark Side of Melanin Secretion in Cutaneous Melanoma Aggressiveness. *Front. Oncol.* **2022**, *12*.

(22) Scott, M. C.; Wakamatsu, K.; Ito, S.; Kadekaro, A. L.; Kobayashi, N.; Groden, J.; Kavanagh, R.; Takakuwa, T.; Virador, V.; Hearing, V. J.; Abdel-Malek, Z. A. Human Melanocortin

1 Receptor Variants, Receptor Function and Melanocyte Response to UV Radiation. *Journal of Cell Science* **2002**, *115* (11), 2349–2355.

(23) Kennedy, C.; Huurne, J. ter; Berkhout, M.; Gruis, N.; Bastiaens, M.; Bergman, W.; Willemze, R.; Bavinck, J. N. B. Melanocortin 1 Receptor (MC1R) Gene Variants Are Associated with an Increased Risk for Cutaneous Melanoma Which Is Largely Independent of Skin Type and Hair Color. *J Invest Dermatol* **2001**, *117* (2), 294–300.

(24) Prota, G. Progress in the Chemistry of Melanins and Related Metabolites. *Medicinal Research Reviews* **1988**, *8* (4), 525–556.

(25) Koike, S.; Yamasaki, K. Melanogenesis Connection with Innate Immunity and Toll-Like Receptors. *International Journal of Molecular Sciences* **2020**, *21* (24), 9769.

(26) Burkhart, C. G.; Burkhart, C. N. The Mole Theory: Primary Function of Melanocytes and Melanin May Be Antimicrobial Defense and Immunomodulation (Not Solar Protection). *International Journal of Dermatology* **2005**, *44* (4), 340–342.

(27) Galván, I.; Alonso-Alvarez, C. The Expression of Melanin-Based Plumage Is Separately Modulated by Exogenous Oxidative Stress and a Melanocortin. *Proceedings of the Royal Society B: Biological Sciences* **2009**, *276* (1670), 3089–3097.

(28) Hong, L.; Simon, J. D. Insight into the Binding of Divalent Cations to Sepia Eumelanin from IR Absorption Spectroscopy. *Photochemistry and Photobiology* **2006**, *82* (5), 1265–1269.

(29) Ghadge, V. A.; Singh, S.; Kumar, P.; Mathew, D. E.; Dhimmar, A.; Sahastrabudhe, H.; Gajjar, A.; Nimse, S. B.; Shinde, P. B. Extraction, Purification, and Characterization of Microbial Melanin Pigments. In *Melanins: Functions, Biotechnological Production, and Applications*; Gosset, G., Ed.; Springer International Publishing: Cham, 2023; pp 91–110.

(30) Xie, H.; Vucetic, S.; Iakoucheva, L. M.; Oldfield, C. J.; Dunker, A. K.; Obradovic, Z.; Uversky, V. N. Functional Anthology of Intrinsic Disorder. 3. Ligands, Post-Translational Modifications, and Diseases Associated with Intrinsically Disordered Proteins. *J. Proteome Res.* **2007**, *6* (5), 1917–1932.

(31) Shimizu, K.; Muraoka, Y.; Hirose, S.; Tomii, K.; Noguchi, T. Predicting Mostly Disordered Proteins by Using Structure-Unknown Protein Data. *BMC Bioinformatics* **2007**, *8* (1), 78.

(32) Meredith, P.; Sarna, T. The Physical and Chemical Properties of Eumelanin. *Pigment Cell Research* **2006**, *19* (6), 572–594.

(33) Meredith, P.; Powell, B. J.; Riesz, J.; Nighswander-Rempel, S. P.; Pederson, M. R.; Moore, E. G. Towards Structure–Property–Function Relationships for Eumelanin. *Soft Matter* **2006**, *2* (1), 37–44.

(34) Hong, L.; Liu, Y.; Simon, J. D. Binding of Metal Ions to Melanin and Their Effects on the Aerobic Reactivity. *Photochemistry and Photobiology* **2004**, *80* (3), 477–481.

(35) Samokhvalov, A.; Liu, Y.; Simon, J. D. Characterization of the Fe(III)-Binding Site in Sepia Eumelanin by Resonance Raman Confocal Microspectroscopy. *Photochemistry and Photobiology* **2004**, *80* (1), 84–88.

(36) Bridelli, M. G.; Ciati, A.; Crippa, P. R. Binding of Chemicals to Melanins Re-Examined: Adsorption of Some Drugs to the Surface of Melanin Particles. *Biophysical Chemistry* **2006**, *119* (2), 137–145.

(37) Larsson, B. S. Interaction Between Chemicals and Melanin. *Pigment Cell Research* **1993**, *6* (3), 127–133.

(38) Berg, S. Z.; Berg, J. Melanin: A Unifying Theory of Disease as Exemplified by Parkinson's, Alzheimer's, and Lewy Body Dementia. *Front. Immunol.* **2023**, *14*.

(39) Panzella, L.; Ebato, A.; Napolitano, A.; Koike, K. The Late Stages of Melanogenesis: Exploring the Chemical Facets and the Application Opportunities. *International Journal of Molecular Sciences* **2018**, *19* (6), 1753.

(40) Mostert, A. B. Melanin, the What, the Why and the How: An Introductory Review for Materials Scientists Interested in Flexible and Versatile Polymers. *Polymers* **2021**, *13* (10), 1670.

(41) Barra, M.; Bonadies, I.; Carfagna, C.; Cassinese, A.; Cimino, F.; Crescenzi, O.; Criscuolo, V.; Marco, d'Ischia; Maglione, M. G.; Manini, P.; Migliaccio, L.; Musto, A.; Napolitano, A.; Navarra, A.; Panzella, L.; Parisi, S.; Pezzella, A.; Prontera, C. T.; Tassini, P. Eumelanin-Based Organic Bioelectronics: Myth or Reality? *MRS Advances* **2016**, *1* (57), 3801–3810.

(42) Kumar, P.; Mauro, E. D.; Zhang, S.; Pezzella, A.; Soavi, F.; Santato, C.; Cicoira, F. Melanin-Based Flexible Supercapacitors. *Journal of Materials Chemistry C* **2016**, *4* (40), 9516–9525.

(43) Wu, T.-F.; Hong, J.-D. Synthesis of Water-Soluble Dopamine–Melanin for Ultrasensitive and Ultrafast Humidity Sensor. *Sensors and Actuators B: Chemical* **2016**, *224*, 178–184.

(44) Vahidzadeh, E.; Kalra, A. P.; Shankar, K. Melanin-Based Electronics: From Proton Conductors to Photovoltaics and Beyond. *Biosensors and Bioelectronics* **2018**, *122*, 127–139.

(45) Meredith, P.; Powell, B. J.; Riesz, J.; Vogel, R.; Blake, D.; Kartini, I.; Will, G.; Subianto, S. Broadband Photon-harvesting Biomolecules for Photovoltaics. In *Artificial Photosynthesis*; John Wiley & Sons, Ltd, 2005; pp 35–65.

(46) Panzella, L.; Pezzella, A.; Napolitano, A.; d'Ischia, M. The First 5,6-Dihydroxyindole Tetramer by Oxidation of 5,5‘,6,6‘-Tetrahydroxy- 2,4‘-Biindolyl and an Unexpected Issue of Positional Reactivity En Route to Eumelanin-Related Polymers. *Org. Lett.* **2007**, *9* (7), 1411–1414.

(47) Wakayama, Y.; Hayakawa, R.; Higashiguchi, K.; Matsuda, K. Photochromism for Optically Functionalized Organic Field-Effect Transistors: A Comprehensive Review. *J. Mater. Chem. C* **2020**, *8* (32), 10956–10974..

(48) Kalachyova, Y.; Guselnikova, O.; Postnikov, P.; Fitl, P.; Lapcak, L.; Svorcik, V.; Lyutakov, O. Reversible Switching of PEDOT:PSS Conductivity in the Dielectric–Conductive Range through the Redistribution of Light-Governing Polymers. *RSC Adv.* **2018**, *8* (20), 11198–11206.

(49) d'Ischia, M.; Napolitano, A.; Pezzella, A.; Meredith, P.; Buehler, M. Melanin Biopolymers: Tailoring Chemical Complexity for Materials Design. *Angewandte Chemie International Edition* **2020**, *59* (28), 11196–11205.

(50) Raper, H. S. The Tyrosinase-Tyrosine Reaction: Production from Tyrosine of 5: 6-Dihydroxyindole and 5: 6-Dihydroxyindole-2-Carboxylic Acid—the Precursors of Melanin. *Biochemical Journal* **1927**, *21* (1), 89–96.

(51) Mason, H. S. THE CHEMISTRY OF MELANIN: III. MECHANISM OF THE OXIDATION OF DIHYDROXYPHENYLALANINE BY TYROSINASE. *Journal of Biological Chemistry* **1948**, *172* (1), 83–99.

(52) Ito, S. A Chemist's View of Melanogenesis. *Pigment Cell Research* **2003**, *16* (3), 230–236..

(53) Chen, C.-T.; Martin-Martinez, F. J.; Jung, G. S.; Buehler, M. J. Polydopamine and Eumelanin Molecular Structures Investigated with Ab Initio Calculations. *Chem. Sci.* **2017**, *8* (2), 1631–1641.

(54) Ito, S.; Wakamatsu, K. Chemistry of Mixed Melanogenesis—Pivotal Roles of Dopaquinone. *Photochemistry and Photobiology* **2008**, *84* (3), 582–592.

(55) Palumbo, A.; d'Ischia, M.; Misuraca, G.; Prota, G. Mechanism of Inhibition of Melanogenesis by Hydroquinone. *Biochimica et Biophysica Acta (BBA) - General Subjects* **1991**, *1073* (1), 85–90.

(56) Pezzella, A.; d'Ischia, M.; Napolitano, A.; Palumbo, A.; Prota, G. An Integrated Approach to the Structure of Sepia Melanin. Evidence for a High Proportion of Degraded 5,6-Dihydroxyindole-2-Carboxylic Acid Units in the Pigment Backbone. *Tetrahedron* **1997**, *53* (24), 8281–8286.

(57) Liu, Y.; Simon, J. D. Isolation and Biophysical Studies of Natural Eumelanins: Applications of Imaging Technologies and Ultrafast Spectroscopy. *Pigment Cell Research* **2003**, *16* (6), 606–618.

(58) d'Ischia, M.; Wakamatsu, K.; Napolitano, A.; Briganti, S.; Garcia-Borron, J.-C.; Kovacs, D.; Meredith, P.; Pezzella, A.; Picardo, M.; Sarna, T.; Simon, J. D.; Ito, S. Melanins and Melanogenesis: Methods, Standards, Protocols. *Pigment Cell & Melanoma Research* **2013**, *26* (5), 616–633.

(59) d'Ischia, M.; Wakamatsu, K.; Cicoira, F.; Di Mauro, E.; Garcia-Borron, J. C.; Commo, S.; Galván, I.; Ghanem, G.; Kenzo, K.; Meredith, P.; Pezzella, A.; Santato, C.; Sarna, T.; Simon, J. D.; Zecca, L.; Zucca, F. A.; Napolitano, A.; Ito, S. Melanins and Melanogenesis: From Pigment Cells to Human Health and Technological Applications. *Pigment Cell & Melanoma Research* **2015**, *28* (5), 520–544.

(60) d'Ischia, M.; Napolitano, A.; Tsiakas, K.; Prota, G. New Intermediates in the Oxidative Polymerisation of 5,6-Dihydroxyindole to Melanin Promoted by the Peroxidase/H2O2 System. *Tetrahedron* **1990**, *46* (16), 5789–5796.

(61) Micillo, R.; Iacomino, M.; Perfetti, M.; Panzella, L.; Koike, K.; D'Errico, G.; d'Ischia, M.; Napolitano, A. Unexpected Impact of Esterification on the Antioxidant Activity and (Photo)Stability of a Eumelanin from 5,6-Dihydroxyindole-2-Carboxylic Acid. *Pigment Cell & Melanoma Research* **2018**, *31* (4), 475–483.

(62) Ito, S. Reexamination of the Structure of Eumelanin. *Biochimica et Biophysica Acta (BBA) - General Subjects* **1986**, *883* (1), 155–161.

(63) Subianto, S.; Will, G.; Meredith, P. Electrochemical Synthesis of Melanin Free-Standing Films. *Polymer* **2005**, *46* (25), 11505–11509..

(64) Pezzella, A.; Barra, M.; Musto, A.; Navarra, A.; Alfè, M.; Manini, P.; Parisi, S.; Cassinese, A.; Criscuolo, V.; d'Ischia, M. Stem Cell-Compatible Eumelanin Biointerface Fabricated by Chemically Controlled Solid State Polymerization. *Materials Horizons* **2015**, *2* (2), 212–220.

(65) Dezidério, S. N.; Brunello, C. A.; da Silva, M. I. N.; Cotta, M. A.; Graeff, C. F. O. Thin Films of Synthetic Melanin. *Journal of Non-Crystalline Solids* **2004**, *338–340*, 634–638.

(66) Bronze-Uhle, E. S.; Batagin-Neto, A.; Xavier, P. H. P.; Fernandes, N. I.; de Azevedo, E. R.; Graeff, C. F. O. Synthesis and Characterization of Melanin in DMSO. *Journal of Molecular Structure* **2013**, *1047*, 102–108.

(67) Paulin, J. V.; McGettrick, J. D.; Graeff, C. F. O.; Mostert, A. B. Melanin System Composition Analyzed by XPS Depth Profiling. *Surfaces and Interfaces* **2021**, *24*, 101053.

(68) Bronze-Uhle, E. S.; Paulin, J. V.; Piacenti-Silva, M.; Battocchio, C.; Rocco, M. L. M.; Graeff, C. F. de O. Melanin Synthesis under Oxygen Pressure. *Polymer International* **2016**, *65* (11), 1339–1346.

(69) Paulin, J. V.; Veiga, A. G.; Garcia-Basabe, Y.; Rocco, M. L. M.; Graeff, C. F. Structural and Optical Properties of Soluble Melanin Analogues with Enhanced Photoluminescence Quantum Efficiency. *Polymer International* **2018**, *67* (5), 550–556.

(70) Cheng, J.; Moss, S. C.; Eisner, M. X-Ray Characterization of Melanins—II. *Pigment Cell Research* **1994**, *7* (4), 263–273.

(71) d'Ischia, M.; Napolitano, A.; Pezzella, A. 5,6-Dihydroxyindole Chemistry: Unexplored Opportunities Beyond Eumelanin. *European Journal of Organic Chemistry* **2011**, *2011* (28), 5501–5516.

(72) Pettinari, M. J.; Pavan, M. E.; López, N. I. Melanin Synthesis in Bacteria: Who, How and Why. In *Melanins: Functions, Biotechnological Production, and Applications*; Gosset, G., Ed.; Springer International Publishing: Cham, 2023; pp 1–25.

(73) Solano, F. Melanins: Skin Pigments and Much More—Types, Structural Models, Biological Functions, and Formation Routes. *New Journal of Science* **2014**, *2014* (1), 498276.

(74) Pezzella, A.; Vogna, D.; Prota, G. Atropoisomeric Melanin Intermediates by Oxidation of the Melanogenic Precursor 5,6-Dihydroxyindole-2-Carboxylic Acid under Biomimetic Conditions. *Tetrahedron* **2002**, *58* (19), 3681–3687.

(75) Pezzella, A.; Vogna, D.; Prota, G. Synthesis of Optically Active Tetrameric Melanin Intermediates by Oxidation of the Melanogenic Precursor 5,6-Dihydroxyindole-2-Carboxylic Acid under Biomimetic Conditions. *Tetrahedron: Asymmetry* **2003**, *14* (9), 1133–1140.

(76) Tran, M. L.; Powell, B. J.; Meredith, P. Chemical and Structural Disorder in Eumelanins: A Possible Explanation for Broadband Absorbance. *Biophysical Journal* **2006**, *90* (3), 743–752.

(77) Pezzella, A.; Iadonisi, A.; Valerio, S.; Panzella, L.; Napolitano, A.; Adinolfi, M.; d'Ischia, M. Disentangling Eumelanin "Black Chromophore": Visible Absorption Changes As Signatures of Oxidation State- and Aggregation-Dependent Dynamic Interactions in a Model Water-Soluble 5,6-Dihydroxyindole Polymer. *J. Am. Chem. Soc.* **2009**, *131* (42), 15270–15275.

(78) Meredith, P.; Riesz, J. Radiative Relaxation Quantum Yields for Synthetic Eumelanin. *Photochemistry and Photobiology* **2004**, *79* (2), 211–216.

(79) Zareba, M.; Szewczyk, G.; Sarna, T.; Hong, L.; Simon, J. D.; Henry, M. M.; Burke, J. M. Effects of Photodegradation on the Physical and Antioxidant Properties of Melanosomes Isolated from Retinal Pigment Epithelium.

(80) Gauden, M.; Pezzella, A.; Panzella, L.; Neves-Petersen, M. T.; Skovsen, E.; Petersen, S. B.; Mullen, K. M.; Napolitano, A.; d'Ischia, M.; Sundström, V. Role of Solvent, PH, and Molecular Size in Excited-State Deactivation of Key Eumelanin Building Blocks: Implications for Melanin Pigment Photostability. *J. Am. Chem. Soc.* **2008**, *130* (50), 17038–17043.

(81) Sarna, T.; Burke, J. M.; Korytowski, W.; Różanowska, M.; Skumatz, C. M. B.; Zaręba, A.; Zaręba, M. Loss of Melanin from Human RPE with Aging: Possible Role of Melanin Photooxidation. *Experimental Eye Research* **2003**, *76* (1), 89–98.

(82) Commoner, B.; Townsend, J.; Pake, G. E. Free Radicals in Biological Materials. *Nature* **1954**, *174* (4432), 689–691.

(83) McGinness, J. E. Mobility Gaps: A Mechanism for Band Gaps in Melanins. *Science* **1972**, *177* (4052), 896–897.

(84) Jastrzebska, M.; Kocot, A.; Tajber, L. Photoconductivity of Synthetic Dopa–Melanin Polymer. *Journal of Photochemistry and Photobiology B: Biology* **2002**, *66* (3), 201–206.

(85) Abbas, M.; D'Amico, F.; Morresi, L.; Pinto, N.; Ficcadenti, M.; Natali, R.; Ottaviano, L.; Passacantando, M.; Cuccioloni, M.; Angeletti, M.; Gunnella, R. Structural, Electrical, Electronic and Optical Properties of Melanin Films. *Eur. Phys. J. E* **2009**, *28* (3), 285–291.

(86) Mostert, A. B.; Powell, B. J.; Pratt, F. L.; Hanson, G. R.; Sarna, T.; Gentle, I. R.; Meredith, P. Role of Semiconductivity and Ion Transport in the Electrical Conduction of Melanin. *Proceedings of the National Academy of Sciences* **2012**, *109* (23), 8943–8947.

(87) Bernardus Mostert, A.; Powell, B. J.; Gentle, I. R.; Meredith, P. On the Origin of Electrical Conductivity in the Bio-Electronic Material Melanin. *Applied Physics Letters* **2012**, *100* (9), 093701.

(88) Motovilov, K. A.; Grinenko, V.; Savinov, M.; Gagkaeva, Z. V.; Kadyrov, L. S.; Pronin, A. A.; Bedran, Z. V.; Zhukova, E. S.; Mostert, A. B.; Gorshunov, B. P. Redox Chemistry in the Pigment Eumelanin as a Function of Temperature Using Broadband Dielectric Spectroscopy. *RSC Adv.* **2019**, *9* (7), 3857–3867.

(89) Mostert, A. B.; Rienecker, S. B.; Noble, C.; Hanson, G. R.; Meredith, P. The Photoreactive Free Radical in Eumelanin. *Science Advances* **2018**, *4* (3), eaaq1293.

(90) Wünsche, J.; Deng, Y.; Kumar, P.; Di Mauro, E.; Josberger, E.; Sayago, J.; Pezzella, A.; Soavi, F.; Cicoira, F.; Rolandi, M.; Santato, C. Protonic and Electronic Transport in Hydrated Thin Films of the Pigment Eumelanin. *Chem. Mater.* **2015**, *27* (2), 436–442.

(91) Sheliakina, M.; Mostert, A. B.; Meredith, P. Decoupling Ionic and Electronic Currents in Melanin. *Advanced Functional Materials* **2018**, *28* (46), 1805514.

Chapter 3: A study on glycosylated eumelanin as multivalent galectin inhibitor

3.1 Introduction

Carbohydrates are the most abundant biopolymers in nature and have long been recognized for their structural and metabolic roles in biological systems (i.e. cellulose, chitin, and glycogen). However, they have historically been overshadowed by proteins and oligonucleotides, which are more widely studied and the understanding of their role as bio-informative molecules has only emerged in recent years.[1,2] Advancements in glycochemistry and glycobiology have renewed interest in oligosaccharides and glycoconjugates.[3] The latter consist in carbohydrates mostly found on cell surfaces linked to other biomolecules like peptides, proteins or lipids.[1,4] Glycoconjugates are crucial in many biological processes and involve glycoproteins, peptidoglycans, and glycolipids. Glycoconjugates are also key components of important drugs promoting cellular uptake and solubility in physiological media including glycosylates.[5,6] While oligonucleotides and oligopeptides can be synthesized by standardized solid-phase methods,[7] oligo/polysaccharides still require specialized synthetic strategies, which limits their production to labs with expertise in carbohydrate chemistry. On the other hand, isolating glycoconjugates from natural sources is a time-consuming and often inefficient process that yields small quantities of material with low purity, hindering their use in advanced biochemical studies.

This chapter will be focused on a poorly studied class of glycoconjugates, namely glycosylated eumelanins. Their preparation entails the initial synthesis of a suitably protected monomer, a 3-thioglycosylated-5,6-diacetoxyindoles, bearing an acetyl protection also in the saccharide moiety. To date application of these

catecholindol-sugar conjugates was reported just once, as precursors for a new model of soluble eumelanins which proved useful to disentangle some chemical and structural features of eumelanin.[8]

In this project it is demonstrated that these glycoconjugates can give birth to a new class of inhibitors for galectins, a family of carbohydrate-binding proteins correlated to various human diseases. Before the discussion, I will briefly cover the complex reactivity of carbohydrates and introduce the biological context of galectins.

3.1.1 Reactivity of Carbohydrates

Carbohydrates are complex molecules that can form both linear and branched polymers. Their monomer units are linked by either alpha or beta glycosidic bonds, and each monosaccharide can exist in two distinct forms (pyranose and furanose). Traditional synthetic techniques for carbohydrates involve numerous protections and deprotection steps and require precise stereochemical control in each glycosylation reaction to ensure the desired outcome. A critical step in the synthesis of oligosaccharides and several glycoconjugates is the glycosylation reaction.

The most important reaction in carbohydrate chemistry is the glycosidation reaction (Scheme 3.1.1), a nucleophilic substitution process committing an electrophilic glycosyl donor and a nucleophilic glycosyl acceptor. The process is nearly always triggered by a promoter, most commonly a Lewis or protic acid, capable of inducing the donor activation by the heterolytic expulsion of a leaving group from the anomeric position.

Scheme 3.1: Glycosylation reaction.

The glycosyl acceptor is typically a sugar bearing a free hydroxyl group in the position which has to be committed in the coupling, the reaction resulting in the formation of a new bond, known as the glycosidic bond.

Owing to the presence of numerous alcohol functionalities in the acceptor residue as well as the presence of a stereocentre in the anomeric centre of glycoside bonds, glycosidation reactions must be region- and stereoselective processes at once.

In nature, these requirements are met by enzymes like glycosyltransferases, which couple a donor activated at the anomeric position with a diphosphate nucleoside leaving group with a well-defined alcohol functionality of a sugar acceptor in a deprotected polyol form.

In this respect, a successful synthetic strategy should ensure the thermal stability of the products, high yields, and excellent stereo- and regioselectivity.

Effective promoters and carefully selected protecting groups (PGs) are essential for the successful synthesis of oligosaccharides. In fact, regioselectivity in glycosylation reactions can be controlled through protection strategies and represent an upstanding way to differentiate functional groups with similar reactivity. Even in the synthesis of a simple disaccharide, it is necessary to distinguish between the donor anomeric position and the acceptor hydroxy group, which acts as the nucleophile. Furthermore, hydroxy (and amino) groups that do not participate in the reaction must be protected to prevent competition with the nucleophile.

Additionally, PGs should be stable and easily removed without affecting the structure of the intermediates designed in the synthetic project. Commonly used protecting groups in organic glycochemistry, such as acetyl, benzoyl, benzyl, and benzylidene or isopropylidene acetals (shown in Table 3.1 and 3.2), provide both stability and ease of manipulation.

COMMON PGs FOR HYDROXY GROUPS		
Acetyl (Esther)		Ac
Chloroacetyl (Esther)	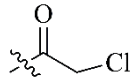	ClAc
Benzoyl (esther)	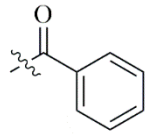	Bz
Methoxycarbonyl (carbonate)	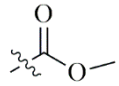	
Trimethylsilyl (silyl ether)	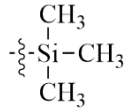	TMS
Trityl (ether)	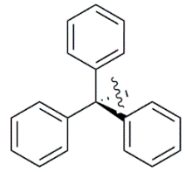	Tr
Benzyl (ether)	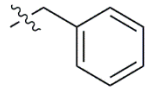	Bn
Benzylidene	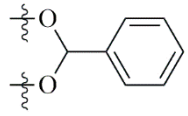	Bzd
Isopropylidene	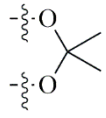	

Table 3.1: Common Protective Groups (PGs) for hydroxy groups used in glycochemistry.

COMMON PGs FOR AMINO GROUPS		
Acetyl (Esther)		Ac
Chloroacetyl (Esther)	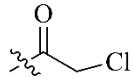	ClAc
Benzoyl (esther)	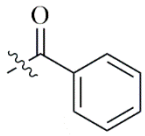	Bz

Table 3.2: Common Protective Groups for amino groups used in glycochemistry.

PGs are also crucial for directing the stereochemistry of a glycosidation reaction. For instance, 1,2-*trans* glycosides can be directly synthesized taking advantage of a reliable mechanism based on a vicinal participation effect. As a matter of fact, when acyl groups are placed at the *O*-2 position of the donor, they can direct the reaction path to form 1,2-*trans* glycosidic bonds stereoselectively (scheme 3.2), while non-interacting groups, such as in ether-based protections, commonly provide a low extent of stereocontrol.

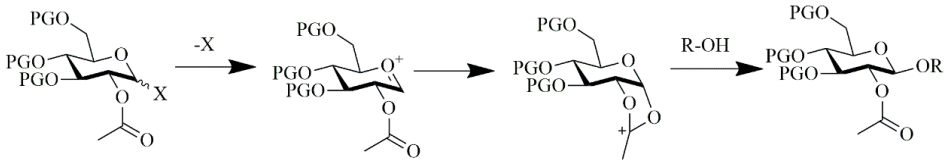

Scheme 3.2: neighbouring group participation.

Other factors affecting the stereoselectivity in glycosidations include the solvent effect, long-range effects, or the presence of bulky groups.[9–12]

In this context, the effect of the promoter must otherwise be considered. As mentioned earlier, the promoter works as an activator for the glycosyl donor in the reaction pathway. Recently, the use of an appropriate promoter led to the development of an efficient method for the highly stereoselective synthesis of α-glycosides, employing an unprecedented, solvent-free combination of promoters, including triethylphosphite, tetrabutylammonium bromide, and N,N-diisopropylethylamine to activate glycosyl chlorides in the presence of air.[13]

3.1.2 Glycomimetics and targets: the galectin Case

Carbohydrates are an intriguing group of biomolecules found in all living organisms. Beyond their vital role in energy storage, they are key components of natural products and are linked to a wide range of soluble and membrane-bound lipids and proteins.[14–16] It is now widely recognized that carbohydrates are involved in many critical biological processes, such as cellular adhesion, migration, and development, and are also involved into the progression of diseases like inflammation, infection, and cancer.[17–21]To better understand and leverage their functions, significant efforts have been made in recent decades to create carbohydrate structural analogues known as glycomimetics. These glycomimetics provide distinct advantages over natural carbohydrates, such as improved stability, availability, and selectivity. They can be designed to resist enzymatic degradation and metabolic processes, while also binding with high affinity and specificity to targeted proteins, thereby minimizing unintended interactions.[22,23]

Galectins are a family of soluble proteins that bind β-D-galactosides, characterized by a conserved carbohydrate recognition domain (CRD).[15] These proteins are found in a wide variety of animal species and in many cell types, including epithelial, endothelial, immune cells, and fibroblasts.[16,17,24] Galectins are categorized into three groups based on their structure: proto-galectins (with one CRD), tandem repeat galectins (with two CRDs connected by a linker peptide), and chimeric galectins (like galectin 3, which has a canonical domain and a long tail).[18] Once synthesized in the cytoplasm, galectins rapidly move to the extracellular space6, where they interact with a broad array of glycans. The attachment of galectins to carbohydrates bound to the extracellular proteins and lipids and other membrane components leads to the formation of a "galectin-glycoprotein lattice".[20] The latter regulates the concentration, positioning, and accessibility of glycosylated receptors on the cell surface. Through this

mechanism, galectins influence various physiological and pathological processes, such as cell-cell interactions, adhesion, proliferation, differentiation, and angiogenesis.[21,25]They also play roles in autoimmune diseases, pulmonary fibrosis, cancer progression, and metastasis.[26,27] Additionally, galectins help control infections by facilitating the endocytosis of pathogens through continuous surveillance of the extracellular space.[28–30] In the intracellular environment, galectins bind to various substrates to regulate biological processes, with their activity mainly driven by protein–protein interactions rather than glycans, although some carbohydrates like lactose can inhibit their intracellular functions.[31]

Since galectins play a crucial role in health and disease, several efforts to develop effective galectin binders for clinical use were carried out. Natural and synthetic carbohydrates, such as lactose and N-acetyllactosamine (LacNAc), can bind to galectins and inhibit their function, demonstrating the therapeutic potential of galectin inhibition. However, these carbohydrates can be degradeted by glucosidase action, limiting their effectiveness. To overcome this issue, modifications like the addition of a sulfur bridge in beta-D-galactopyranosyl-(1-1)-thio-β-D-galactopyranoside (TDG)[22] have been explored, improving stability without sacrificing affinity for galectins. TDG derivatives, including 4-aryl-1,2,3-triazolyl (TD139),[32] now show promising results, with TD139 recently approved by the FDA for treating idiopathic pulmonary fibrosis.[33]

One of the key strategies in designing effective glycomimetics is to incorporate the concept of multivalency. In the case of protein-carbohydrate interaction, multivalent ligands are molecular entities that contain several carbohydrate moieties that can bind to multiple receptors simultaneously, leading to enhanced affinity and selectivity.[34] Valuable unleashed perspective arises in the multivalent presentation of top small molecules ligands (antagonists) on biocompatible macromolecular backbones, which could lead to super-inhibitors featuring sub-

nanomolar affinities. Neo-glyco proteins (chiefly based on serum albumins), dendrimers with 3,5-di-(2-aminoethoxy)benzoic acid-based [35] as well as calixarenes[36] have been among the first large chemical scaffolds employed as multivalent galectin ligands. A promising application of glycomimetics in lectin inhibition is in the prevention of bacterial infections. A notable example in this field was reported from Yan et al. that developed the construction of mannose-based multivalent antagonist to inhibit FimH, a virulence factor of *E. coli*, to prevent bacterial adhesion to cells.[37] By developing mannose-based polymeric glycomimetics, it was possible to effectively block bacterial attachment and reduce the severity of infections. Vrbat et al synthesized a library of C-3 aryl-substituted thiodigalactoside galectin inhibitors and their multivalent N-(2-hydroxypropyl)methacrylamide (HPMA)-based counterparts with two different glycomimetic contents demonstrating that the multivalent presentation of such inhibitors on a suitable biocompatible carrier can enhance the overall affinity toGal-3 and favourably modify the interaction with Gal-3-overexpressing cells.[38]

3.1.3 3-thioglycosylated eumelanins

During my thesis work, I had the opportunity to work in laboratories where several synthetic methods were elaborated to obtain 3-thiogalactosyl-5,6-diacetoxyindole **3.3** eumelanin precursor, the first eumelanin glycoconjugate**.**[8] The synthesis of this glycoconjugate involves the exploit of a peculiar thioglycosylating agent **3.1**, bearing a S-SePh bond.[39] The coupling reaction between the glycosyl donor **3.1** and the eumelanin monomer synthetic step involved process was carried out by adding N-bromosuccinimide in the presence of the thioglycosylating agent, selenophenyl thioglycoside, and O-protected DHI, 5,6-diacetoxyindole **3.1** (DAI) (Scheme 3.3).

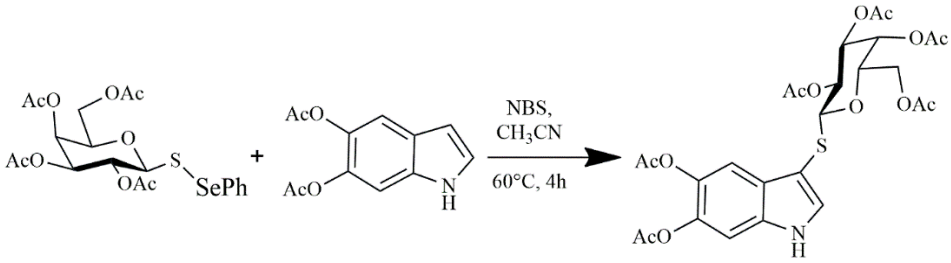

3.1 **3.2** **3.3**

Scheme 3.3: Synthesis of the 3-thiogalactosyl-5,6-diacetoxyindole conjugate.

To validate the water-soluble eumelanin model, the conjugate was subjected to oxidation using horseradish peroxidase (HRP) and hydrogen peroxide (H_2O_2). This is currently one of the most efficient oxidative systems for the isolation of oligomeric species of 5,6-dihydroxyindoles, as previously mentioned in chapter 2.

Model chemical studies have demonstrated that DHI undergoes oxidative conjugation primarily through 2,4′- and 2,7′-bonds, leading to the formation of dimers and complex mixtures of oligomers via different mechanisms. The isolation of the 2-4' and 2-7' dimers (**3.4** and **3.5**, figure 3.1) of the 3-thiogalactose-5,6-diacetoxyindole conjugate showed that the oxidative behaviour exhibited by the conjugate is very similar to the DHI precursor.

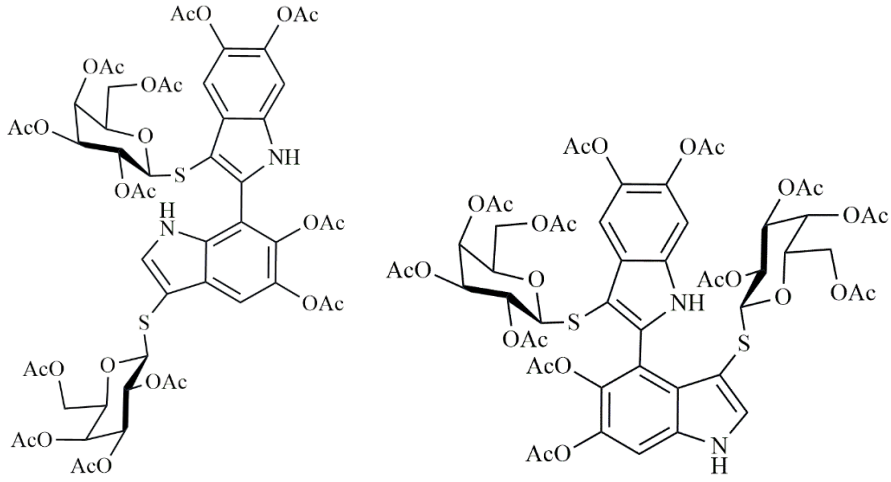

3.4 **3.5**

Figure 3.1: Structures of the isolated dimers 2-7’ (left) and 2-4’ (right) from the oxidation of **3.3** after reduction and acetylation steps.

Thus, the thioglycoside functionalization does not significantly alter the reactivity of the conjugate but, it does affect the solubility in aqueous systems.

By consequence, the oligomer is water-soluble and displays binding patterns akin to those found in natural eumelanin. This provided the model for investigating the typical properties of eumelanins in solution.

In particular, the 3-thioglycosylated water-soluble eumelanin models clarified some structural and optical properties of eumelanin dark polymer. Spectroscopical studies of this glycosylated model revealed that the dark colour of eumelanin polymers isn't solely due to individual chromophores but is significantly influenced by the aggregation and oxidation state of the polymer chains. Not only, it was proved that eumelanin chain consists in both reduced and oxidized structure, with a coexistence of both forms.

Subsequently, in the interest of extending this new class of compounds, a simpler and more effective method for thioglycosidation of DAI was developed, making it easier to attach different types of thioglycosides including disaccharides, deoxy sugars, and amino sugars (scheme 3.4).[40]

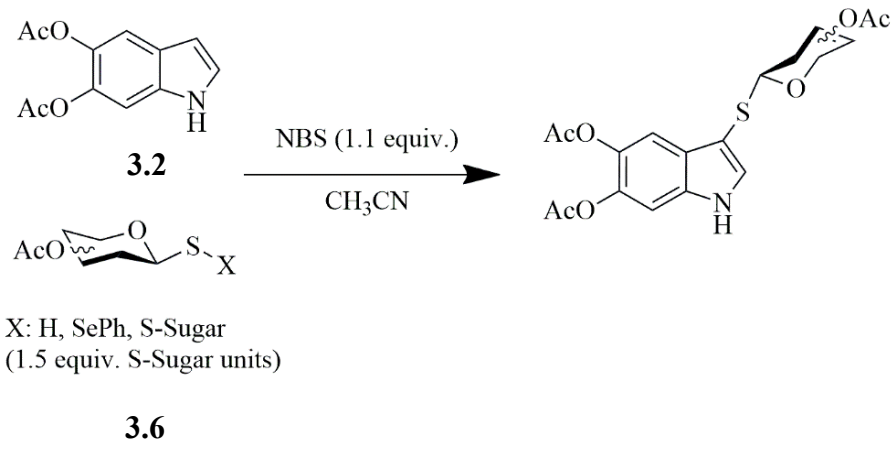

Scheme 3.4: thioglycosidation of 5,6-diacetoxyindoles.

This new approach improved the efficiency by using a thioglycosyl mixture **3.6**, eliminating the need to isolate intermediate products during the process, and results in higher yields of thioglycosides compared to previous methods.

3.1.4 Aim of the project

Considering the importance of glycoconjugate-lectin interactions in pathophysiological processes, the synthesis of new molecules capable of interacting with lectins could open up new avenues for drug discovery and disease treatment. By understanding how these molecules interact, we can develop more effective therapies and deepen our understanding of various biological processes. In this context, thioglycosylated eumelanin polymer, a biocompatible scaffold with exposed multivalent glycans (Figure 3.2), represents as a golden candidate for the development of lectin inhibitors. Indeed, exposed sugar units offer the possibility of selective cell attachment to glycoeumelanin by exploiting possible interactions between saccharide units and lectins. In this study, we take advantage of the oxidative polymerization process of DHI and thioglycosylated eumelanin precursors to create both a multivalent ligand and its structural framework simultaneously. This allows to achieve the buildup of a multivalent ligand and its structural motif via the nascent eumelanin backbone. The goal is to ultimately test how this ligand interacts with biological targets.

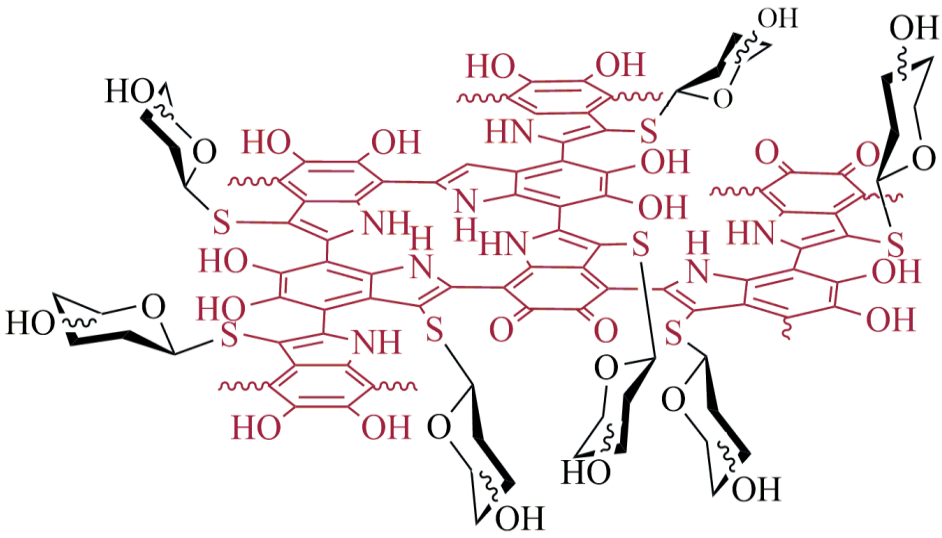

Figure 3.2: cartoon of putative thioglycosylated eumelanin polymer.

In summary this project, developed in collaboration with Prof. Iadonisi from University of Naples and Dr. Pedone and co-workers from CNR of Naples, involves the following key steps:

1. **Ligand Design**: Starting from the vast library of 3-thioglycosylated-5,6-diacetoxyindoles, I aimed to design, synthesize, and characterize novel 5,6-dihydroxyindole glycoderivatives to create a variety of galectin ligands, both derivatized and underivatized. Synthetic methodology improvements represent also a key step to develop an easier methodology to scale-up;

2. **Polymer Preparation and structural characterization**: Synthesis of polymers via oxidative coupling of the dihydroxyindole glycoderivatives. This step includes choosing suitable biocompatible reaction conditions, performing chemical and physical characterization, and evaluating the

biocompatibility, bioactivity, stability, and degradation products of the polymers;

3. **Binding Assays**: Testing the interaction of the ligands with galectin carbohydrate recognition domains (CRD).

3.2 Results and discussion

3.2.1 Deacetylation of LacSDAI

In the perspective of better understanding how to control the development of glycomelanin and how the monomer and the multivalent polymer interact with their target, we focused our experiments on the 3-thiolactose derivative LacSDAI **3.7** (see scheme 3.5). This choice was motivated by the fact that *β*-lactosides are the natural ligand for galectins.

For this reason, we investigated the possibility of *O*-deacetylating the monomer **3.7** to obtain the corresponding deprotected monomer **3.8** through Zemplen *O*-deacetylation conditions, also reported for the isolation of dimeric products in Gal-S-DHI (Scheme 3.5).[8]

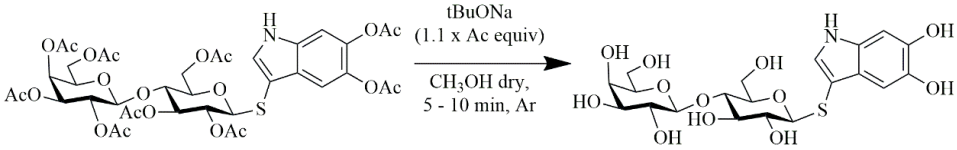

3.7
LacSDAI

3.8
LacSDHI

Scheme 3.5: Zemplen *O*-deacetylation for 3-thioglycoside monomers.

This procedure allows to access to a series of deprotected monomers that exposed to opportune conditions, give rise to multivalent polymers, derived from the one-pot Zemplen *O*-deacetylation and in situ oxidation of 3-thioglycosylated eumelanin monomers.

After deacetylation, this experiment enables the polymer synthesis to take place in a single reaction system (one-pot), with an appropriate biocompatible buffer

and pH adjustments made on-site. Later, lyophilization can be employed to lower the levels of volatile salts. This time-consuming step is useful for eliminating salts that may affect the monitoring of the oxidation reaction conditions.

To investigate the structure of LacSDHI from the deacetylated monomeric LacSDAI precursor, we conducted a deeper analysis using NMR spectroscopy. The lyophilized sample, previously deprotected and brought to pH 7.4, was dissolved in deoxygenated D_2O. NMR spectra confirmed complete deacetylation of lactose (Figure 3.3).

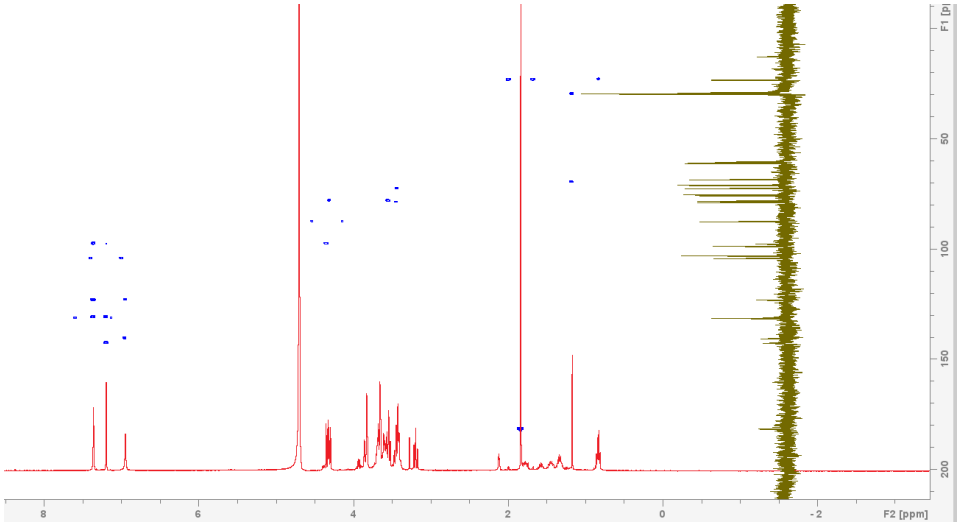

Figure 3.3: HMBC NMR spectrum of *O*-deacetylated 3-thiolactosydic-5,6-diacetoxyindole.

3.2.2 Polymeric LacSDHI synthesis

For the synthesis of polymeric LacSDHI-p **3.9** we performed a multi-step one-pot deprotection and oxidation reaction. We first performed the in situ Zemplen de-O-acetylation and then performed a biocompatible oxidation according to scheme 3.6.

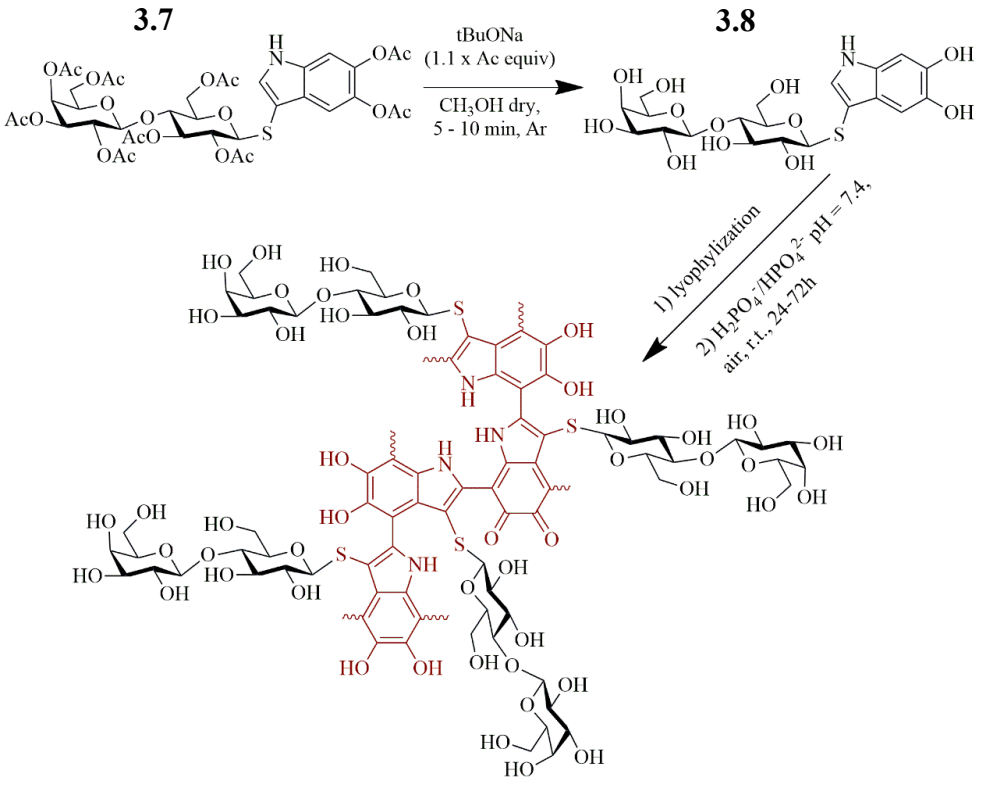

Scheme 3.6: Synthesis of LacSDHI polymer LacSDHI-p. The eumelanin backbone is shown in red.

As mentioned earlier, the Zemplen system allows for the *in-situ* addition of an appropriate buffer and pH adjustment. Later, freeze-drying can be used to reduce the content of volatile salts.

The investigation of LacSDHI-p polymer formation was conducted dissolving the lyophilized sample (to obtain it in 20 mM Na_3PO4, 150 mM NaCl pH 7.4), filtering with a 0.1 µm filter and exposing to air at r.t. Firstly, the process was followed by observing the progressive darkening of LacSDHI solution (Figure 3.4).

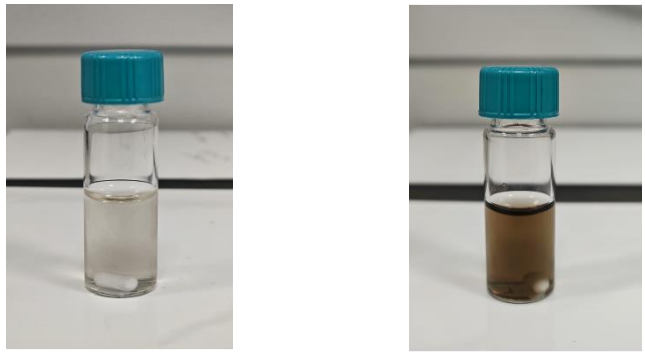

Figure 3.4: 5 mM solution of LacSDHI after 0h (left) and 48 h (right).

3.2.3 UV-Vis spectroscopy

UV-Vis spectroscopy experiments were carried out for two main purposes: first, to accurately measure the concentration of the monomeric LacSDHI solution right after it was dissolved, and second, to monitor the polymerization process. The concentration was determined using the Lambert-Beer law, based on the measured absorbance at a wavelength of 298 nm where the calculated molar absorption coefficient was $\varepsilon = 6300\ cm^{-1}\ M^{-1}$. The monomeric LacSDHI exhibited a distinct absorbance peak at $\lambda = 298$ nm, along with a shoulder at $\lambda = 268$ nm.

After determining the correct concentration, the oxidation experiment was carried out. Firstly, the solution was diluted with the same phosphate buffer at pH 7.4, reaching a final concentration of 4 mM LacSDHI. The sample was then exposed to continuous oxidation by maintaining contact with air for up to 72 hours at 25°C. As aforementioned, the DHI polymerization reaction is highly dependent from a set of boundary conditions, such as the concentration of DHI sample itself, the pH, the temperature and the concentration of the oxidizing agent. This data set was established to be as the standard experimental procedure that guaranteed a high degree of reproducibility for all the oxidation experiments of LacSDHI. From this point onwards, all the discussed experiments were conducted under these established conditions.

UV-Vis spectra of the LacSDHI samples were recorded at different times (Figure 3.5) after the correct dilution to 0.1mM. As polymerization continues, the main peak gradually red-shifted to a longer wavelength, and the little peak at $\lambda = 268$ nm, typical of not oxidized DHI monomer, disappears. After 24 hours, when polymerization the polymerization was completed showing a new peak appears at $\lambda = 320$ nm and a UV-Vis profile that remained unchanged for the next 24 h. This unique spectroscopic pattern allowed for real-time tracking of the polymerization

reaction, helping to standardize the preparation protocol and precisely determine the sample concentration.

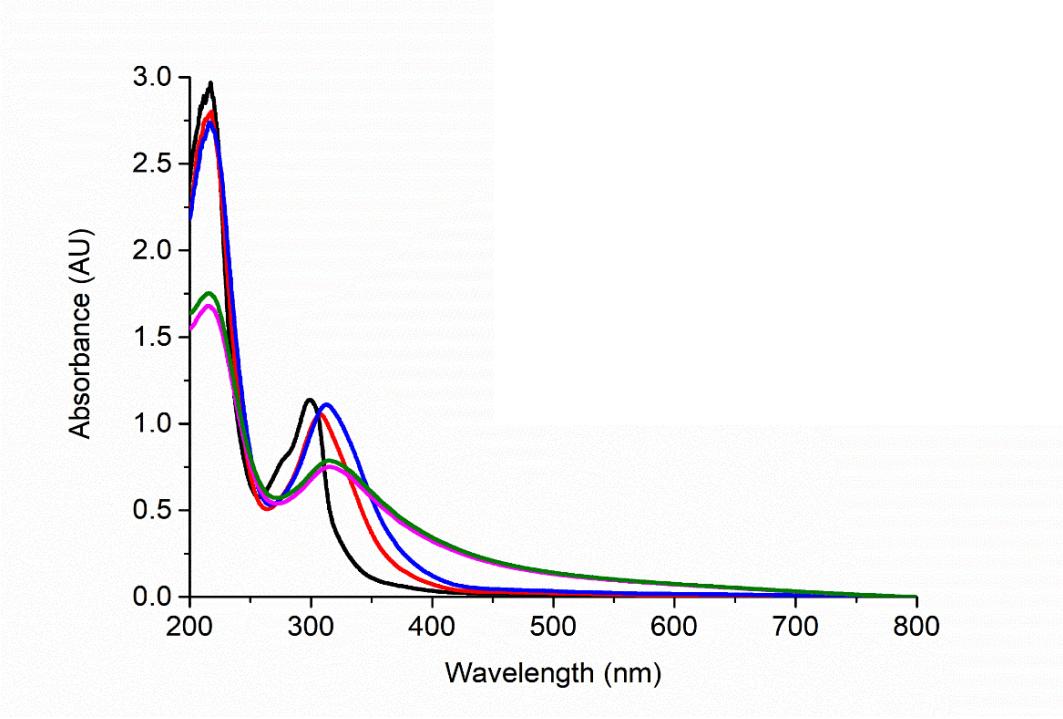

Figure 3.5: UV-Vis spectra of 0.1 mmol/L LacSDHI after 1 min (black line), 1 h (red line), 2h (blue line), 24 h (purple line), 48 h (green line).

3.2.4 DLS measurements

Dynamic light scattering (DLS) is a technique that is used to determine the size distribution profile of polymers in solution. In this case, DLS was used by Pirone and co-workers to follow the growing of the LacSDHI polymer, measuring the diameters at the same critical times used for UV-vis spectroscopic analysis. The following table (Table 3.3) summarizes the information about DLS measurements.

Time (h)	Hydrodynamic diameter (nm)	Deviation (nm)
0	1.17	0.2
8	2.48	0.4
24	5.28	0.9
72	5.28	1.1

Table 3.3

The collected data (Table 3.3 and figure 3.6) showed that after solubilizing the lyophilized sample (t = 0 h), LacSDHI presents a single peak of 1.16 nm of diameter likely diameter for a monomer/dimer. When the UV spectrum of the LacSDHI polymer was first detected (t = 24 h) the corresponding diameter was measured to be 5.2 nm, value that remains stable for the next 48 h (from t = 24 h to t = 72 h). This diameter is the biggest measured in these specific conditions (4 mM, 25 °C, followed for 72 h after solubilization).

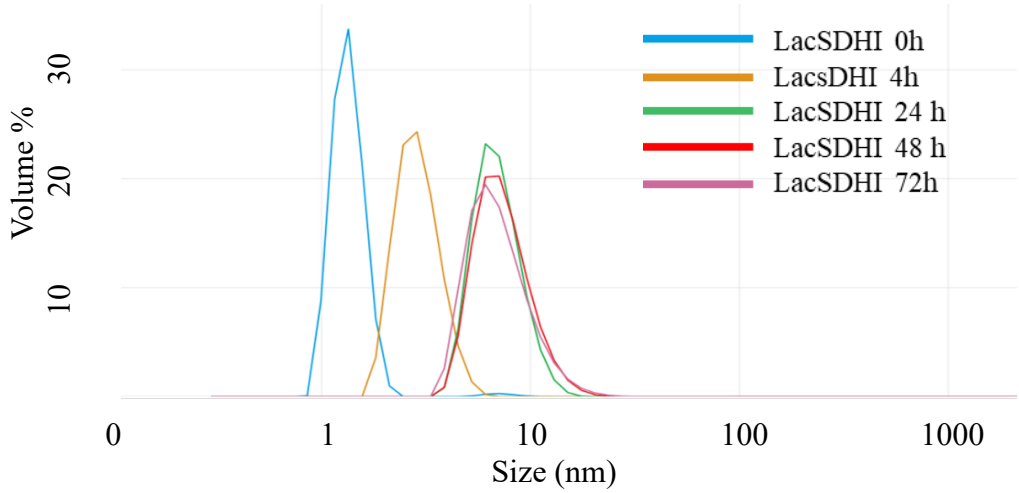

Figure 3.6: DLS experiments of LacSDHI. LacSDHI diameter measurement at t=0 h (blue peak), t=4 h (yellow peak), t=24 h (green peak), t=48 h (red peak) and t=72 h (pink peak). The diameter values ± standard deviation. are reported in the table 3.3.

3.2.5 NMR structural study of LacSDHI monomer and polymer

To better understand LacSDHI polymeric structure, we conducted a deeper analysis using NMR spectroscopy. The lyophilized sample, previously deprotected and brought to pH 7.4, was dissolved in deoxygenated D_2O. NMR spectra confirmed complete deacetylation of lactose. Then, the sample was exposed to air to start the polymerization reaction. UV-Vis spectroscopy was used to follow the formation of a species exhibiting a red-shifted absorption band. After 48h, DLS analysis indicated the formation of a species of interest with a diameter of 5.2 nm.

At this point, a comparison between initial and 48h NMR spectra highlighted significant changes, particularly in the aromatic region with the total disappearance of signals (figure 3.7 yellow and green line, respectively, for intermediate times see materials and methods figure 3.11). Diffusion-Ordered Spectroscopy (DOSY) is a powerful NMR technique that correlates each nuclear magnetic resonance signal to the rate of diffusion of the detected atom, returning a 2D graph. Typically, it is used to distinguish the signals of different molecules within a mixture basing on their diffusion coefficients.

DOSY NMR experiments were employed in this case to investigate the molecular weight on the same sample at time 0 and time 48h confirmed the growth of the species after oxidation (figure 3.7 blue and red line, respectively).

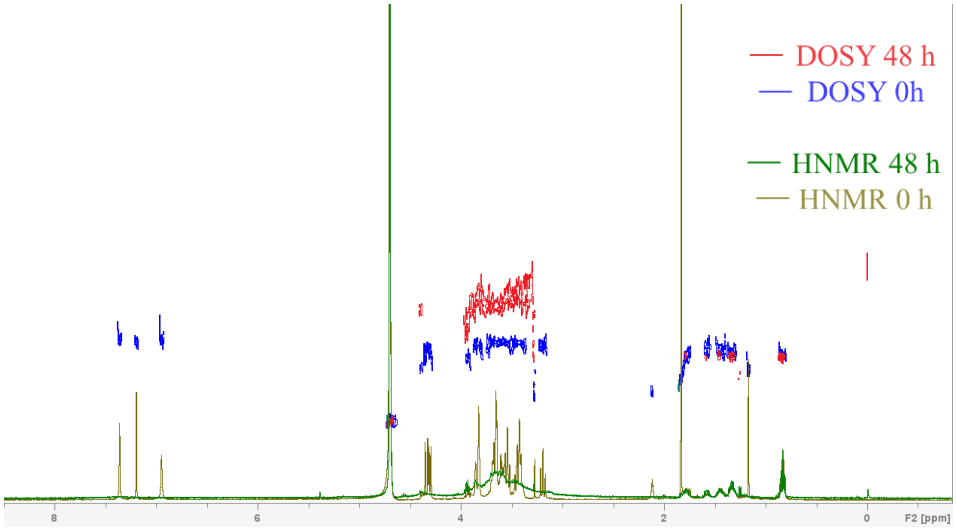

Figure 3.7: HNMR and DOSY NMR superimposed spectra of *O*-deacetylated 3-thiolactosydic-5,6-diacetoxyindole at 0 h (yellow and blue lines) and 48h (red and green lines).

An important observation was the presence of two new raising peaks in the NMR spectra at 5.4 and 4.5 ppm. We suppose that this phenomenon might be related to a partial release of lactose, that starts approximately after one day after the exposition to aerobic environment. This species persisted at a maximum of 10% relative to initial signals after 2 days (doublets at 5.4 and 4.5 ppm, see also materials and methods figure 3.12. We think that lactose release could be inducted to the quinone formation according to a mechanism similar to scheme 3.7.

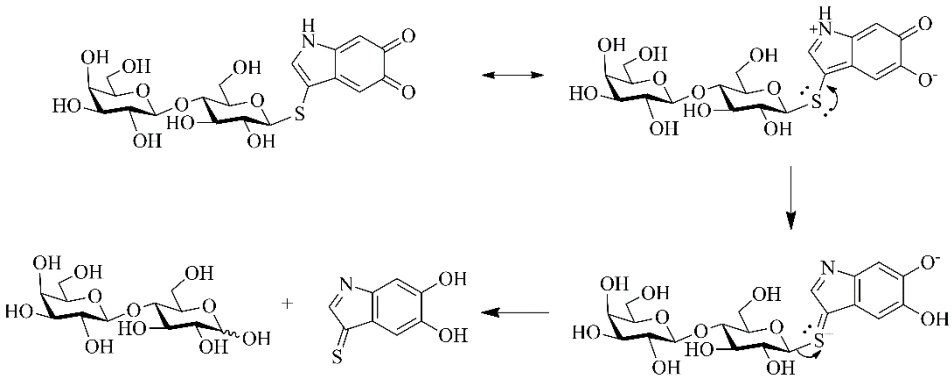

Scheme 3.7: mechanism of lactose release from LacSDAI.

To verify this hypothesis, we stored the monomer in a deoxygenated argon atmosphere for two weeks and studied the evolution of the NMR spectra at different times (figure 3.8).

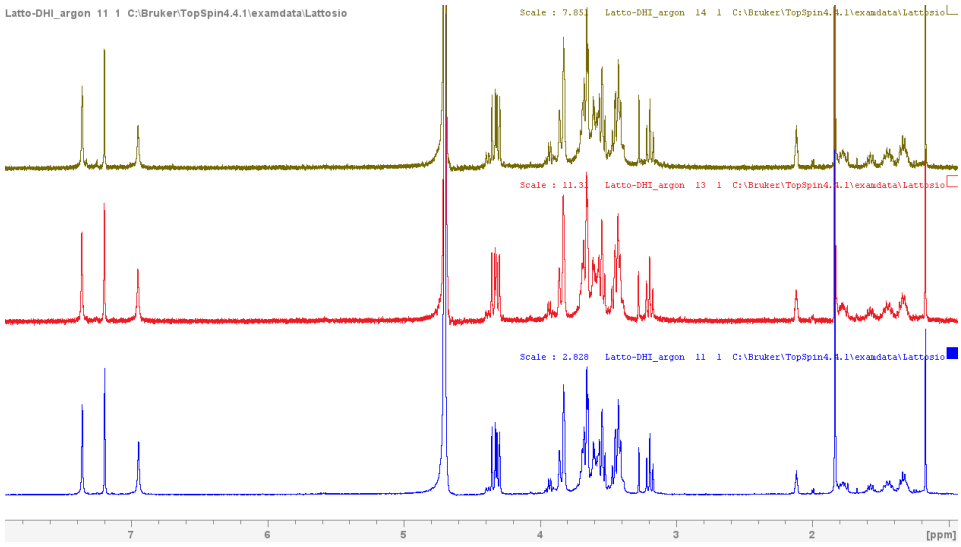

Figure 3.8: NMR spectra of LacSDHI in agon after 0 h (blue line), 1 week (red line) and 2 weeks (yellow line).

The absence of lactose and conjugated peaks under these conditions supports the idea that lactose release is induced by the formation of quinone species during polymerization.

3.2.6 Binding affinity analysis of LacSDHI monomer to Gal-3^{CRD}

Pirone and coworkers (CNR institute of Naples) evaluate the interaction of monomeric LacSDHI and Gal-3^{CRD} by Isothermal Titration Calorimetry experiments, the gold-standard method to determine the affinity of monovalent glycans to lectins. Gal-3^{CRD} expression and purification will be not treated here. The experiments LacSDHI and Lactose vs Gal-3^{CRD} were performed fixing 270 µL of 20 µmol/L protein in the chamber and titrating it with 39.4 µL of 400 µmol/L monomeric LacSDHI and 750 µM of Lactose, used as reference (Figure 3.9 A/B). The K_D value measured (Table 3.4) showed improved affinity of LacSDHI compared to the Lactose alone. Two different experimental controls were run: the first technical control was made injecting a total volume of 39.4 µL of 400 µM LacSDHI in the chamber containing just buffer (Figure 3.9 D); the second experimental control was made by injecting the same volume of 500 µM DHI in the chamber containing 270 µL of 20 µM Gal-3^{CRD} (Figure 3.9 C), in order to assess which part of LacSDHI molecule is directly involved in the interaction with Gal-3^{CRD}. The latter experiment showed a no-binding, allowing DHI to be excluded as a factor in binding with Gal-3. In this binding, enthalpy plays a dominant role in promoting the interaction by stabilizing the global system (Table 6); however, the negative $-T\Delta S$ contribution suggests an entropy loss, probably due to the enhancement of rigidity during the formation of the complex. Altogether, it may be assumed that the binding of LacSDHI is specific and all borne by the sugar moiety.

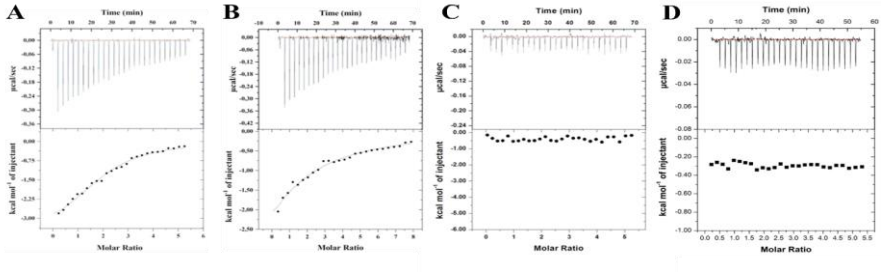

Figure 3.9: ITC binding studies on Gal-3^{CRD}. (A) Titration with LacSDHI, (B) Lactose (used as reference), (C) DHI and in (D) the titration of buffer (negative control) is shown. The top panels of the graphs correspond to the injections while the bottom panels correspond to the integrations of the peaks according to the molar ratio of the tested molecules.

Ligand	**K_D (µM)**	**ΔG (Kcal/mol)**	**ΔH (Kcal/mol)**	**−TΔS (Kcal/mol)**	***n***
LacSDHI	19.6 ± 3	−6.4	−5.2 ± 0.6	−3.6 ± 0.4	0.97 ± 0.2
Lactose	40.8 ± 5	−6.1	−2.4 ± 0.9	−3.7 ± 0.3	1.03 ± 0.2

Table 3.4: Thermodynamic parameters from ITC binding experiments between Gal-3^{CRD} and LacSDHI/Lactose.

3.2.7 BLI binding analysis

For the evaluation of the interaction of the 5.2 nm polymeric LacSDHI, Bio-layer interferometry (BLI) was performed by Pirone and co-workers (CNR of Naples), a technique suitable to estimate the interaction between the target and multivalent ligands.

LacSDHI-polymer was tested via BLI to assess the effect of polymerization on the ability to binding Gal-3^{CRD}. The experimental binding curves confirm the dose-response binding and by fitting them with a binding model 1:1 it was possible to obtain a solid steady state analysis (Figure 3.10) that provided a K_D value of 830 nmol/L (Table 3.5). The polymerization process on LacSDHI results in the formation of polymer, exhibiting a 24-fold decrease in the K_D value compared to its monomeric form. Furthermore, dissociation curves showed a very slow dissociation of polymeric LacSDHI from galectin ligand, paving the way for speculation on the potential link between the acquired multivalency and the polymeric LacSDHI enhanced avidity for the galectin, considering the strong increase in affinity between the monomeric and the polymeric state of LacSDHI.

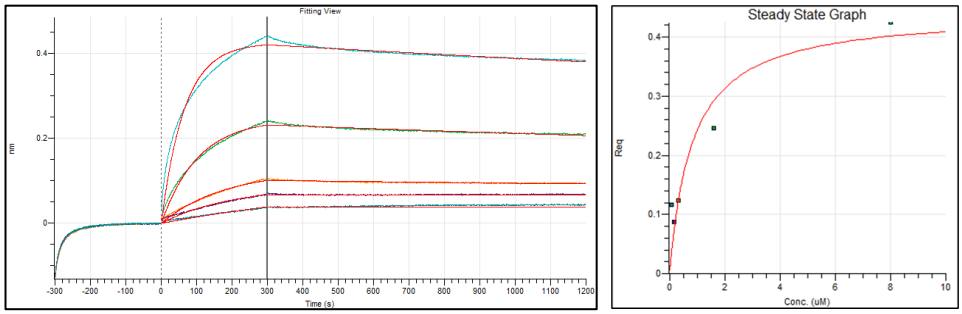

Figure 3.10: BLI experiment. Left) the experimental curves of Gal-3^{CRD} loading, LacSDHI polymer association and complex dissociation; in association and dissociation panels are shown in red the fitting model curve, used to interpolate data. Right) the steady state graph provides data to extract the dose-response binding curve.

Steady State Results	
	Values
χ^2	0.0089
R^2	0.88
R_{max}	0.44
R_{max} error	± 0.06
K_D (M)	8.3 E-07
K_D error	± 3 E-07

Table 3.5: Summary of binding parameters and statistical analysis from Steady State results.

3.2.8 Development of new methodologies for the synthesis of LacSDAI

LacSDHI polymer, with its multiple sugar exposures, has gained significant attention. To fully exploit its potential, we aimed to establish more efficient and scalable methods for synthesizing thioglycosylated indoles. Previous efforts to directly glycosylate 5,6-diacetoxyindole at the 3-position using various electrophilic agents were unsuccessful.

While the use of selenophenyl thioglycosides **3.1** and thioglycosidic pools **3.6** with NBS provided a workable solution, the multi-step nature and time-consuming purifications, especially for compounds like LacSDAI, hampered large-scale synthesis. In fact, the similar retention factors of LacSDHI and its disulfide byproduct further complicated its purification, requiring extensive chromatography.

An expedient solution to this problem came, however, utilizing a tributyl phosphine reduction protocol followed by in-situ acetylation (Scheme 3.8).

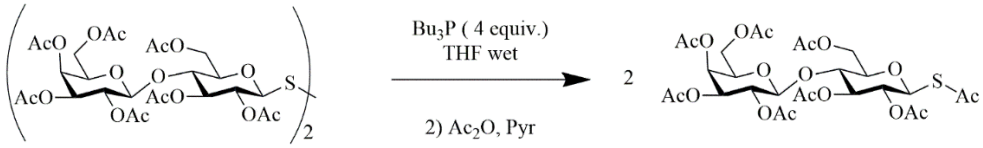

3.10 **LacSAc 3.11**

Scheme 3.8: tributyl phosphine reduction of diglycosyl disulfides.

Treating the crude product with this methodology effectively converted the disulfide to the corresponding thioacetate **3.11**, simplifying the purification. However, the additional synthetic steps and chromatography still hindered large-

scale synthesis. To satisfy the need for a scalable route to study LacSDAI for galectin inhibition studies, we attempted to develop a new synthetic protocol.

In this context, inspired by some clues from the success of previous synthetic protocols that utilized diglycosyl disulfides in the same reaction medium with selenophenyl thioglycosides and their corresponding thiols, we explored a new approach to generate soft thioglycosidation agents directly from these disulfides. These derivatives could be prepared by a straightforward sequence of three fast reactions and a single chromatographic purification step. The first results were obtained by reacting directly easily obtainable disulfides in presence of NBS, TBAB and diphenyl diselenide.[41] Whereas direct coupling of 5,6-diacetoxyindole with NBS alone, NBS and TBAB was unproductive, activation with a catalytic amount of diphenyl diselenide resulted in the neat generation of the desired conjugate number in satisfactory yields (scheme 3.9).

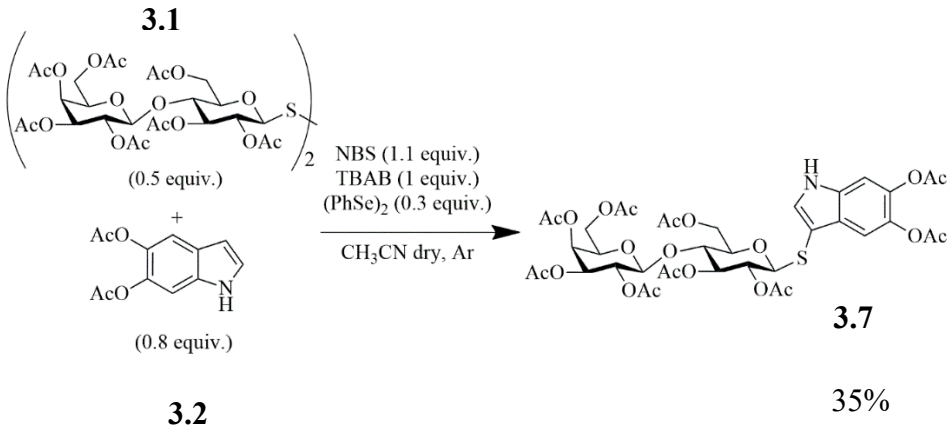

Scheme 3.8: synthesis of LacSDAI from diglycosidic disulfides.

This approach allowed us to get the desired product **3.7** with a 35% yield, thanks to careful optimization of both the stoichiometry and the solvent. When it comes to large-scale processes, this method is much more efficient, as the synthesis of

disulfides requires much faster chromatography and generally needs far fewer equivalents of diphenyl diselenide, which is a highly expensive reagent, as well as a reduced number of saccharide units. Although the reaction is still under mechanistic study, it is possible that the coupling reaction mechanism is activated by the presence of Br· radicals, since study of the reaction in absence of light results in minimal reaction yield.

3.3 Materials and methods

General information: All commercially available reagents were used as received and all the solvents were of analytical grade. Synthesis of 5,6-dihydroxiindole, 5,6-diacetoxyindole, were performed according to the already known protocols.[42] The reactions were monitored using TLC plates, which were visualized under UV-visible light. After visualization, the plates were immersed in a solution of ethanol/sulfuric acid (conc.) 95:5 and then heated to 230°C. For indolic compounds, after UV-visible light visualization, the plates were exposed to ammonia vapours before proceeding with carbonization (AISSP). The products obtained were separated using flash chromatography, with Merck Kieselgel 60 (63-200 mesh) silica as the stationary phase, and the purified products were characterized using NMR spectroscopy. The ^{1}H and ^{13}C NMR spectra were recorded on a Bruker spectrometer (400 MHz). Chemical shifts in ppm were referenced to tetramethylsilane.

General procedure for the synthesis of symmetrical lactose disulfide: to a solution of lactose octaacetate (678 mg, 1 mmol), dissolved in DCM-dry (2 mL) I_2 (280 mg, 1.1 mmol), and Et3SiH (177 µL, 1.1 mmol) were added subsequently (caution: exothermic reaction). The reaction mixture was refluxed until the starting material was fully consumed (15 minutes, monitored by TLC). The mixture was then diluted with DCM, and the organic phase was washed with aqueous sodium carbonate containing sodium thiosulfate, which was added gradually until the residual iodine in the organic phase was completely consumed. The organic phase was washed with water, dried, and concentrated. Thiourea (114 mg, 1.5 mmol) was then added to the crude residue, which was suspended in 2 mL

of acetonitrile and heated to 60°C. After 15–30 minutes, TLC showed complete consumption of the glycosyl iodide and the formation of a polar product. The mixture was cooled to room temperature, and phenyl diselenide (9.4 mg, 0.03 mmol) and TEA (0.55 mL, 4 mmol) were added sequentially. After 10 minutes, the reaction vessel was placed in an oil bath at 50°C for 1 hour. The mixture was then concentrated under vacuum, the residue dissolved in DCM, and the organic phase washed with water. The aqueous phase was re-extracted with DCM, and the combined organic phases were dried and concentrated. Flash chromatography on silica gel (eluent: hexane/ethyl acetate 6:4) afforded lactose disulfide as a foam (240 mg, 50% overall yield).

General procedure for the synthesis of LacSDAI: DAI (186 mg, 0.8 mmol) and lactose disulfide (650 mg, 0.5 mmol) were dissolved under an argon atmosphere in acetonitrile (7 mL), which had been deoxygenated by purging with argon for 15 minutes prior to use. To this solution, NBS (196 mg, 1.1 mmol), diphenyl diselenide (93 mg, 0.3 mmol), and TBAB (322 mg, 1 mmol) were added under argon. The mixture was then stirred under laboratory illumination at r.t.. Upon completion of the reaction, the mixture was diluted with CH_2Cl_2, and the organic phase was washed with aqueous thiosulfate. The aqueous phase was re-extracted with CH_2Cl_2, and the combined organic phases were dried and concentrated under vacuum. The resulting residue was purified by silica gel flash chromatography using a hexane/ethyl acetate mixture as the eluent.

General procedure for the synthesis of LacSAc 3.11: to a solution of lactose disulfide (650 mg, 0.5 mmol), dissolved in CH_3CN-dry (7 mL), water (20 µL) and Bu_3P (0.49 mL) were added subsequently under deoxygenated Ar atmospher. The reaction mixture was stirred until fully consumption of lactose disulfide (3 h, monitored by TLC). The mixture was then quenched diluting with acetic

anhydride (200 µL, 4 mmol) and THF dried at rotary evaporator. After this Pyridine (400 µL) was introduced. After 1h, the reaction was quenched with methanol, diluted with DCM and the organic phase was extracted with water., which was added gradually until the residual iodine in the organic phase was completely consumed. The organic phase was washed with water, dried, and concentrated. The aqueous phase was re-extracted with DCM, and the combined organic phases were dried and concentrated. Flash chromatography on silica gel (eluent: hexane/ethyl acetate) afforded the formation of lactose thioacetate as a foam (640 mg, 90% overall yield).

UV-Vis Spectroscopy: Far UV-Vis spectra of monomeric LacSDHI have been recorded using V-730 UV-vis/NIR Spectrophotometer (Jasco, Cremella, LC, Italy) in the λ range from 200 to 800 nm, at 200 nm *x* min^{-1} speed scan. The baseline correction spectrum has been recorded using empty cuvette, to remove any background noise. Blank spectrum has been recorded using only buffer and subtracted from all experimental absorbance curves. At each time, the sample has been diluted in buffer, for a final concentration of 100 µmol/L. By applying the Beer-Lamber law ($A=\varepsilon c l$, where A is the absorbance, ε is the molar absorptivity (L *x* mol^{-1} *x* cm^{-1}), c is the concentration (mol *x* L^{-1}) and l is the path length (cm)) it was accurately determined the concentration of the samples at λ_{298} nm; at this wavelength, the solution has a molar absorptivity (ε) of 6'300 L *x* mol^{-1} *x* cm^{-1}. Next, UV-Vis spectra were analysed using Spectra Manager™ Suite and SpectraGryph v. 1.2 software.

LacS-DHI-p synthetic procedure: 8.8 mg of LacSDAI ($1*10^{-5}$ mol) were dissolved in 1 mL of CH_3OH dry, previously degassed with argon for 15 minutes. Then, 9.6 mg of sodium tert-butoxide (10 eq.) were added to the solution. After 1

minute, the reaction was monitored with TLC analysis and after completion (complete disappearance of LacSDAI) the solution was diluted with buffer phosphate 10 mM, pH = 7.4, brought to pH 7.4 with HCl 1M and then lyophilized. The oxidation of LacSDHI was performed dissolving the lyophilized sample in D_2O, resulting in the formation of a solution of 4 mM LacSDHI 10 mM phosphate buffer, pH 7.4, and exposing the sample to air for 48 hours.

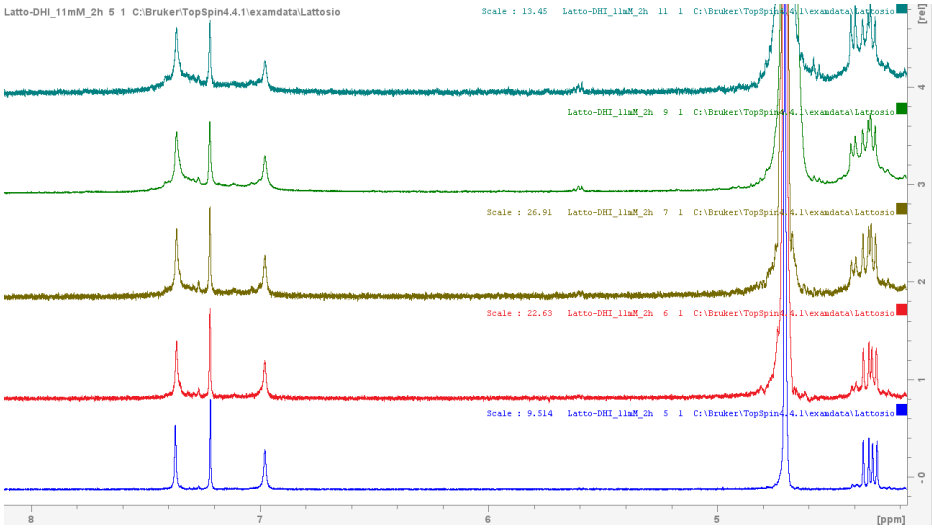

Figure 3.11: NMR spectra of LacSDHI after 0h (blue line), 8 h (red line), 16h (yellow line), 24 h (green line), 36 h (dark green line).

Procedure for LacSDHI ^{1}HNMR analysis in de-oxygenated environment: 8.8 mg of LacSDAI ($1*10^{-5}$ mol) were dissolved in 1 mL of CH_3OH dry, previously degassed with Ar for 15 minutes. Then, 9.6 mg of sodium tert-butoxide (10 eq.) were added to the solution. After 1 minute, the reaction was monitored with TLC analysis and after completion (complete disappearance of LacSDAI) the solution was diluted with buffer phosphate 10 mM, pH = 7.4, brought to pH 7.4 with HCl

1M and then lyophilized. The lyophilized sample was dissolved with de-oxygenated D_2O (previously degassed with Ar), under Ar atmosphere. The sample was transferred into NMR cuvette under Ar atmosphere and sealed. The cuvette was stored at r.t. for 2 weeks and NMR spectra were collected after 0h, 1 week and 2 weeks.

DLS Analysis: DLS analyses were performed by Pirone and co-workers on Zetasizer (Malvern Panalytical Ltd, UK). LacSDHI, dissolved in 20 mM Na3PO_4 150 mM NaCl pH 7.4 as previously described, was placed in a disposable cuvette at the concentration of 4 mM. All measurements were carried out at 25 °C. While the polymerization was followed in the same buffer without DTT over time at 25 C°. For each sample, the measurements were recorded three times with 11 sub-runs using the multimodal mode. The Z-average diameter was calculated from the correlation function using the Malvern technology software ZS Xplorer version 3.2.0.84.

ITC Experiments: the interactions between all compounds mentioned (750 μM Lactose, 500 μM LacSDHI and 500 μM DHI with Gal-1 and Gal-3^{CRD} were performed by isothermal titration calorimetry (ITC) experiments by Pirone and co-workers. The analyses were carried out on an ITC200 calorimeter (MicroCal/GE Healthcare, Boston, MA, USA) at 25 °C in 20 mM Na_3PO_4, 150 mM NaCl pH 7.5 buffer for Lactose experiments, and 20 mM $NaPO_4$, 150 mM NaCl, 1 mM DTT pH 7.5 buffer for LacSDHI and DHI experiments (galacto?) All of experiments were carried out using a fixed concentration (20 μM) of Gal-1 or Gal-3^{CRD} in chamber. A solution of 39.4 μL of the ligands was titrated in aliquots of 1.5 μL into the chamber containing 270 μL of protein. Injections were

performed every 150 s, for a total of 27 injections (0.4 µL for the first injection), under 750 rpm stirring. Control experiments were carried out by performing identical injections of ligands into the chamber containing just buffer. The binding stoichiometry, enthalpy, and equilibrium association constants were determined by fitting the corrected data to a one-set-of-site- binding model with MicroCal analysis software (GE Healthcare). The data obtained from the measurements were analyzed by peak integration using ORIGIN 7.0 software (OriginLab, Northampton, USA) and the free energy change (ΔG) and entropy contributions (TΔS) were derived from Equation : $\Delta G = \Delta H - T\Delta S = -RT \ln K_a$

BLI Analysis: BLI experiments were performed by Pirone and co-workers using the Octet R8 (8-channel instrument – Sartorius, Gottinga, Germania). AR2G biosensors were used following the manufacturer instructions. Briefly, biosensors were hydrated in KB 1X (Sartorius, Gottinga, Germany) and subsequently activated in 20 mM NaOAc, 10 mM NHS pH 4.5 solution for 300 s; after loading 10 mg/mL Gal-3^{CRD} for 600 s, the quenching step was made to avoid non-specific binding by immersing biosensors in 1 M ethanolamine pH 8.5. Then, baseline, association and dissociation steps (450 s, 300 s, 900 s, respectively) were performed using analyte suitable diluted. All the incubations were performed at 25 °C with 750 rpm of shaking. All the samples were diluted in KB 1x (Sartorius, Gottinga, Germania) in 96-well back plates (Greiner Bio-One, Stonehouse, UK). The associations were obtained using the polymeric from of LacSDHI of 5.2 nm of diameter in a range of concentrations from 8 mM - 0.08 mM. The dissociations were performed incubating the biosensors in kinetic buffer for 600 s. Every run included a reference well. All data were analysed using the Octet Analysis Studio 12.2 software and were modelled using the 1:1 global model within the Octet software.

3.4 Conclusion and perspectives

In conclusion, this work aimed to develop a new multivalent ligand for interacting with galectin, a class of carbohydrate-binding proteins exploiting the already known 3-thioglycosyl-5,6-diacetoxyindoles. Among the latter, the lactose derivative, LacSDHI, was identificated to be the suitable ligand for this application.

A large-scale synthesis of the acetylated derivative LacSDAI was performed, and the development of a biocompatible deacetylation procedure was carried out. After, the best biocompatible condition for the interaction with galectins was found and the polymer formation was characterised through UV-Vis spectroscopy, DLS and Nuclear magnetic resonance spectroscopy.

Concerning the interaction with galectins, LacSDHI and its polymer demonstrated the ability to bind galectins effectively at low concentrations, marking for the first time the pioneering use of an eumelanin precursor as a protein ligand. The presence of DHI in the polymer structure allows the exploitation of its oxidative polymerization, enabling the simultaneous formation of both the multivalent ligand and its structural motif via the nascent eumelanin backbone. This innovation holds promise for various applications, particularly in the precise control of the ligand's structure and its modifiable activity, facilitated by the redox chemistry of DHI.

Furthermore, this approach offers the potential to selectively promote oxidative polymerization in specific cellular environments, such as the reduced intracellular conditions found in tumour cells, allowing for the targeted formation of the polymer as a protein inhibitor. In the end, the combination of Gal3/LacSDHI binding and LacSDHI's oxidative polymerization could lead to the development of other thioglycosylated eumelanin-based ligands with customized selectivity, further expanding the range of possible applications in targeted therapies.

Finally, this work also aimed to develop a better synthetic strategy for the 3-thioglycosyl-eumelanin monomers. 3-thiolactosyl-5,6-diacetoxyindole can be easily synthesized within a day from symmetrically prepared lactose disulfide, with the final step involving a coupling reaction mediated by N-bromosuccinimide, tetrabutylammonium, and diphenyl diselenide. This method improves both the time efficiency (requiring one less purification step) and the cost-effectiveness (due to a reduced need for expensive reagents). Additionally, the conjugation reaction is notably accelerated under light exposure when catalysed by diphenyl diselenide.

3.5 References

(1) Varki, A. Biological Roles of Oligosaccharides: All of the Theories Are Correct. *Glycobiology* **1993**, *3* (2), 97–130.

(2) Ratner, D. M.; Adams, E. W.; Disney, M. D.; Seeberger, P. H. Tools for Glycomics: Mapping Interactions of Carbohydrates in Biological Systems. *ChemBioChem* **2004**, *5* (10), 1375–1383.

(3) Wiederschain, G. Ya. Glycobiology: Progress, Problems, and Perspectives. *Biochemistry Moscow* **2013**, *78* (7), 679–696.

(4) Broussard, A. C.; Boyce, M. Life Is Sweet: The Cell Biology of Glycoconjugates. *MBoC* **2019**, *30* (5), 525–529.

(5) Sung, Y.-S.; Kerimoglu, B.; Ooi, A.; Tomat, E. Aroylhydrazone Glycoconjugate Prochelators Exploit Glucose Transporter 1 (GLUT1) to Target Iron in Cancer Cells. *ACS Med. Chem. Lett.* **2022**, *13* (9), 1452–1458.

(6) Cimmino, G.; De Nisco, M.; Alonso, C.; Gravina, C.; Piscopo, V.; Lemos, R.; Coderch, L.; Piccolella, S.; Pacifico, S.; Pedatella, S. Novel Synthesized Seleno-Glycoconjugates as Cosmeceutical Ingredients: Antioxidant Activity and in Vitro Skin Permeation. *European Journal of Medicinal Chemistry Reports* **2024**, *12*, 100240.

(7) Kent, S. B. H. Total Chemical Synthesis of Proteins. *Chem. Soc. Rev.* **2009**, *38* (2), 338–351.

(8) Pezzella, A.; Iadonisi, A.; Valerio, S.; Panzella, L.; Napolitano, A.; Adinolfi, M.; d'Ischia, M. Disentangling Eumelanin "Black Chromophore": Visible Absorption Changes As Signatures of Oxidation State- and Aggregation-Dependent Dynamic Interactions in a Model Water-Soluble 5,6-Dihydroxyindole Polymer. *J. Am. Chem. Soc.* **2009**, *131* (42), 15270–15275.

(9) Wulff, G.; Röhle, G. Results and Problems of O-Glycoside Synthesis. *Angewandte Chemie International Edition in English* **1974**, *13* (3), 157–170.

(10) Schmidt, R. R.; Rücker, E. Stereoselective Glycosidations of Uronic Acids. *Tetrahedron Letters* **1980**, *21* (15), 1421–1424.

(11) Plante, O. J.; Palmacci, E. R.; Andrade, R. B.; Seeberger, P. H. Oligosaccharide Synthesis with Glycosyl Phosphate and Dithiophosphate Triesters as Glycosylating Agents. *J. Am. Chem. Soc.* **2001**, *123* (39), 9545–9554.

(12) Adinolfi, M.; Iadonisi, A.; Schiattarella, M. An Approach to the Highly Stereocontrolled Synthesis of α-Glycosides. Compatible Use of the Very Acid Labile Dimethoxytrityl Protecting Group with Yb(OTf)3-Promoted Glycosidation. *Tetrahedron Letters* **2003**, *44* (34), 6479–6482.

(13) Traboni, S.; Vessella, G.; Bedini, E.; Iadonisi, A. Solvent-Free, under Air Selective Synthesis of α-Glycosides Adopting Glycosyl Chlorides as Donors. *Org. Biomol. Chem.* **2020**, *18* (27), 5157–5163.

(14) Gabius, H.-J.; Siebert, H.-C.; André, S.; Jiménez-Barbero, J.; Rüdiger, H. Chemical Biology of the Sugar Code. *ChemBioChem* **2004**, *5* (6), 740–764.

(15) Laaf, D.; Bojarová, P.; Elling, L.; Křen, V. Galectin–Carbohydrate Interactions in Biomedicine and Biotechnology. *Trends in Biotechnology* **2019**, *37* (4), 402–415.

(16) Cooper, D. N. W. Galectinomics: Finding Themes in Complexity. *Biochimica et Biophysica Acta (BBA) - General Subjects* **2002**, *1572* (2), 209–231.

(17) Johannes, L.; Jacob, R.; Leffler, H. Galectins at a Glance. *Journal of Cell Science* **2018**, *131* (9), jcs208884.

(18) Ludwig, A.-K.; Michalak, M.; Xiao, Q.; Gilles, U.; Medrano, F. J.; Ma, H.; FitzGerald, F. G.; Hasley, W. D.; Melendez-Davila, A.; Liu, M.; Rahimi, K.; Kostina, N. Y.; Rodriguez-Emmenegger, C.; Möller, M.; Lindner, I.; Kaltner, H.; Cudic, M.; Reusch, D.; Kopitz, J.; Romero, A.; Oscarson, S.; Klein, M. L.; Gabius, H.-J.; Percec, V. Design–Functionality Relationships for Adhesion/Growth-Regulatory Galectins. *Proceedings of the National Academy of Sciences* **2019**, *116* (8), 2837–2842.

(19) Stegmayr, J.; Zetterberg, F.; Carlsson, M. C.; Huang, X.; Sharma, G.; Kahl-Knutson, B.; Schambye, H.; Nilsson, U. J.; Oredsson, S.; Leffler, H. Extracellular and Intracellular Small-Molecule Galectin-3 Inhibitors. *Sci Rep* **2019**, *9* (1), 2186.

(20) Sciacchitano, S.; Lavra, L.; Morgante, A.; Ulivieri, A.; Magi, F.; De Francesco, G. P.; Bellotti, C.; Salehi, L. B.; Ricci, A. Galectin-3: One Molecule for an Alphabet of Diseases, from A to Z. *International Journal of Molecular Sciences* **2018**, *19* (2), 379.

(21) Colin Hughes, R. Galectins as Modulators of Cell Adhesion. *Biochimie* **2001**, *83* (7), 667–676.

(22) Cumpstey, I.; Carlsson, S.; Leffler, H.; Nilsson, U. J. Synthesis of a Phenyl Thio-β-D-Galactopyranoside Library from 1,5-Difluoro-2,4-Dinitrobenzene: Discovery of Efficient and Selective Monosaccharide Inhibitors of Galectin-7. *Org. Biomol. Chem.* **2005**, *3* (10), 1922–1932.

(23) Vašíček, T.; Spiwok, V.; Červený, J.; Petrásková, L.; Bumba, L.; Vrbata, D.; Pelantová, H.; Křen, V.; Bojarová, P. Regioselective 3-O-Substitution of Unprotected Thiodigalactosides: Direct Route to Galectin Inhibitors. *Chemistry – A European Journal* **2020**, *26* (43), 9620–9631.

(24) Houzelstein, D.; Gonçalves, I. R.; Fadden, A. J.; Sidhu, S. S.; Cooper, D. N. W.; Drickamer, K.; Leffler, H.; Poirier, F. Phylogenetic Analysis of the Vertebrate Galectin Family. *Molecular Biology and Evolution* **2004**, *21* (7), 1177–1187.

(25) Etulain, J.; Negrotto, S.; Tribulatti, M. V.; Croci, D. O.; Carabelli, J.; Campetella, O.; Rabinovich, G. A.; Schattner, M. Control of Angiogenesis by Galectins Involves the Release of Platelet-Derived Proangiogenic Factors. *PLOS ONE* **2014**, *9* (4), e96402.

(26) de Oliveira, F. L.; Gatto, M.; Bassi, N.; Luisetto, R.; Ghirardello, A.; Punzi, L.; Doria, A. Galectin-3 in Autoimmunity and Autoimmune Diseases. *Exp Biol Med (Maywood)* **2015**, *240* (8), 1019–1028.

(27) Liu, F.-T.; Rabinovich, G. A. Galectins as Modulators of Tumour Progression. *Nat Rev Cancer* **2005**, *5* (1), 29–41.

(28) Pirone, L.; Del Gatto, A.; Di Gaetano, S.; Saviano, M.; Capasso, D.; Zaccaro, L.; Pedone, E. A Multi-Targeting Approach to Fight SARS-CoV-2 Attachment. *Front. Mol. Biosci.* **2020**, *7*.

(29) Di Gaetano, S.; Capasso, D.; Delre, P.; Pirone, L.; Saviano, M.; Pedone, E.; Mangiatordi, G. F. More Is Always Better Than One: The N-Terminal Domain of the Spike Protein as Another Emerging Target for Hampering the SARS-CoV-2 Attachment to Host Cells. *International Journal of Molecular Sciences* **2021**, *22* (12), 6462.

(30) Baum, L. G.; Garner, O. B.; Schaefer, K.; Lee, B. Microbe–Host Interactions Are Positively and Negatively Regulated by Galectin–Glycan Interactions. *Front. Immunol.* **2014**, *5*.

(31) Liu, F.-T.; Patterson, R. J.; Wang, J. L. Intracellular Functions of Galectins. *Biochimica et Biophysica Acta (BBA) - General Subjects* **2002**, *1572* (2), 263–273.

(32) Delaine, T.; Collins, P.; MacKinnon, A.; Sharma, G.; Stegmayr, J.; Rajput, V. K.; Mandal, S.; Cumpstey, I.; Larumbe, A.; Salameh, B. A.; Kahl-Knutsson, B.; van Hattum, H.; van Scherpenzeel, M.; Pieters, R. J.; Sethi, T.; Schambye, H.; Oredsson, S.; Leffler, H.; Blanchard, H.; Nilsson, U. J. Galectin-3-Binding Glycomimetics That Strongly Reduce Bleomycin-Induced Lung Fibrosis and Modulate Intracellular Glycan Recognition. *ChemBioChem* **2016**, *17* (18), 1759–1770.

(33) Rajput, V. K.; MacKinnon, A.; Mandal, S.; Collins, P.; Blanchard, H.; Leffler, H.; Sethi, T.; Schambye, H.; Mukhopadhyay, B.; Nilsson, U. J. A Selective Galactose-Coumarin-Derived Galectin-3 Inhibitor Demonstrates Involvement of Galectin-3-Glycan Interactions in a Pulmonary Fibrosis Model. *J Med Chem* **2016**, *59* (17), 8141–8147.

(34) Quintana, J. I.; Atxabal, U.; Unione, L.; Ardá, A.; Jiménez-Barbero, J. Exploring Multivalent Carbohydrate–Protein Interactions by NMR. *Chem. Soc. Rev.* **2023**, *52* (5), 1591–1613.

(35) André, S.; Pieters, R. J.; Vrasidas, I.; Kaltner, H.; Kuwabara, I.; Liu, F.-T.; Liskamp, R. M. J.; Gabius, H.-J. Wedgelike Glycodendrimers as Inhibitors of Binding of Mammalian Galectins to Glycoproteins, Lactose Maxiclusters, and Cell Surface Glycoconjugates. *ChemBioChem* **2001**, *2* (11), 822–830.

(36) André, S.; Sansone, F.; Kaltner, H.; Casnati, A.; Kopitz, J.; Gabius, H.-J.; Ungaro, R. Calix[n]Arene-Based Glycoclusters: Bioactivity of Thiourea-Linked Galactose/Lactose Moieties as Inhibitors of Binding of Medically Relevant Lectins to a Glycoprotein and Cell-Surface Glycoconjugates and Selectivity among Human Adhesion/Growth-Regulatory Galectins. *ChemBioChem* **2008**, *9* (10), 1649–1661.

(37) Yan, X.; Sivignon, A.; Yamakawa, N.; Crepet, A.; Travelet, C.; Borsali, R.; Dumych, T.; Li, Z.; Bilyy, R.; Deniaud, D.; Fleury, E.; Barnich, N.; Darfeuille-Michaud, A.; Gouin, S. G.; Bouckaert, J.; Bernard, J. Glycopolymers as Antiadhesives of E. Coli Strains Inducing Inflammatory Bowel Diseases. *Biomacromolecules* **2015**, *16* (6), 1827–1836

(38) Vrbata, D.; Filipová, M.; Tavares, M. R.; Červený, J.; Vlachová, M.; Šírová, M.; Pelantová, H.; Petrásková, L.; Bumba, L.; Konefał, R.; Etrych, T.; Křen, V.; Chytil, P.; Bojarová, P.

Glycopolymers Decorated with 3-O-Substituted Thiodigalactosides as Potent Multivalent Inhibitors of Galectin-3. *J. Med. Chem.* **2022**, *65* (5), 3866–3878.

(39) Valerio, S.; Iadonisi, A.; Adinolfi, M.; Ravidà, A. Novel Approaches for the Synthesis and Activation of Thio- and Selenoglycoside Donors. *J. Org. Chem.* **2007**, *72* (16), 6097–6106.

(40) Adinolfi, M.; d'Ischia, M.; Iadonisi, A.; Leone, L.; Pezzella, A.; Valerio, S. Glycosylated Eumelanin Building Blocks by Thioglycosylation of 5,6-Diacetoxyindole with an Expedient Selenium-Based Dynamic-Mixture Methodology. *European Journal of Organic Chemistry* **2012**, *2012* (23), 4333–4338.

(41) Adinolfi, M.; Capasso, D.; Gaetano, S. D.; Iadonisi, A.; Leone, L.; Pastore, A. A Straightforward Synthetic Access to Symmetrical Glycosyl Disulfides and Biological Evaluation Thereof. *Org. Biomol. Chem.* **2011**, *9* (18), 6278–6283.

(42) Edge, R.; D'Ischia, M.; Land, E. J.; Napolitano, A.; Navaratnam, S.; Panzella, L.; Pezzella, A.; Ramsden, C. A.; Riley, P. A. Dopaquinone Redox Exchange with Dihydroxyindole and Dihydroxyindole Carboxylic Acid. *Pigment Cell Research* **2006**, *19* (5), 443–450.

Chapter 4: A new class of selenoglycosides through 3-Selenoglycosydation of Eumelanin Monomers.

4.1 Introduction

4.1.1 Introduction on seleno glycoconjugates

As previously mentioned, saccharide structures are often linked to non-saccharide bioactive compounds in the frame of a strategy aimed at improving the properties of the active moiety in terms of solubility, stability, activity. In some of these applications the glycoconjugates are purportedly designed so to bear specific saccharide structures recognized by suitable receptors, creating an opportunity for improving their selectivity.

Selenoglycosides, a new class of glycomimetics, exhibit promising biological activities, including immunostimulatory and anti-metastatic effects (compound **4.1** in figure 4.1.1 is shown as an example).[1]

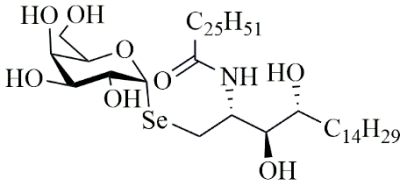

4.1

Figure 4.1.1: immunostimulant α-Se-GalCer.

From a synthetic perspective, selenoglycosides display unique reactivity as glycosyl donors. The C-Se bonds at the anomeric position can be easily ionized under photochemical conditions, producing highly reactive cationic and radical-

cationic species.[2] In addition, soft electrophiles can also be used for a similar purpose.[3–6]

In 2018, Zhu et al. proposed a stereoretentive method for the synthesis of selenoglycosides. This approach involves a copper-catalysed cross-coupling reaction between anomeric stannanes and symmetrical diselenides, resulting in either anomeric product.[7] The reaction mechanism involves the replacement of Cu with a Sn-substituent, creating an intermediate that retains its configuration at the anomeric C. Interestingly, when cross-coupling occurs between anomeric stannanes and symmetric diselenides, the result is a 1,1-selenodisaccharide. This process ensures that the anomeric configuration is perfectly preserved throughout, providing precise stereocontrol over the final product by carefully choosing the right coupling partners. The same method was also applied to the synthesis of selenium-containing glycopeptides. In this case, the cross-coupling of protected glycosyl stannanes with seleno-L-cysteine successfully produced selenocysteine glycoconjugates in good yields.

The main general strategy for the synthesis of selenoglycosides relies on the *in situ* generation of glycosyl selenolates with suitable electrophilic agents. Glycosyl selenolates are in turn obtained from an initial substitution process committing a suitable nucleophilic selenium species (i.e. selenourea, selenocyanate or selenobenzoate salts, etc..) and an electrophilic glycosyl donor (more commonly glycosyl halides).[1,8–16]

Recently, Iadonisi et al. developed a highly efficient and cost-effective method to synthesize peracetylated diglycosyl diselenides (**4.2-4.7**) by reacting elemental selenium, preliminarily reduced in situ with sodium borohydride, and glycosyl iodides (the latter serving as highly reactive glycosyl donors) in the key selenoglycosydation step (scheme 4.1.1).[17]

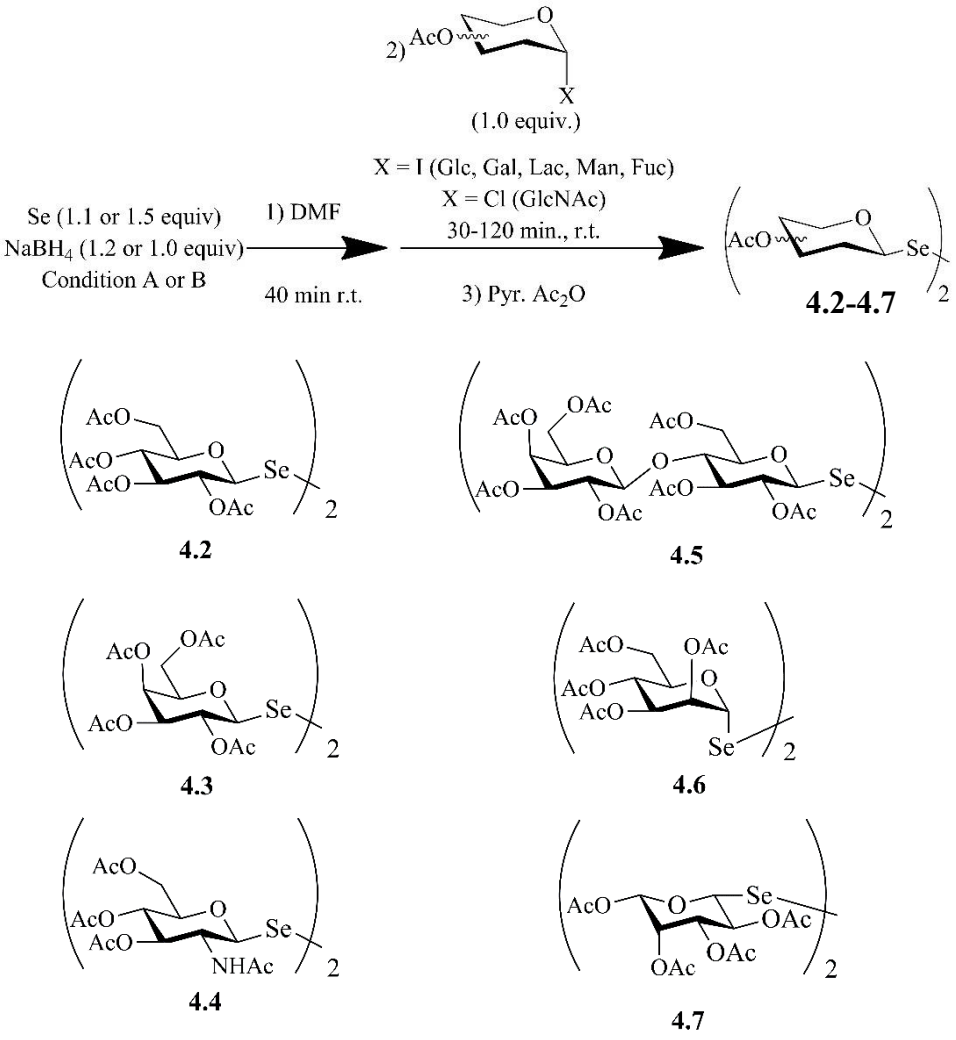

Scheme 4.1.1: synthesis of diglycosidic diselenides.

This approach for the synthesis of diselenides differs from other protocols described in literature in the usage of a cheap and non-toxic selenium source and can also be exploited to access unsymmetrical diglycosyl selenides.

Recently, a selenoglycosidation approach was designed by Lim and Paradisi in order to allow selenoglycosidation of electron rich aromatic systems, which can also be structural motifs of bioactive and pharmaceutically relevant compounds.[18] This process was based on the use of unprotected glycosyl diselenides as selenoglycosyl donors, and involved the use of a large excess (20 equivalents) of both the aromatic substrate and copper sulphate, enabling the synthesis of selenoglycosylated conjugates with various aromatic compounds in water. The products obtained included promising drug candidates, such as selenoglycosylated indole and other pharmaceutically relevant molecules. These compounds featured a new selenoether bond and were isolated in moderate yields.

Spurred by the current broad interest towards the pharmaceutical potential of selenoorganic compunds,[19] we considered the possibility to generate a selenium-based analogue of the 3-thioglycosylated eumelanin glycoconjugate[20,21] discussed in the previous chapter (figure 4.1.2).

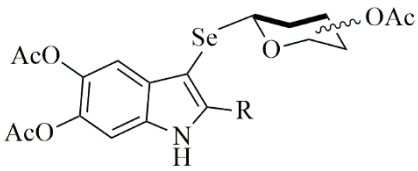

R = H, COOH

Figure 4.1.2: synthetic targets of this work.

These compounds can have many applications. Firstly, they could help to clarify unresolved structural aspects of melanin's three-dimensional structure. Secondly, they could function as multivalent scaffolds with potential pharmaceutical applications, especially in their interactions with lectins.

Increasing the solubility of glycosylated eumelanin precursors could facilitate the structural study of oligomers. This would provide valuable insights into the structure of natural polymers and identify characteristic structural motifs of melanins. To probe eumelanin's structural models, isolating oligomeric intermediates at different polymerization stages is crucial. This would reveal how precursors couple, the structure of oligomeric subunits, and their tendency to form aggregates through σ or π interactions. However, the instability of polymerization products, which readily auto-oxidize in both aqueous and organic environments, complicates this process.

Given the recent optimization of a rapid synthetic method for symmetric diselenides, we wanted to explore their potential as selenoglycosyl donors in conjugation reactions with DHI and DHICA to generate selenoglycosylated indoles. However, O-protection of DHI and DHICA is necessary to prevent spontaneous polymerization. Even in a non-oxidizing environment, an aqueous medium containing Cu(II) ions can lead to undesired side reactions due to Cu(II) chelation. Additionally, DHI and DHICA have poor water solubility and photochemical approaches face challenges due to the potential degradation and polymerization of eumelanin monomers. All these considerations made unpractical the application of the above mentioned selenoglycosidation strategy described by Paradisi et al, where a larges excess of both $CuSO_4$ and the aromatic substrate was needed.

The development of an alternative approach for synthesizing the mentioned targets was therefore addressed in this investigation.

4.1.2 Aim of the study

The next chapter will discuss the development of a new synthetic protocol for the 3-selenoglycosylation of both *O*-protected eumelanin key monomers, 5,6-diacetoxyindole (DAI) and 5,6-diacetoxyindole-2-carboxylic acid (DAICA), this latter being for the first time glycoconjugated.

Therefore, we investigate the development of an innovative synthetic methodology compatible with both DAI and DAICA by systematically studying different experimental conditions for the use of symmetrical glycosyl diselenides as glycosyl donors.

This new methodology exploits the activation of Se-Se bond through an unusual combination of promoters such as N-iodosuccinimmide (NIS) and tetrabutylammonium bromide (TBAB). Moreover, the procedure exhibits a broad synthetic scope, affording a vast library of selenoglycosidic functionalized eumelanin monomers as well as the first aminoacid-functionalized melanin monomer, starting from symmetrical N-protected seleno-L-Cystine. This new compound represents a promising conjugate in the horizon of the combination of two natural polymeric macromolecules, melanin and proteins, aiming to tailor different functions and properties into eumelanin polymers.

In conclusion, the main objective of this study is to simplify and make more versatile the glycosylation of eumelanin derivatives, allowing the synthesis of new monomeric units. These compounds could help resolve structural questions about melanins and serve as multivalent scaffolds for pharmaceutical applications, especially in lectin interactions. The increased solubility of glycosylated eumelanin precursors will also help to study oligomeric structures and identifying melanin-specific motifs.

4.2. Results and discussion

Following the previously mentioned considerations about the compatibility of the substrate and considering the amazing result of Gal3-CRD interaction with 3-thiolactosydic-DHI polymer, lactose diselenide **5** was chosen as a model glycosyl donor to investigate the reaction with the model substrate DAI (and later DAICA) for the formation of the new lactose-Se-Indole conjugate **4.8** (and later **4.9**) (scheme 4.2.1).

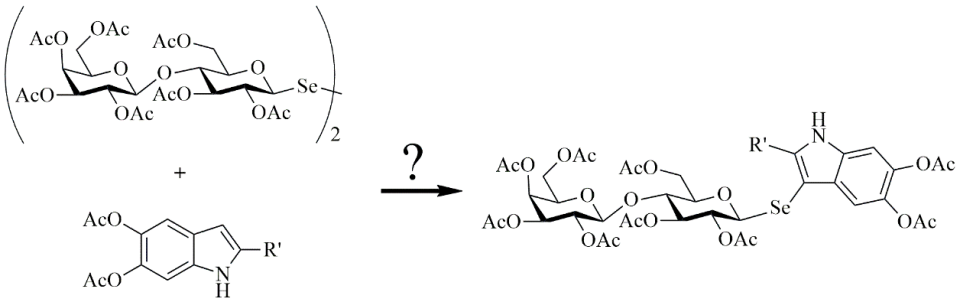

Scheme 4.2.1: selenoglycosylation reaction model.

In preliminary experiments, inspired by some examples of weak halogen-chalcogen interactions in literature, we explored the activation of the Se-Se bond utilizing soft electrophilic agents commonly employed in organic chemistry such as NIS (N-Iodosuccinimide) and NBS (N-Bromosuccinimide).[22,23]

Owing to the well-established affinity of selenium towards soft electrophiles such as some N-halosuccinimides like NIS (N-Iodosuccinimide) and NBS (N-Bromosuccinimide), these latter were initially tested for their ability to activate

the symmetrical diselenide using a stoichiometric amount (1 equivalent relative to the total monomeric units present in the diselenide) in acetonitrile dry as the solvent. The choice of this solvent was based on its use in the previously described approach for the thioglycosylation of DAI. The first trials were conducted at r.t. and they gave different results depending on the halosuccinimide used as depicted in scheme 4.2.2.

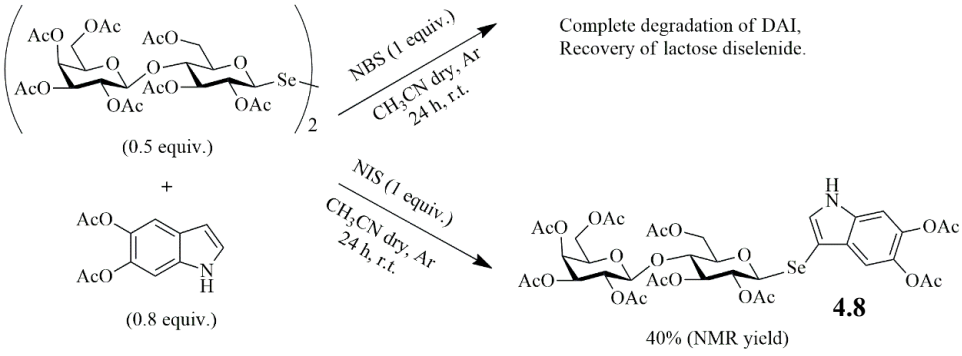

Scheme 4.2.2: preliminary reaction conditions explored for the synthesis of 8.

In the first case, the employment of NBS resulted in a complete degradation of DAI without affording the desired product. On the contrary, when NIS was used in the reaction, a 40% yield of the target product was obtained. The determination of NMR yield analysis was supposed on the integration of the aromatic region of DAI and the newly formed product **4.8.** In particular, it was very surprising that the Se-Se bond is activated only by a specific halogen. This may suggest that a specific interaction between Selenium and iodine is involved in the reaction pathway, maybe related to the higher softness of the halogen atom.

In the perspective of improving the reaction yield, the reactivity of NBS and NIS was examined in the combination with tetrabutylammonium halides such as

TBAB (tetrabutylammonium bromide) and TBAI (tetrabutylammonium iodide). Actually, it was reported that NBS and NIS can form adducts with TBAB and TBAI which retain the ability to serve as a source of halonium species, being capable of promoting electrophilic halogenation reactions of alkenes. Starting from these considerations, the model reaction was revisited by associating 1 equivalent of NXS (X = Br, I) with substoichiometric amounts of TBAY (Y = Br, I) (scheme 4.2.3).

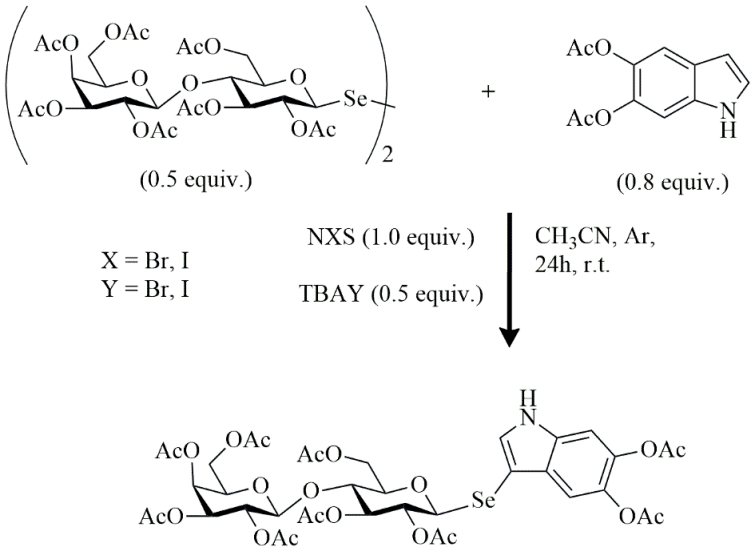

Scheme 4.2.3: Study of the effects of NXS/TBAY on the model reaction.

The results of these experiments, along with two previous tests, are summarized in table 4.2.1.

Entry	NXS (1.0)	TBAY (0.5)	Yield[a]	Comments
1	NBS	-	-	DAI completely degradated. Lac-OH.
2	NIS	-	40 %	LacSeDAI + partial reacovery of DAI + partial recovery of **5**
3	NBS	TBAB	-	Recovery of DAI. Lac-OH mostly present
4	NBS	TBAI	-	Halogenation of DAI, Lac-OH mostly present
5	**NIS**	**TBAB**	**75 %**	**LacSeDAI + recovery of a little amount of 5**
6	NIS	TBAI	-	Halogenation of DAI. Lac-OH + partial recovery of **5**

Table 4.2.1: Study on the effect of NXS/TBAY on the reaction. The yield refers to NMR yield comparing DAI and LacSeDAI **4.8**.

In the case of NBS, it was observed that both TBAB and TBAI caused significant degradation of the lactosyl diselenide (table 4.2.1, entry 3 and 4), which was found in the final crude reaction product predominantly in its hemiacetal form (Lac-OH). In stark contrast, when no additives were used (table 4.2.1, entry 1), the lactosyl

diselenide was largely recovered. NIS proved to be the most effective activator for this reaction, and specifically, the combination with TBAB (Table 4.2.1, entry 5) led to an important improvement in yield, over 30% higher than the reaction without TBAB (table 4.2.1, entry 2).

After identifying the NIS/TBAB combination as the best activator for glycosyl diselenides, comparative tests were performed to evaluate the effect of different solvents. The reaction was repeated in dichloromethane, dioxane, and tetrahydrofuran. Among these, dioxane provided a synthetically useful yield (c.a 50 %), although it was still lower than the yield achieved with acetonitrile, which remained the solvent of choice for subsequent experiments.

The final experiments investigated the effect of stoichiometry of the activating agents. It was observed that reducing the amount of NIS, compared to the previous stoichiometric ratio, led to a gradual decrease in the activation of the lactosyl diselenide. On the other hand, using a higher excess of NIS caused observable hydrolysis of the selenoglycosidic bond, as indicated by the presence of lactose in its hemiacetal form. In the end, the stoichiometry used in the initial tests (NIS/TBAB 1:0.5) proved to be the most efficient for the reaction.

Based on this outcome, the scope of the synthetic methodology was assessed with glycosylated diselenides derived from other sugars, achieving very satisfactory results with glycosylated diselenides from glucose, galactose, and *N*-acetylglucosamine (scheme 4.2.4).

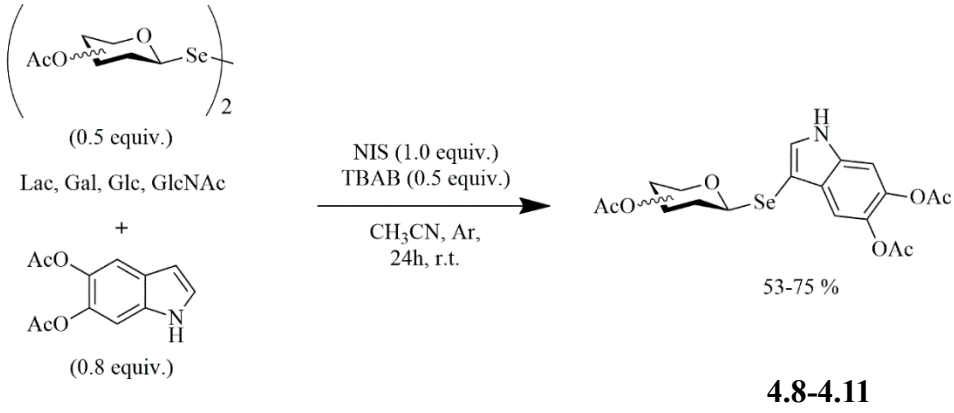

Scheme 4.2.4: Synthesis of selected 3-selenoglycosylated 5.6-diacetoxyindoles.

In all cases (products **4.8-4.11**), yields were over 50%, and the reactions were performed at room temperature, as summarized in table 4.2.2.

Entry	Sugar	Product	Yield (%)
1	**4.5**	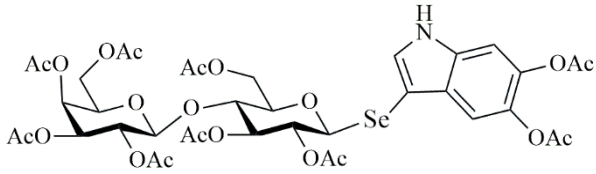 **4.8**	75 %
2	**4.3**	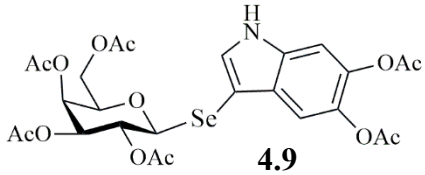 **4.9**	55 %
3	**4.2**	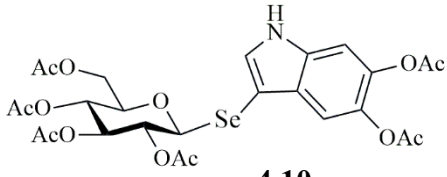 **4.10**	64 %
4	**4.4**	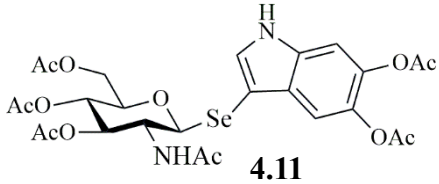 **4.11**	53 %

Table 4.2.2: Synthesis of selected 3-selenoglycosylated 5,6-diacetoxyindoles. The yield refers to the isolated product.

In the subsequent stage of investigation, we aimed to extend the methodology to DAICA, the other key eumelanin precursor in its protected diacetylated form. In the beginning, the reaction was evaluated using once again the model glycosyl donor **5** for the optimization of conditions. When the lactose diselenide was reacted with DAICA using the previously established stoichiometry (1 equivalent NIS, 0.5 equivalents TBAB), 40% reaction yield was achieved, obtaining for the first time a glycoconjugated 5,6-diacetoxyindole-2-carboxylic acid derivative. To increase the yield several NIS/TBAB stoichiometric combinations were tested, and a slight improvement to a 45% yield was recorded upon using 0.8 equivalents for both reagents. Since DAICA bears an electron withdrawing group on the C-2 position of the indole ring and thus is less reactive than DAI, it was hypothesized that increasing the amount of TBAB, and consequently the content of the NIS/TBAB adduct, would boost the reactivity and the reaction yield.

Anyway, using the established stoichiometry, the reaction methodology was successfully extended to all other sugars, resulting in DAICA derivatives (**4.12-4.15**) as shown in scheme 4.2.5.

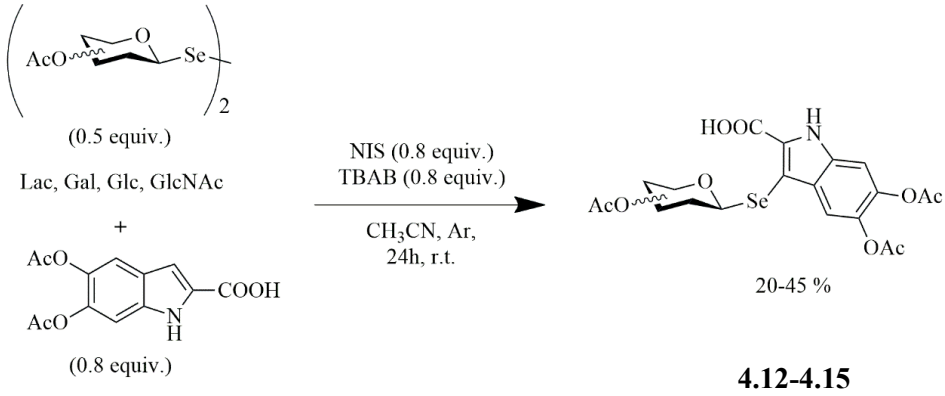

Scheme 4.2.5: Synthesis of selected 3-selenoglycosylated 5.6-diacetoxyindole-2-carboxylic acids.

A summary of the results obtained with DAICA is shown in the following table (table 4.2.3).

Entry	Sugar	Product	Yield (%)
1	**4.5**	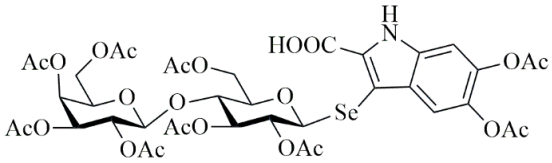 **4.12**	45 %
2	**4.3**	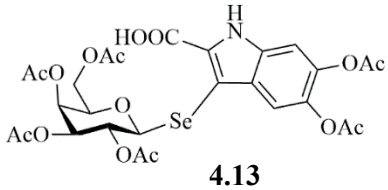 **4.13**	20 %
3	**4.2**	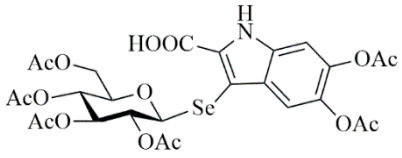 **4.14**	38 %
4	**4.4**	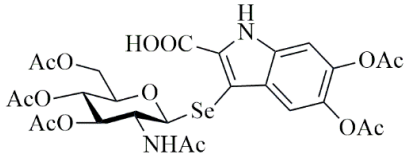 **4.15**	28 %

Table 4.2.3: Synthesis of selected 3-selenoglycosylated 5.6-diacetoxyindole-2-carboxylic acids. The yield refers to the isolated product after chromatography.

As expected, a lower reactivity of DAICA compared to DAI was observed (Table 4.2.3). However, it was still possible to isolate the 3-selenoglucosylated product in useful yields with all the glycosyl diselenides under scrutiny.

It is reasonable that the methodology may require further optimization with DAICA in terms of stoichiometry and temperature. Nevertheless, the results obtained are already sufficient to generate a new class of water-soluble glycosylated eumelanins, previously only obtained via the polymerization of a thioglycosylated DAICA derivative.

Following the demonstration of the methodology's broad scope, mechanistic experiments were carried out to investigate the effect of the TEMPO radical (tetramethylpiperidinyl N-oxyl) **4.16** on the reaction outcome. The model compounds DAI and peracetylated lactose diselenide were therefore reacted with catalytic or substoichiometric amount of TEMPO, as shown in scheme 4.2.6.

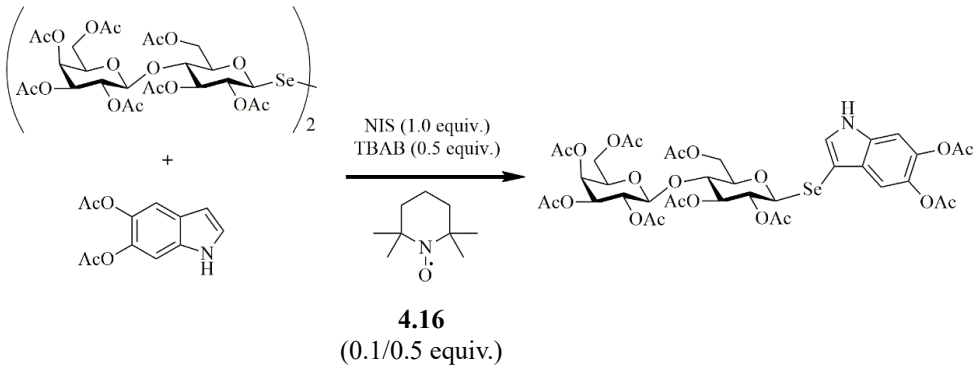

Scheme 4.2.6: Mechanicistic experiment on selenoglycosidic model reaction.

Addition of TEMPO did not reveal significant differences in the reaction pathway, suggesting an ionic mechanism rather than a radical one. It is proposed that the initial step involves the formation of an intermediate where a halonium

ion bonds to one of the selenium atoms in the glycosyl diselenide. In contrast, a previous study on a similar 3-thioglycosylation reaction showed evidence of a chain radical mechanism, as TEMPO inhibited the reaction even with catalytic amounts. This highlights a key difference between the two methods. Furthermore, the selenoglycosylation method offers a practical advantage over thioglycosylation due to the simpler purification process. As a matter of fact, with the latter reaction similar chromatographic properties of the starting glycosyl disulfide and the resulting DAI-conjugated thioglycoside make separation especially challenging.

A valuable extension of the selenoglycosylation method was discovered by applying the activation conditions with NIS and TBAB to an amino acid diselenide, specifically L-selenocystine. To test the method, commercially available selenocystine (**4.17**) hydrochloride was initially protected on the amine group with tBoc (tert-butoxycarbonyl) protecting group (scheme 4.2.7).

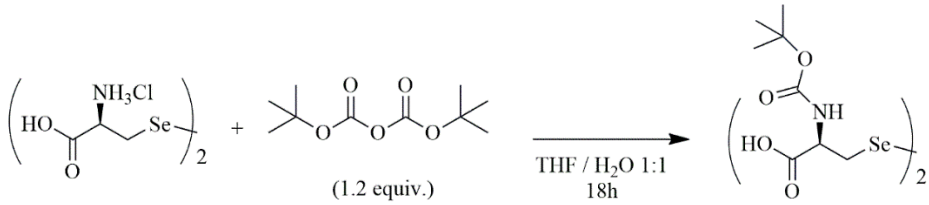

Scheme 4.2.7: tBoc protection reaction of Seleno-L-Cystine.

This derivative **4.18** was purified through simple liquid-liquid extraction and was coupled with DAI under the same conditions described in scheme 4.2.4 for selenoglycosydation of DAI. The reaction proceeded with an excellent yield (90%) and a significantly reduced reaction time (3 hours) compared to glycosyl diselenides (scheme 4.2.8). The presence of two different functional groups in the

amino acid could potentially inspire future applications in the development of novel molecular systems inspired by eumelanins.

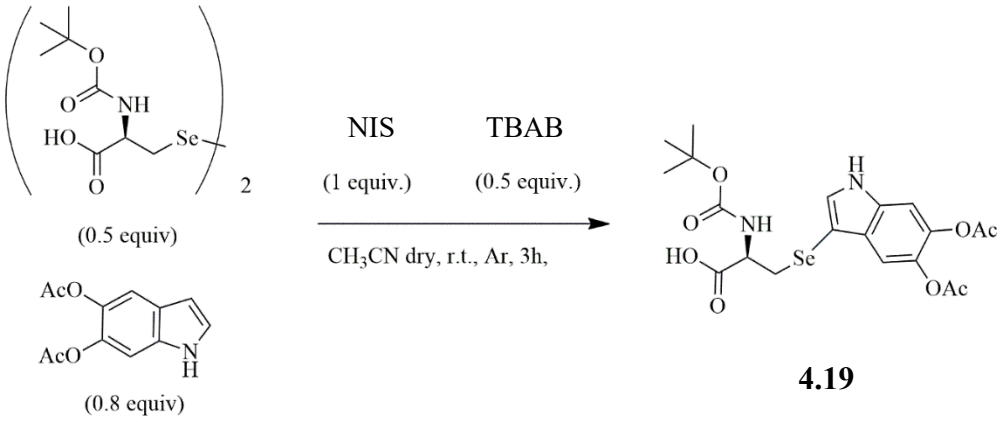

Scheme 4.2.8: Synthesis of selenocysteine-functionalized 5,6-diacetoxyindole

Additionally, the method can activate also aromatic diselenides. DAI successfully reacted with a commercially available substrate, diphenyl diselenide. Once again, the isolated yield exceeded 90% in 4 hours. A summary of the reaction conditions is shown in table 4.2.4. It's important to highlight that with diglycosyl diselenides Se-Se bond are much less reactive than alkyl and aryl diselenides, reactions with these latter being complete in much shorter times and with higher yields.

Entry	Diselenide	Product	Isolated yield (time)
1		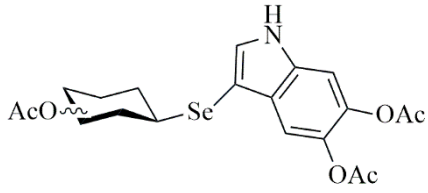	53-75 % (24 h)
2	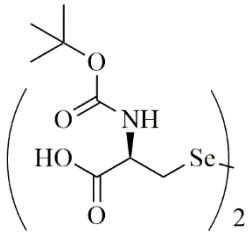	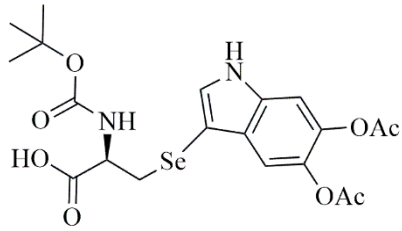	90 % (3h)
3	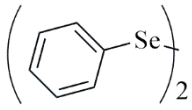	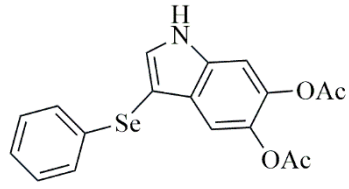	93 % (4h)
		4.20	

Table 4.2.4: Synthesis of selected 3-selenoconjugated-5,6-diacetoxyindoles. The yield is referred to the isolated product after chromatography.

4.3 Materials and methods:

All the commercial chemical reagents used were employed without prior purification. The reactions were monitored using TLC plates, which were visualized under UV-visible light. After visualization, the plates were immersed in a solution of ethanol/sulfuric acid (conc.) 95:5 and then heated to 230°C. For indolic compounds, after UV-visible light visualization, the plates were exposed to ammonia vapours before proceeding with carbonization (AISSP). The products obtained were separated using flash chromatography, with Merck Kieselgel 60 (63-200 mesh) silica as the stationary phase, and the purified products were characterized using NMR spectroscopy. The ^{1}H and ^{13}C NMR spectra were recorded on a Bruker spectrometer (400 MHz). Chemical shifts in ppm were referenced to tetramethylsilane.

All commercially available reagents were used as received and all the solvents were of analytical grade. Synthesis of 5,6-dihydroxiindole, 5,6-diacetoxyindole, were performed according to the already known protocols.[24]

Lac-Se-DAI x OAc 4.8:

^{1}H NMR ($CDCl_3$, 400 MHz) d 8.65 (1H, d, J = 1.6 Hz, -NH), 7.43 (1H, s), 7.19 (1H, d, J = 1.6 Hz), 7.16 (1H, s), 5.28 (1H, bd, J = 2.4 Hz, H-4'), 5.10 (1H, t, J = 9.2 Hz, H-3), 5.28 (1H, dd, J = 8.0 e 10.4 Hz, H-2'), 4.88 (1H, dd, J = 2.4 e 10.4 Hz, H-3'), 4.75 (1H, t, J = 10.0 Hz, H-2), 4.61 (1H, d, J = 10.0 Hz, H-1), 4.37 (1H, bd, J = 12.4 Hz, H-6a), 4.33 (1H, d, J = 8.0 Hz, H-1'), 4.10 – 3.93 (3H, m, H-6b e H_2-6'), 3.77 (1H, bt, J = 6.8 Hz, H-5'), 3.55 – 3.48 (2H, sovrapposti, H-4 e H-5), 2.31 (x2), 2.10, 2.09, 2.02, 2.00, 1.98, 1.97, 1.93 (27H, 8 x s, 9 x -$COCH_3$). ^{13}C NMR ($CDCl_3$, 100 MHz) d 170.4, 170.3 , 170.1, 170.0, 169.7, 169.6, 169.5, 169.3, 169.0, 138.4, 136.4, 134.0, 133.2, 128.9, 114.5, 105.6, 100.8, 79.9, 75.8, 73.8, 70.9, 70.7, 70.5, 68.9, 66.5, 62.1, 60.5, 20.8 -20.3.

Gal-Se-DAI x OAc 4.9:

^{1}H NMR ($CDCl_3$, 400 MHz) d 8.55 (1H, bs, -NH), 7.49 (1H, s), 7.32 (1H, d, J = 1.8 Hz), 7.19 (1H, s), 5.27 (1H, bd, J = 2.8 Hz, H-4), 5.10 (1H, t, J = 10.0 Hz, H-2), 4.95 (1H, dd, J = 2.8 e 10.0 Hz, H-3), 4.67 (1H, d, J = 10.0 Hz, H-1), 4.09 (1H, dd, J = 6.8 e 11.2 Hz, H-6a), 3.93 (1H, dd, J = 6.8 e 11.2 Hz, H-6b), 3.78 (1H, bt, J = 6.8 Hz, H-5), 2.31, 2.30, 2.11, 2.01, 1.92, 1.79 (18H, 6 x s, 6 x -$COCH_3$). ^{13}C NMR ($CDCl_3$, 100 MHz) d 170.2 (x2), 169.9, 169.4, 169.1, 168.9, 138.5, 136.8, 133.6, 133.1, 128.6, 114.7, 105.4, 81.2, 75.2, 71.8, 67.7, 67.0, 61.5, 20.8, 20.6, 20.5. 20.4, 20.0.

Glc-Se-DAI x OAc 4.10:

^{1}H NMR ($CDCl_3$, 400 MHz) d 8.66 (1H, bs, -NH), 7.45 (1H, s), 7.29 (1H, d, J = 1.6 Hz), 7.15 (1H, s), 5.13 (1H, t, J = 9.6 Hz, H-3), 4.90 - 5.00 (2H, sovrapposti, H-2 e H-4), 4.67 (1H, d, J = 10.0 Hz, H-1), 4.10 -4.00 (2H, m, H_2-6), 3.55 (1H, m, H-5), 2.33, 2.32, 2.12, 1.99 (x2), 1.97 (18H, 5 x s, 6 x -$COCH_3$). ^{13}C NMR ($CDCl_3$, 100 MHz) d 170.7, 170.2, 169.4, 169.3, 169.2 (x2), 138.5, 136.8, 133.8, 133.2, 128.2,114.4, 105.9, 95.0, 80.4, 74.5, 70.5 (x2), 68.0, 62.0, 20.8, 20.7, 20.6.

GlcNAc-Se-DAI x OAc 4.11:

^{1}H NMR ($CDCl_3$, 400 MHz) d 9.00 (1H, bs, -NH), 7.46 (1H, s), 7.26 (1H, d, J = 1.2 Hz), 7.15 (1H, s), 6.00 (1H, J = 9.2 Hz, NH-2), 5.13 (1H, t, J = 10.0 Hz, H-3), 4.94 (1H, t, J = 10.0 Hz, H-4), 4.85 (1H, d, J = 10.0 Hz, H-1), 4.20 -4.05 (2H, m, H_2-6), 3.90 (1H, q, J = 9.6 Hz, H-2), 3.60 (1H, m, H-5), 2.35, 2.33, 2.03, 2.00, 1.99 (x2) (18H, 5 x s, 6 x -$COCH_3$). ^{13}C NMR ($CDCl_3$, 100 MHz) d 170.9, 170.8, 170.4, 169.4, 138.2, 136.6, 133.6, 133.2, 128.7, 114.1, 106.0, 82.0, 76.5, 73.5, 68.3, 62.2, 53.9, 23.3, 20.8, 20.7, 20.6.

Lac-Se-DAICA x OAc 4.12:

^{1}H NMR ($CDCl_3$, 400 MHz) d 10.22 (1H, bs, -NH), 7.61 (1H, s), 7.30 (1H, s), 5.31 (1H, bd, J = 2.8 Hz, H-4'), 5.12 (1H, t, J = 9.6 Hz, H-3), 5.05 (1H, dd, J = 8.0 e 10.4 Hz, H-2'), 4.94 (1H, dd, J = 2.8 e 10.4 Hz, H-3'), 4.83 (1H, t, J = 10.0 Hz, H-2), 4.44 (1H, d, J = 10.0 Hz, H-1), 4.35 (1H, bd, J = 11.6 Hz, H-6a), 4.15 – 4.00 (4H, sovrapposti, , H-6b, H_2-6', e H-1'), 3.84 (1H, bt, J = 6.8 Hz, H-5'), 3.67 (1H, t, J = 9.6 Hz, H-4), 3.56 (1H, m, H-5), 2.33, 2.32, 2.12, 2.08, 2.04, 2.00, 1.99, 1.97, 1.94 (27H, 8 x s, 9 x -$COCH_3$).

Gal-Se-DAICA x OAc 4.13:

^{1}H NMR ($CDCl_3$, 400 MHz) d 9.88 (1H, bs, -NH), 7.66 (1H, s), 7.34 (1H, s), 5.36 (1H, bd, J = 2.8 Hz, H-4), 5.09 (1H, t, J = 10.0 Hz, H-2), 4.98 (1H, dd, J = 2.8 e 10.0 Hz, H-3), 4.89 (1H, d, J = 10.0 Hz, H-1), 4.14 (1H, dd, J = 6.8 e 11.2 Hz, H-6a), 4.04 (1H, dd, J = 6.8 e 11.2 Hz, H-6b), 3.88 (1H, bt, J = 6.8 Hz, H-5), 2.35, 2.34, 2.11, 2.03, 1.98, 1.95 (18H, 6 x s, 6 x -$COCH_3$). ^{13}C NMR ($CDCl_3$, 100 MHz) d 176.4, 170.4, 170.3, 170.0, 169.8, 169.8, 169.0, 168.5, 163.9, 161.0, 141.9, 138.2, 133.5, 130.8, 129.1, 116.7, 106.5, 82.5, 75.7, 71.7, 67.8, 67.1, 61.6, 20.8 - 20.4.

Glc-Se-DAICA x OAc 4.14:

^{1}H NMR ($CDCl_3$, 400 MHz) d 10.10 (1H, bs, -NH), 7.63 (1H, s), 7.35 (1H, s), 5.14 (1H, t, J = 9.6 Hz, H-3), 5.02 (1H, t, J = 9.6 Hz, H-2), 4.94 (1H, t, J = 9.6 Hz, H-4), 4.90 (1H, d, J = 10.0 Hz, H-1), 4.20 -4.00 (2H, m, H_2-6), 3.63 (1H, m, H-5), 2.33, 2.32, 2.09, 2.06, 1.99, 1.95 (18H, 6 x s, 6 x -$COCH_3$). ^{13}C NMR

($CDCl_3$, 100 MHz) d 176.4, 170.9, 170.2, 169.9, 169.4, 169.1, 168.6, 162.9, 141.7, 138.1, 133.6, 130.8, 129.1, 116.3, 106.8, 81.8, 73.8, 70.8, 67.9, 62.0, 20.7 - 20.5.

GlcNAc-Se-DAICA x OAc 4.15:

^{1}H NMR (acetone d-6, 400 MHz) d 11.32 (1H, bs, -NH), 7.72 (1H, s), 7.44 (1H, s), 5.33 (1H, d, J = 10.0 Hz, H-1), 5.24 (1H, t, J = 9.6 Hz, H-3), 4.94 (1H, t, J = 9.6 Hz, H-4), 4.20 (1H, dd, J = 5.6 e 12.4 Hz, H-6a), 4.00 – 3.90 (2H, sovrapposti, H-2, H-6b), 3.74 (1H, m, H-5), 2.31 (x2), 1.98, 1.93, 1.91, 1.86 (18H, 5 x s, 6 x -$COCH_3$).

^{13}C NMR (acetone d-6, 100 MHz) d 176.4, 169.9, 169.6, 169.0, 168.6, 168.2, 161.3, 141.5, 138.0, 133.7, 131.58, 129.0, 116.0, 106.6, 83.2, 76.5, 73.6, 68.7, 62.0, 53.9, 22.2, 19.7 - 19.5.

Cysteine-Se-DAI x OAc 4.18:

^{1}H NMR ($CDCl_3$, 400 MHz) d 9.26 (1H, bs, -NH), 7.39 (1H, s), 7.16 (1H, s), 7.15 (1H, d, J = 2.4 Hz), 5.50 (1H, d, J = 4.4 Hz, -NHtBoc), 4.42 (1H, m, -C_aH-CO), 3.00 (1H, d, -C_bH-CO-), 2.34, 2.33 (6H, 2 x s, 2 x -$COCH_3$), 1.47 (1H, s, -$C(CH_3)$).

^{13}C NMR ($CDCl_3$, 100 MHz) d 175.1, 169.8, 169.5, 155.8, 138.1, 136.6, 133.5, 133.4, 127.8, 113.2, 106.2, 96.2, 80.6, 53.0, 29.7, 29.3, 20.8, 20.7.

SeCystine-tBoc 4.17:

^{1}H NMR (acetone d-6, 400 MHz) d 6.34 (1H, d, J = 7.6 Hz, NH), 4.52 (1H, m, H-a), 3.55 (1H, dd, J = 5.2 e 12.8 Hz, Ha-a), 3.55 (1H, dd, J = 5.2 e 12.8 Hz, Ha-b), 3.55 (1H, dd, J = 5.2 e 12.8 Hz, Ha-b), 1.41 (9H, s, -t-Boc CH_3).

^{13}C NMR (acetone d-6, 100 MHz) d 171.6, 155.4, 78.8, 54.3, 31.9, 27.7.

General Procedure for the Synthesis of Symmetric Glycosyl Diselenides: The first step in the synthesis of diglycosyl diselenides involves the formation of glycosyl iodide: to a solution of 1 mmol of peracetylated sugar (678 mg for lactose octaacetate), dissolved in DCM-dry (2 mL) I_2 (280 mg, 1.1 mmol), and Et3SiH (177 µL, 1.1 mmol) were added subsequently (caution: exothermic reaction). The reaction mixture was refluxed until the starting material was fully consumed (15 minutes, monitored by TLC). The mixture was then diluted with DCM, and the organic phase was washed with aqueous sodium carbonate containing sodium thiosulfate, which was added gradually until the residual iodine in the organic phase was completely consumed. The organic phases were collected and fried to give the glycosyl iodide. Meanwhile, a mixture of elemental selenium (87 mg, 1.1 mmol or 118 mg 1.5 mmol, see rif[17]) and sodium borohydride (1.2 or 1.0 mmol see rif[17]) is prepared, suspended in DMF (3-4 mL), and maintained under magnetic stirring at room temperature. After 40 minutes, the mixture is added to the flask containing the previously synthesized glycosyl iodide (or GlcNAcChloride) (1.0 mmol) in DMF (3 mL). The flask is washed with small amounts of DMF, which are then added to the reaction flask (totalling 3 mL). The reaction is conducted at room temperature under magnetic stirring until complete (usually less than two hours). The reaction is quenched with acetic acid (0.25 mL), and the mixture is transferred to a separatory funnel and diluted with DCM. The organic phase is washed with an aqueous solution of sodium carbonate, and the aqueous phase is re-extracted with DCM. The collected organic phase is dried with sodium sulphate, filtered, and concentrated. Pyridine (1 mL) and acetic anhydride (0.5 mL) are added for 1 hour at room temperature. The mixture is then treated with methanol in a cold bath, transferred to a separatory funnel, and the organic phase extracted with DCM, washing with an aqueous solution of sodium carbonate. The aqueous phase is re-extracted with DCM, and the two organic phases are combined, dried over sodium sulphate, filtered, and concentrated. The final

product is purified by flash chromatography (using mixtures of hexane/acetate or dichloromethane/methanol).

General Procedure for the Selenoglycosidation of DAI (6,7,8,9): DAI (19 mg, 0.08 mmol) and glycosyl diselenide (41 mg/70 mg for mono-/di-saccharides, 0.05 mmol) are placed in a flask and dissolved under argon in acetonitrile (1 mL) previously flushed with argon for 15 minutes. To this solution, NIS (23 mg, 0.1 mmol) and TBAB (16 mg, 0.05 mmol) are added. The reaction is carried out at room temperature under magnetic stirring in an inert atmosphere. After the reaction is complete, the mixture is diluted with DCM, and the organic phase is washed with a 10% aqueous sodium thiosulfate solution. The aqueous phase is re-extracted, and the organic phases are combined, dried with sodium sulphate, filtered, and concentrated. The crude product is purified by flash chromatography on silica gel, using mixtures of hexane and ethyl acetate.

General Procedure for the Selenoglycosidation of DAICA (10,11,12,13): DAICA (22 mg, 0.08 mmol) and glycosyl diselenide (41 mg/70 mg for mono-/disaccharides, 0.05 mmol) are dissolved under an argon atmosphere using acetonitrile (1 mL) previously flushed with argon for 15 minutes. NIS (18 mg, 0.08 mmol) and TBAB (26 mg, 0.08 mmol) are then added to the reaction flask. The reaction is conducted overnight at room temperature, under magnetic stirring in an inert atmosphere. After the reaction is complete, the mixture is diluted with DCM, and the organic phase is washed with a 10% aqueous sodium thiosulfate solution. The aqueous phase is re-extracted with DCM, and the two organic phases are combined, dried with sodium sulphate, filtered, and concentrated. The crude product is purified by flash chromatography on silica gel, using mixtures of hexane, ethyl acetate, and acetic acid.

4.4 Conclusions

In this chapter, an original method of glycoconjugation of DAI and DAICA, important indole derivatives at the basis of significant biochemical processes, has been described. The attachment of the sugar to the indole moiety occurs through the generation of a selenoglycoside bond, taking advantage of the feasible activation of symmetrical glycosyl diselenides with the NIS/TBAB combination. An optimization study conducted on peracetylated lactose diselenide demonstrated that a different NIS/TBAB stoichiometric combination was best performing in the

After this optimization, the methodology has been extended to a range of sugars (including an amino sugar), with satisfying yields. Remarkably, among these experiments there are the first examples of DAICA glycofunctionalization which proved expectedly more difficult than with DAI.

The method was demonstrated to be versatile and could be applied also to non saccharidic diselenides, leading to new DAI derivatives with modifications at position C-3. In this regard, it is especially remarkable the smooth and high-yielding DAI conjugation with *N*-tBoc protected selenocysteine.

Moreover, the methodology was proven to have high efficiency, as the resulting products were easily separated and purified from the starting materials due to their different chemical properties.

Future studies will verify the possibility of O-deacetylation from the modified molecule (5) and investigate how the attached sugar influences the formation of oligomeric products (dimers, polymers). Moreover, the capability of creating multivalent conjugate and their action in biological field will be evaluated.

Particular attention will be paid to the derivatives synthesized from 5,6-diacetossiindole-2-carboxylic acid and selenocysteine, as these represent a new frontier in the field of water-soluble eumelanins.

4.5 References

(1) McDonagh, A. W.; Mahon, M. F.; Murphy, P. V. Lewis Acid Induced Anomerization of Se-Glycosides. Application to Synthesis of α-Se-GalCer. *Org. Lett.* **2016**, *18* (3), 552–555.

(2) Furuta, T.; Takeuchi, K.; Iwamura, M. Activation of Selenoglycosides by Photoinduced Electron Transfer. *Chem. Commun.* **1996**, No. 2, 157–158.

(3) Valerio, S.; Iadonisi, A.; Adinolfi, M.; Ravidà, A. Novel Approaches for the Synthesis and Activation of Thio- and Selenoglycoside Donors. *J. Org. Chem.* **2007**, *72* (16), 6097–6106.

(4) Mehta, S.; Mario Pinto, B. Phenylselenoglycosides as Novel, Versatile Glycosyl Donors. Selective Activation over Thioglycosides. *Tetrahedron Letters* **1991**, *32* (35), 4435–4438.

(5) Mehta, S.; Pinto, B. M. Novel Glycosidation Methodology. The Use of Phenyl Selenoglycosides as Glycosyl Donors and Acceptors in Oligosaccharide Synthesis. *J. Org. Chem.* **1993**, *58* (12), 3269–3276.

(6) Zuurmond, H. M.; Van Der Meer, P. H.; Van Der Klein, P. A. M.; Van Der Marel, G. A.; Van Boom, J. H. Iodonium-Promoted Glycosylations with Phenyl Selenoglycosides. *Journal of Carbohydrate Chemistry* **1993**, *12* (8), 1091–1103.

(7) Zhu, F.; O'Neill, S.; Rodriguez, J.; Walczak, M. A. Stereoretentive Reactions at the Anomeric Position: Synthesis of Selenoglycosides. *Angewandte Chemie International Edition* **2018**, *57* (24), 7091–7095.

(8) Suzuki, T.; Makyio, H.; Ando, H.; Komura, N.; Menjo, M.; Yamada, Y.; Imamura, A.; Ishida, H.; Wakatsuki, S.; Kato, R.; Kiso, M. Expanded Potential of Seleno-Carbohydrates as a Molecular Tool for X-Ray Structural Determination of a Carbohydrate–Protein Complex with Single/Multi-Wavelength Anomalous Dispersion Phasing. *Bioorganic & Medicinal Chemistry* **2014**, *22* (7), 2090–2101.

(9) Shimabukuro, J.; Makyio, H.; Suzuki, T.; Nishikawa, Y.; Kawasaki, M.; Imamura, A.; Ishida, H.; Ando, H.; Kato, R.; Kiso, M. Synthesis of Seleno-Fucose Compounds and Their Application to the X-Ray Structural Determination of Carbohydrate-Lectin Complexes Using Single/Multi-Wavelength Anomalous Dispersion Phasing. *Bioorganic & Medicinal Chemistry* **2017**, *25* (3), 1132–1142.

(10) André, S.; Kövér, K. E.; Gabius, H.-J.; Szilágyi, L. Thio- and Selenoglycosides as Ligands for Biomedically Relevant Lectins: Valency–Activity Correlations for Benzene-Based Dithiogalactoside Clusters and First Assessment for (Di)Selenodigalactosides. *Bioorganic & Medicinal Chemistry Letters* **2015**, *25* (4), 931–935.

(11) Wagner, G.; Nuhn, P. Synthese von Selenoglykosiden Mit Acetyl-Glykosyl-Isoselenuronium-Bromiden. 4. Mitt. Über „Selenoglykoside". *Archiv der Pharmazie* **1964**, *297* (8), 461–473.

(12) Manna, T.; Misra, A. K. Glycosyl Selenoacetates: Versatile Building Blocks for the Preparation of Stereoselective Selenoglycosides and Selenium Linked Disaccharides. *Org. Biomol. Chem.* **2019**, *17* (39), 8902–8912.

(13) Kawai, Y.; Ando, H.; Ozeki, H.; Koketsu, M.; Ishihara, H. A Facile Method for β-Selenoglycoside Synthesis Using β-p-Methylbenzoyl Selenoglycoside as the Selenating Unit. *Org. Lett.* **2005**, *7* (21), 4653–4656.

(14) Nanami, M.; Ando, H.; Kawai, Y.; Koketsu, M.; Ishihara, H. Stereoselective Synthesis of Various α-Selenoglycosides Using in Situ Production of α-Selenolate Anion. *Tetrahedron Letters* **2007**, *48* (7), 1113–1116.

(15) Zhu, M.; Alami, M.; Messaoudi, S. Room-Temperature Pd-Catalyzed Synthesis of 1-(Hetero)Aryl Selenoglycosides. *Org. Lett.* **2020**, *22* (16), 6584–6589.

(16) Saravanan, V.; Porhiel, E.; Chandrasekaran, S. Tetraethylammonium Tetraselenotungstate: A New and Efficient Selenium Transfer Reagent for the Chemoselective Synthesis of Functionalised Diselenides. *Tetrahedron Letters* **2003**, *44* (11), 2257–2260.

(17) Iadonisi, A.; Traboni, S.; Capasso, D.; Bedini, E.; Cuomo, S.; Gaetano, S. D.; Vessella, G. Switchable Synthesis of Glycosyl Selenides or Diselenides with Direct Use of Selenium as the Selenating Agent. *Org. Chem. Front.* **2021**, *8* (8), 1823–1829.

(18) Lim, D.; Paradisi, F. Investigations into the Aqueous Synthesis of Selenoglycoconjugates. *European Journal of Organic Chemistry* **2023**, *26* (34), e202300496.

(19) Álvarez-Pérez, M.; Ali, W.; Marć, M. A.; Handzlik, J.; Domínguez-Álvarez, E. Selenides and Diselenides: A Review of Their Anticancer and Chemopreventive Activity. *Molecules* **2018**, *23* (3), 628.

(20) Adinolfi, M.; d'Ischia, M.; Iadonisi, A.; Leone, L.; Pezzella, A.; Valerio, S. Glycosylated Eumelanin Building Blocks by Thioglycosylation of 5,6-Diacetoxyindole with an Expedient Selenium-Based Dynamic-Mixture Methodology. *European Journal of Organic Chemistry* **2012**, *2012* (23), 4333–4338.

(21) Pezzella, A.; Iadonisi, A.; Valerio, S.; Panzella, L.; Napolitano, A.; Adinolfi, M.; d'Ischia, M. Disentangling Eumelanin "Black Chromophore": Visible Absorption Changes As Signatures of Oxidation State- and Aggregation-Dependent Dynamic Interactions in a Model Water-Soluble 5,6-Dihydroxyindole Polymer. *J. Am. Chem. Soc.* **2009**, *131* (42), 15270–15275.

(22) *Regioselective Deiodination of Thyroxine by Iodothyronine Deiodinase Mimics: An Unusual Mechanistic Pathway Involving Cooperative Chalcogen and Halogen Bonding | Journal of the American Chemical Society*.

(23) Bayse, C. A.; Rafferty, E. R. Is Halogen Bonding the Basis for Iodothyronine Deiodinase Activity? *Inorg. Chem.* **2010**, *49* (12), 5365–5367.

(24) Edge, R.; D'Ischia, M.; Land, E. J.; Napolitano, A.; Navaratnam, S.; Panzella, L.; Pezzella, A.; Ramsden, C. A.; Riley, P. A. Dopaquinone Redox Exchange with Dihydroxyindole and Dihydroxyindole Carboxylic Acid. *Pigment Cell Research* **2006**, *19* (5), 443–450.

Chapter 5: Chalcogen-loaded eumelanins

5.1 Introduction

A major limiting factor for the practical implementation of eumelanin-based electronic devices is the low conductivity of this pigment, coupled with the fact that the underlying conduction mechanisms remain a subject of debate.[1–3] Various strategies are emerging to overcome the limitation of poor conductivity, aiming to take advantage of eumelanin's biocompatibility and favourable physico-chemical properties.[4–7] Among the approaches under investigation, a promising strategy is hybridization with a suitable conductive counterpart.[8,9]

For instance, blending and treatments like in situ polymerization of DHI in the presence of PEDOT:PSS have led to the development of a hybrid material that can be used as an electrode for optoelectronic devices.[5,10–12]

In the literature, to control the optoelectronic properties of organic semiconductors and enhance the performance of organic electronic devices, several molecular design strategies have been proposed. For example, common organic semiconductor polymers, which consist of alternating electron-rich (donor) and electron-deficient (acceptor) units, are known as donor–acceptor (D–A) copolymers.[13–15] The energy levels of the highest occupied molecular orbital (HOMO) and the lowest unoccupied molecular orbital (LUMO) can be effectively tuned through D–A design strategies or by extending the conjugated length of organic semiconductors. In alternative, chemical modifications such as installing electron-withdrawing substituents like nitro, halogen or cyano groups into organic semiconductors can lower LUMO levels, while electron-donating groups are used to increase HOMO levels.[16,17]

Despite these advancements, organic semiconductors still face significant challenges, including weak charge transport, low light and thermal power conversion efficiencies, which result from their inherently narrow bandwidth, poor planarity, and weak intermolecular interactions. A universal solution to address all these issues simultaneously is still lacking. In recent years, incorporating heavy atoms such as chalcogens into the conjugated backbone of organic semiconductors has gained increasing interest to regulate their optoelectronic properties. The higher nuclear charge of heavy atoms compared to light atoms results in stronger Coulombic interactions between electrons and heavy atoms, which can alter the energy distribution and induce the "heavy atom effect''.

In this perspective, following the introduction or substitution of chalcogens in organic materials, I explored the possibility of enhancing eumelanin properties with the incorporation of chalcogens into eumelanin moieties. A brief introduction on chalcogens will focus on their properties and uses in organic electronics, introducing the perspective on the application of these elements in eumelanin-like materials.

5.1.1 Chalcogens and organic electronics

Chalcogens are Group 16 elements (O, S, Se, Te and Po, highlighted in figure 5.1) of the periodic table that find applications in a range of devices such as computer memories, telecommunications, chemical sensors, photodetectors, and ionic sensors.[18] The term “chalcogen” refers to "ore-forming" materials and is derived from the Greek word *khalkós*, meaning copper (ore or coin), and the Latinized Greek word *genēs*, meaning born or produced. Chalcogenide compounds are often associated with the elements of the oxygen family, including sulphides, selenides, tellurides, and the radioactive element polonium (Po).

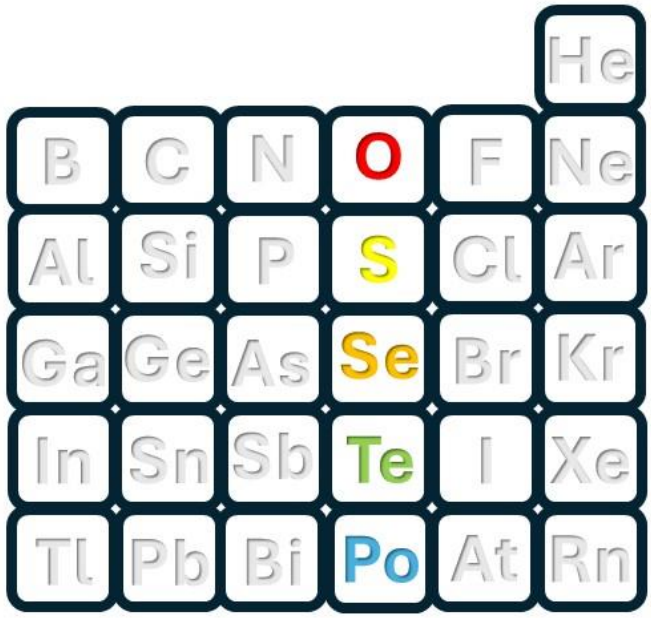

Figure 5.1: p-block of the periodic table. Group 16 (chalcogens) is highlighted with different colour for each constituent element.

Oxygen is typically treated separately from the other chalcogens due to its distinct chemical behaviour, and sometimes even excluded from the term ‘’chalcogen’’. Sulphur-based materials are widely used in optoelectronic and energy storage devices, selenium-based materials instead are primarily applied in imaging, biomedical fields, ion-selective sensors, and modern solar cells, while tellurium-based materials are commonly used in phase-change memory devices and infrared detectors.

Chalcogens display an interesting property such as their ability to form specific non-covalent interactions known as chalcogen bonding. Although some aspects about the terminology of this phenomenon are still on debate,[19] the most agreed description is that during this event the chalcogen atom is acting as an electrophilic species and interacts with a nucleophilic site (electron rich species).[20] The general structure of chalcogen bonding between a chalcogen atom K and a nucleophile Nu:, is depicted in Figure 5.2.

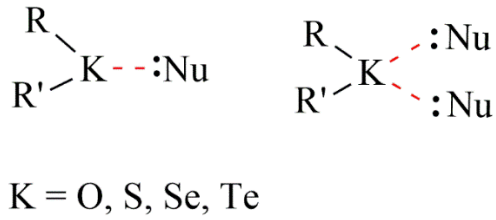

Figure 5.2: Directional chalcogen bond interaction.

Chalcogen bonding, although often considered a weak interaction, can range from a few kJ/mol to several hundred kJ/mol in strength.[21] This electrostatic phenomenon is typically explained starting from the positive electrostatic potential on the surface of the chalcogen atom. This is an electron deficient region, known as the "σ-hole". The size of the σ-hole increases from lighter to heavier

chalcogens, as polarizability increases and electronegativity decreases (O < S < Se < Te). The σ-hole elongates the R–K bond and directs it towards the electron-rich species in a highly linear, directional arrangement, maximizing the interaction.

Other factors that influence this engagement are the steric and electronic characteristics of the substituent groups attached to the chalcogen atom. Also, due to their amphoteric nature (i.e. they exhibit both electrophilic and nucleophilic behaviours), chalcogens can participate in multiple chalcogen bonds at the same time. In summary, the key properties of chalcogen bonding are:[21]

a) Directionality: the geometry of the chalcogen bond is highly directional. The electrostatic interaction has a linear geometry that ensures maximal attraction between the σ-hole and the electron-rich region around lone pairs or a π-system, while minimizing repulsion between other electron-rich areas. The stronger the chalcogen bond, the shorter the distance between the chalcogen and the donor.

b) Tunability: chalcogen bonding strength can be easily tuned by modifying the substituent group R or the nucleophilic center, or by replacing the chalcogen atom (O, S, Se, or Te);

c) Hydrophobicity: Compared to traditional hydrogen bonds, chalcogen bond donors are more hydrophobic. The positive electrostatic potential on the chalcogen atom is often shielded by the attached covalent bonds, which limits the solubility of organochalcogen compounds in polar solvents or water;

d) Steric hindrance sensitivity: the larger atomic size of chalcogen atoms (with van der Waals radii ranging from 1.52 Å for oxygen to 2.06 Å for tellurium) compared to hydrogen (1.20 Å) makes chalcogen bonds more sensitive to steric hindrance. This difference leads to variations in physical and chemical properties between chalcogen bonds and hydrogen bonds, influencing how these interactions behave in various molecular and material contexts;

e) Multiplicity: Unlike hydrogen atoms, chalcogen atoms can exhibit multiple valence states, such as di-, tetra-, or hexa-valence, allowing for the formation of multiple chalcogen bonds.

These characteristics make chalcogen bonding interesting to study in fields like synthetic chemistry, catalysis and materials science where molecular interactions are crucial.

In material science, organochalcogens-containing compounds or coordination compounds showing chalcogen bonds have gained significant importance, since they often display unique properties such as enhanced electric and thermal conductivities. Recently, the effect of substitution using heavier chalcogen atoms, such as selenium or tellurium, with their larger atomic size and increased polarizability, showed great promise in the field of organic thermoelectric materials with inter- and intramolecular chalcogen bonding both in solution and in the solid state. This effect is also known as heavy atom effects.

5.1.2 The Heavy Atom effect

During the last decades, many strategies were proved to be effective in enhancing thermoelectric properties of organic materials. Among these, the effect of substitution of an heavier atom (heavy atom effect) inside the monomeric structure (and polymeric after) has received more and more attention.

Polymers incorporating Group 16 heterocycles such as furan, selenophene, and tellurophene (chalcogenophenes, shown in figure 5.3) have gained significant attention in organic electronics.

Figure 5.3: Chalchogenophenes family, from left to right (furan, thiophene, selenophene, tellurophene).

Through Polythiophene and its derivatives, notable progresses in understanding how molecular structure, solid-state organization, and electronic performance interact in CPs were made. Substituting heteroatoms in polythiophenes can lead to improve the performance of the device and control self-assembly, optoelectronic and transport properties, providing valuable insights into designing CPs with desirable properties.

Due to their larger atomic radius and higher polarizability, Se and Te are more likely to engage in intermolecular interactions through their lone pairs, which can enhance charge transport.

For example, strong Te–Te interactions are found in the crystal structures of 3,4-dimethoxytellurophene.[22] The latter could also play a crucial role in the molecular organization and solid-state morphology of polytellurophenes. In comparing the structural, magnetic, energetic, and electronic properties of aromatic rings, the trend of aromaticity is as follows: benzene > thiophene > selenophene > tellurophene > furan. Aromaticity profoundly impacts the thermodynamic stability and reactivity of these heterocycles, with electrophilic aromatic substitution rates inversely related to aromaticity.

In this perspective, heavy atom effects can be used to improve intermolecular interactions, control quinoidal resonance properties, expand bandwidths, and adjust diradical characters, all of which have a substantial impact on organic optoelectronic devices. Additionally, the incorporation of heavy atoms has been shown to facilitate charge transfer, enhance air stability, and boost device performance in the realm of organic thermoelectrics (OTEs).[23]

As we move from S to Se to Te, the Van Der Waals radii increase from 1.80 to 1.90 to 2.10 Å, while their electronegativities decrease from 2.58 to 2.55 to 2.10 on the Pauling scale. The larger atomic radii of heavier atoms in this series result in stronger interactions between atoms, thereby enhancing both intramolecular and intermolecular interactions. The larger atomic radius of heavy atoms enhances the interaction between them and their neighbouring atoms in the conjugated framework, resulting in more effective electron orbital overlap. This leads to better molecular stacking and an increased bandwidth.

Consequently, introducing heavier atoms with larger atomic sizes into the conjugated backbone gradually strengthens molecular interactions, impacting the optoelectronic and thermoelectric properties. The lack of strong intermolecular interactions in organic semiconductors limits charge transport and electrical conductivity. However, introducing heavy atoms can significantly improve these interactions.

Widening the bandwidth typically raises the electronic energy levels, thereby improving the electrical conductivity of organic semiconductors. This is particularly important for devices like organic field-effect transistors and organic solar cells, where wider bandwidth is associated with higher electron mobility and broader absorption spectra. By controlling the bandwidth through heavy atom substitution, the electronic structure of OSCs can be modulated, improving charge transport, optimizing device performance, and enhancing their response to light across various wavelengths.

For instance, quinoidal bithiophene (QBT) and the selenium analogue quinoidal biselenophene (QBS) were recently tested as bipolar organic field-effect transistor materials.[24] The difference in sulphur and selenium showed a high impact on the macroscopic properties. More specifically, QBS showed higher crystallinity and stronger diffraction peaks than QBT, indicating a higher degree of crystallinity likely due to the stronger intermolecular interactions from selenium atom. AFM images revealed that annealed QBS films had larger domain sizes and rougher surfaces, while QBT remained amorphous.

In 2019, Ding et al. reported enhanced thermoelectric performance of selenium-substituted diketopyrrolopyrrole (DPP) derivatives. PDPPSe-12 achieved a power factor of 364 $mWm^{-1}K^{-2}$ and a ZT of 0.25, more than doubling the performance of sulphur-based DPP derivatives, setting a new record for p-type organic thermoelectric materials.[25]

On the molecular level, the exchange for heavier heteroatoms (Se, Te) moves the equilibrium towards the quinoidal form (scheme 5.1), improving molecular planarity and broadening electron delocalization, which facilitates electron transport and positively impacts optoelectronic properties.

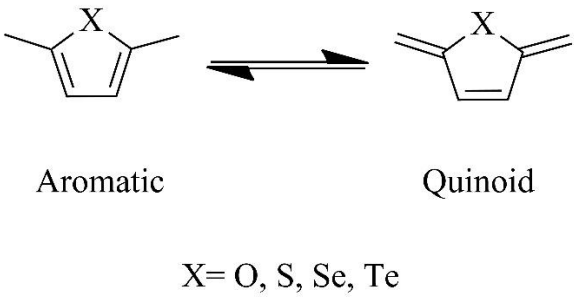

Scheme 5.1: quinoidal and aromatic equilibrium of chalcogenophenes.

Patra et al. demonstrated the advantages of the selenium analogue PEDOS (poly(3,4-ethylenedioxyselenophene)), showing that replacing sulphur with selenium in PEDOS enhanced the quinoidal character.[26] This computational study calculated that a higher twisting energy for PEDOS was required due to its better planarity and shorter C─C bond in the inner ring.

Moreover, when quinoidal chalcogenophenes go from a quinoidal structure to an aromatic structure, they acquire two unpaired electrons, forming diradicals.[27,28] A recent study showed that the presence of heavy atoms enhances these diradical characteristics, effectively promoting charge delocalization, improving the air stability of n-doped devices, and potentially enhancing thermoelectric performance.[29] It reported the use of quinoidal oligothiophene (QOT)-based 2DQQT-S and 2DQQT-Se, where heavy atom incorporation resulted in longer C─C double bonds and shorter C─C single bonds, enhancing diradical properties. Due to the larger size of selenium, 2DQQT-Se exhibited more enhanced spin delocalization, and its electron paramagnetic resonance (EPR) signal was broader than that of 2DQQT-S. NMR spectra indicated that the conjugate skeleton of 2DQQT-Se was more shielded, further supporting the difference in diradical properties between the two molecules. Quantum chemical calculations revealed that the open-shell diradical states of both 2DQQT-S and 2DQQT-Se were more

energetically favourable than their closed-shell states and that partially separated singly occupied molecular orbitals (SOMOs) in both compounds were delocalized across the conjugated chain, which might enhance charge transport and electrical conductivity. The small energy differences between the open-shell singlet and triplet states (3.74 kcal/mol for 2DQQT-S and 3.56 kcal/mol for 2DQQT-Se) indicate that these compounds exhibit paramagnetic properties, which can be thermally activated at room temperature, as shown by strong EPR signals at g=2.00595 and 2.00719.

5.1.3 Aim of the project

Taking inspiration from the successful incorporation of additional physicochemical properties into eumelanin polymers, such as 3-thioglycomelanin (described in Chapter 3), and the influence of heavy atoms in the chalcogenophenes series, this project set out to develop a new class of melanin monomers that integrate chalcogen elements, particularly sulphur and selenium.
By introducing functional groups derived from these elements, the aim was to enhance both the physicochemical and biological properties of the polymerized eumelanin.
The project was structured as follows:

- Identify a set of eumelanin monomers that could be easily functionalized with chalcogen-based groups, such as sulphur and selenium;
- Investigate the effects of these functional groups on the stability and reactivity of the monomers;
- Polymerize the monomers to produce the corresponding melanin and analyse its physicochemical properties, with particular focus on how the incorporation of heavy atoms influences melanin's conductivity, redox properties, and free-radical behaviour.

The project identified, as we will briefly discuss, suitable chalcogen-based groups which can be easily attached to the catecholindole C-3-position from commercially available products serving as sources of thiocyanate and selenocyanate groups. The adopted strategy is better depicted in figure 5.4, where *O*-protected monomers are first chemically modified and then allowed to polymerize to obtain the corresponding chalcogen-loaded material.

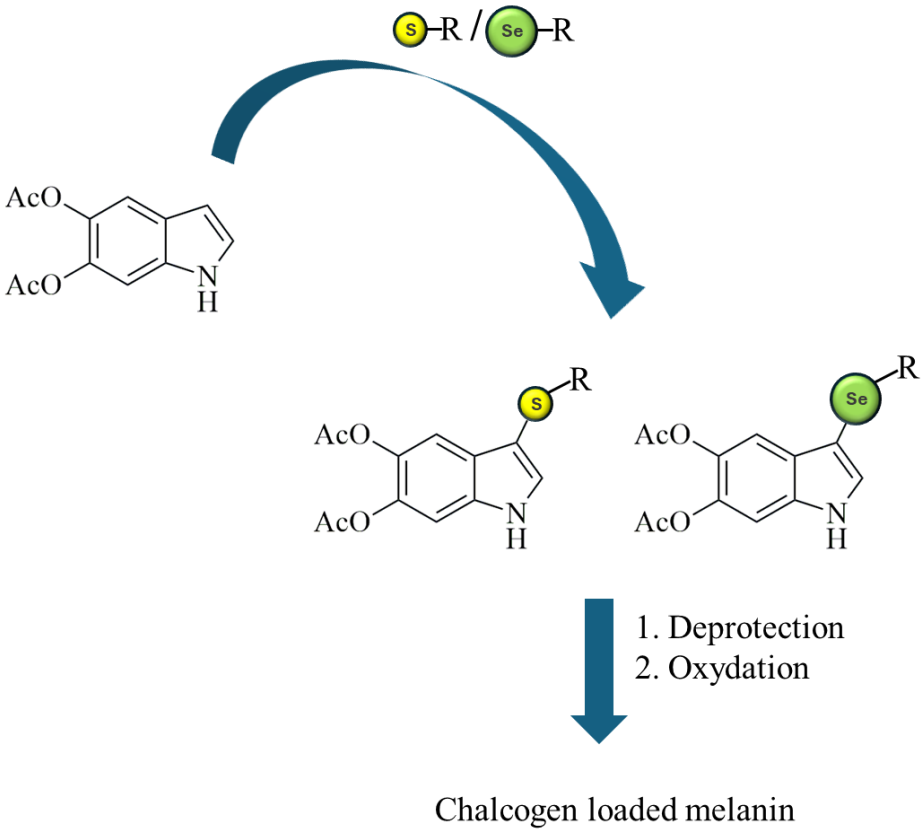

Figure 5.4: Strategy for the study of chalcogen-loaded melanin.

5.2 Results and discussion

5.2.1 Synthesis of chalcogen-containing eumelanin monomers and polymers

At this point, the identification of chalcogen containing melanin monomers was taken into account. The 3-thiocyanate-5,6-diacetyloindole (DAISCN, figure 5.5) is an already known compound, previously reported from my research group.[30]

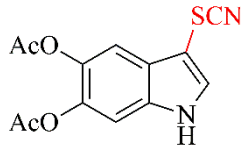

Figure 5.5: 3-thiocyano-5,6-diacetoxyindole (DAISCN).

The synthesis is based on the exposure in dry methanol of 5,6-diacetoxyindole (DAI) to a thiocyanate salt (NH_4SCN) in the presence an oxidizing agent known as oxone, which is indeed a mixture of three salts including potassium peroxymonosulphate ($2KHSO_5 \cdot KHSO_4 \cdot K_2SO_4$). The synthetic procedure results to be very efficient in terms of isolated yields (up to 90%),and reduced experimental effort (the reaction is complete in less than three hours and the product is purified through a fast liquid-liquid extraction).

For these reasons we started to identify other chalcogen analogues of DAISCN. Since selenocyanate salts are easily available, the instalment of selenocyanate on the 3-position of DAI was taken into account.

Albeit selenocyanate and thiocyanate groups in literature are described to have the same reactivity, 3-substituted selenocyano-indoles molecules could lead to a more reactive and activated soft group rather than thiocyanate. The synthesis of the 3-selenocyanate 5,6-dihydroxyindole was performed successfully using potassium selenocyanate salt in the presence of the same oxidizing agent in dry methanol (Scheme 5.2), with an isolated yield of 60% in 3h time of reaction.

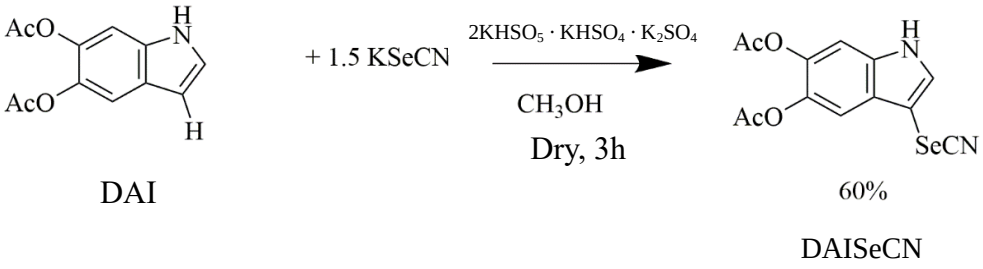

Scheme 5.2: synthetic reaction scheme of DAISeCN.

In figure 5.6 are summarized the structures of the monomers (DAI, DAISCN, and DAISeCN) that were then elaborated:

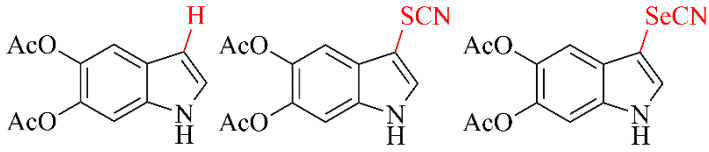

Figure 5.6: (left) 5,6-diacetoxyindole (DAI); (center) 3-thiocyano-5,6-diacetoxyindole (DAISCN); (right) 3-selenocyano-5,6-diacetoxyindole (DAISeCN).

5.2.2 Polymerization of DAI, DAISCN and DAISeCN and film surface characterization

To synthesize the respective eumelanins, two approaches of polymerization are possible. The first approach involved a classic Zemplen O-deprotection strategy in methanol, followed by an attempt to adjust the pH and finally extract the solution with an appropriate organic solvent to obtain the O-deacetylated monomers (scheme 5.3). Then, the final step involved the treatment with AISSP (Ammonia-Induced Solid-State Polymerization)[31] of the deposited films.

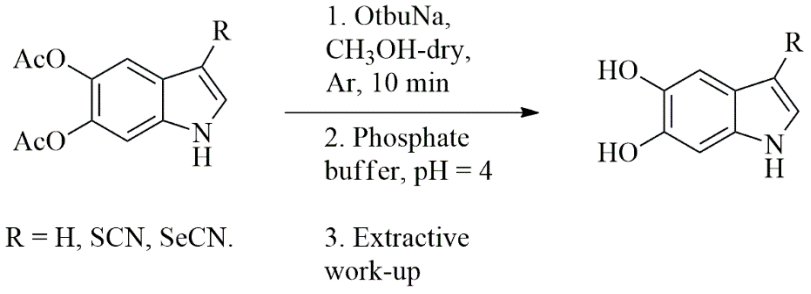

Scheme 5.3: 1st designed strategy for the O-deacetylation procedure to obtain eumelanin monomers.

This strategy had both advantages and disadvantages, such as a high number of steps and uncertainty regarding the amount of material extracted, which made it

difficult to control the film formation, although it ensured the removal of acetate salts.

The second alternative procedure involves performing AISSP directly on films of the O-protected monomers, bypassing a multi-step O-deprotection strategy that required controlled atmosphere and long times. In this way, we thought that AISSP could act as both O-deprotecting and polymerizing procedure in the solid-state in a single step. Specifically, our hypothesis suggests that the ammonia vapours, condensing on the film surface, could create a sufficiently alkaline environment to simultaneously deprotect and oxidize the material (scheme 5.4).

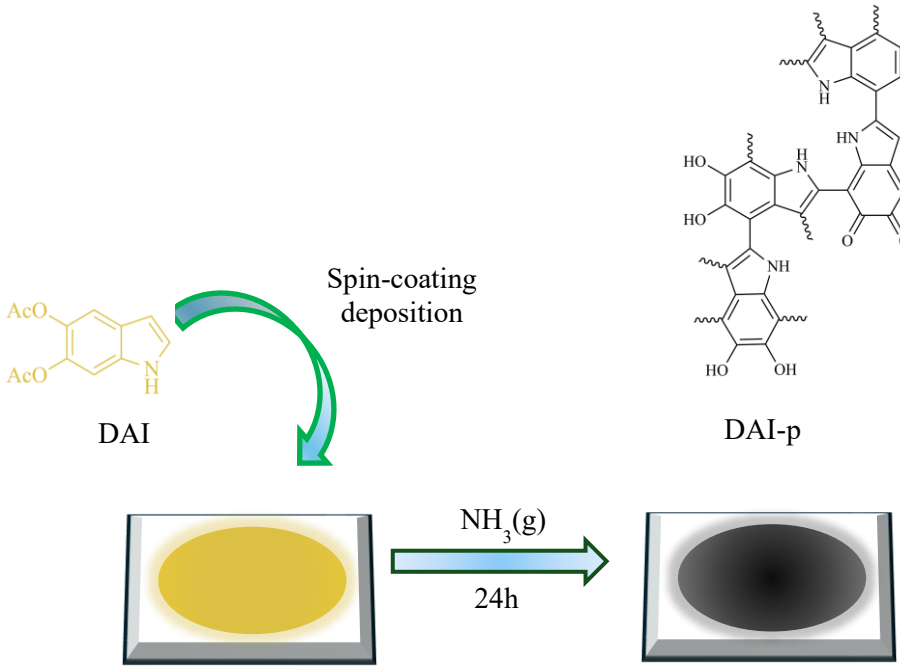

Scheme 5.4: Synthesis of DAI-p films.

For simplicity, we attempted this second option, exposing drop-casted deposited films of acetylated monomers to ammonia vapours for 24 hours. After this treatment, we observed complete darkening of the samples (figure 5.7).

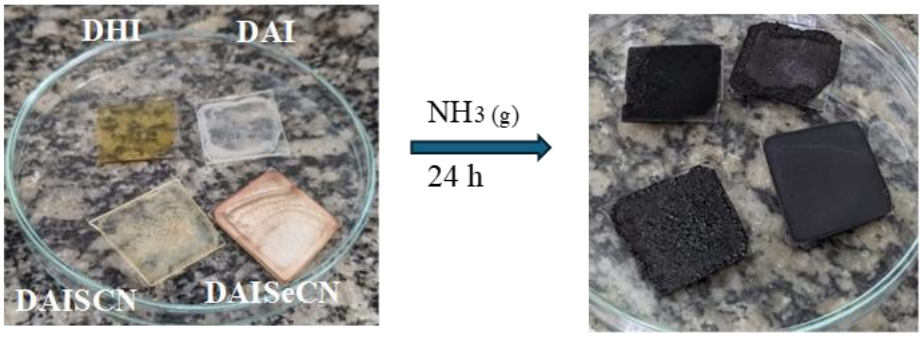

Figure 5.7: drop-casted samples of DHI, DAI, DAISCN DAISeCN before (left) and after (right) AISSP treatment.

Considering 5,6-diacetoxyindole, treatment with this process would lead to the formation of acetate salts and deacetylated catechol, which, when exposed to ammonia vapours, polymerizes to yield the corresponding eumelanin product.

DAI, DAISCN, and DAISeCN polymers (denoted from now on as DAI-p, DAISCN-p and DAISeCN-p) were synthesized using the AISSP technique. The process started with a spin-coating deposition of the O-protected eumelanin monomer films on glass substrates, followed by exposure to ammonia vapours for 24 hours to induce polymerization and, afterwards, a drying procedure.

Interestingly, the film morphology differed significantly (see Figure 5.27 A, B, and C, Materials and Methods). DAI-p exhibited a hill-like, heterogeneous, and spotty surface with a high external contact area, while the surfaces of DAISCN-p and DAISeCN-p presented a more homogeneous pattern. The surface of DAISCN-p showed wrinkle-like features, whereas DAISeCN-p had a flatter and uniform surface, suggesting a densely packed arrangement, likely due to stronger internal noncovalent interactions found in heavy chalcogens organic materials.[32]

Moreover, DAI exhibited a different adhesion from the other two samples. The latter remained more attached to the substrate during the deposition. The different kinetics of polymerization and darkening were observed as follows: DAI > DAISCN > DAISeCN.

5.2.3 UV-Vis-NIR measurements of DAI, DAISCN and DAISeCN films

The observed phenomenon of darkening of the O-protected monomers DAI, DAISCN and DAISeCN through AISSP treatment was investigated performing UV-Vis-NIR spectroscopy on quartz substrates. DAI, DAISCN, and DAISeCN were deposited through spin-coating, exposed to ammonia vapours, heated for 15 minutes at 100°C and investigated at different times of exposure (0h, 1h, 4h and 24h) (figure 5.8, figure 5.9 and figure 5.10).

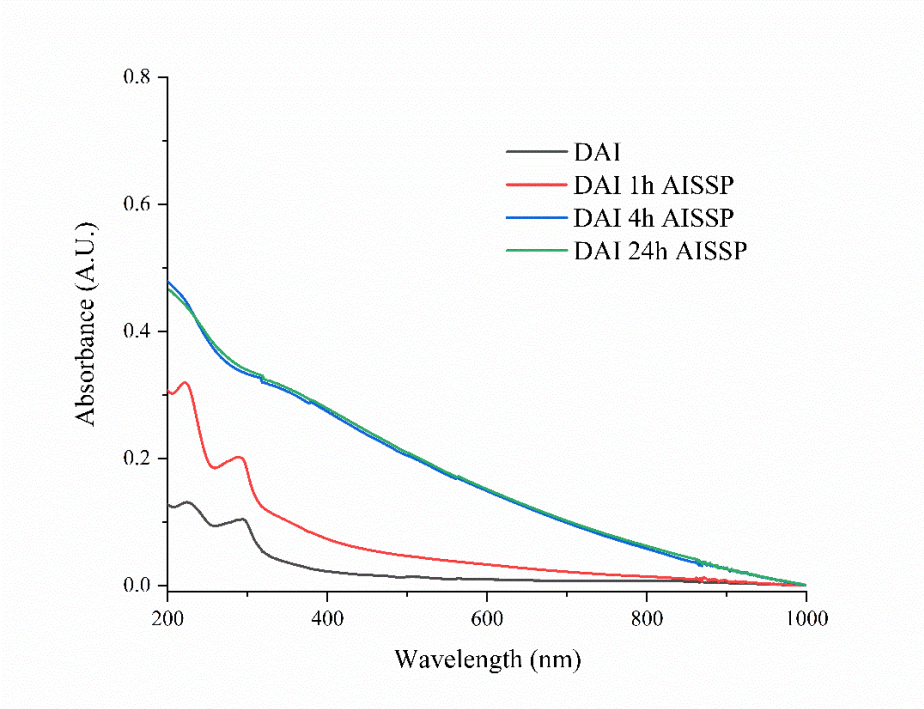

Figure 5.8: UV-Vis spectra of DAI films. Black, red, blue and green lines represent, respectively, 0h, 1h, 4h and 24h of AISSP for each sample.

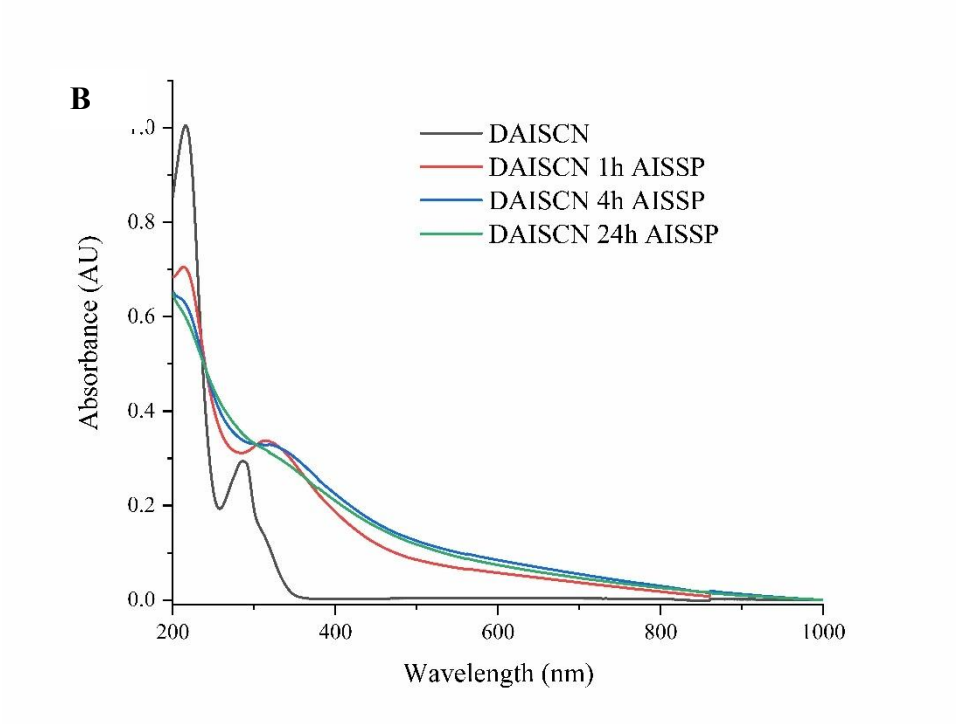

Figure 5.9: UV-Vis spectra of DAISCN films. Black, red, blue and green lines represent, respectively, 0h, 1h, 4h and 24h of AISSP for each sample.

C

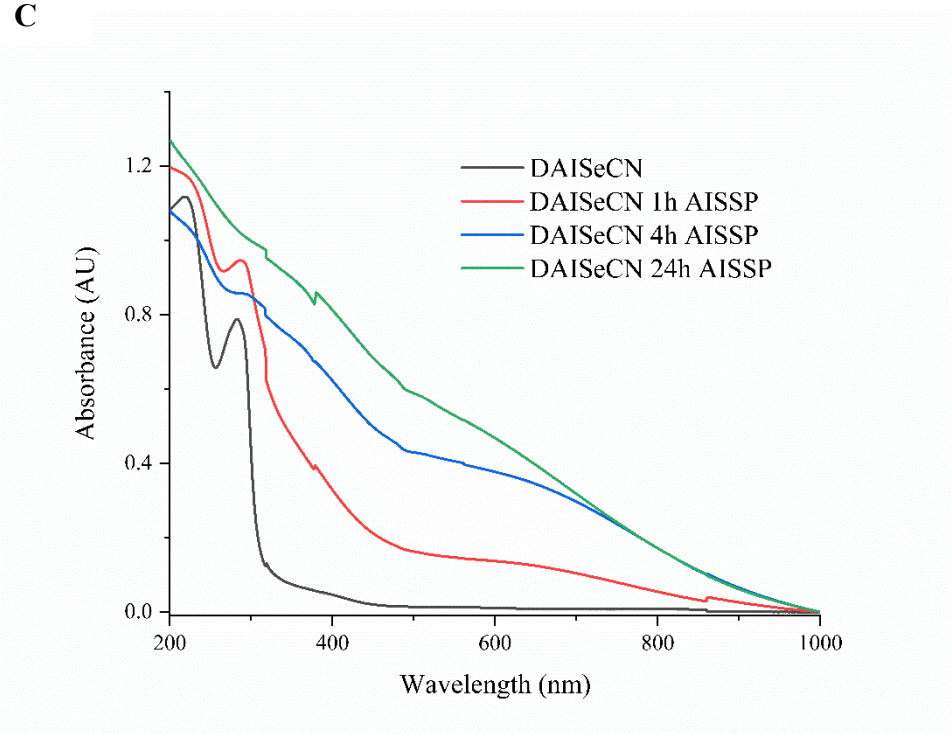

Figure 5.10: UV-Vis spectra of DAISeCN films. Black, red, blue and green lines represent, respectively, 0h, 1h 4h and 24h of AISSP for each sample.

In all the samples (figure 5.8, figure 5.9 and figure 5.10) similar UV-Vis spectra are shown at time 0 (black lines), exhibiting two maximum peaks at around λ = 220 nm (max 1) and λ = 290 nm (max 2), although the different height ratio of absorption between these two peaks are characteristic of each sample (A_{max1}/A_{max2}). After 1h (figure 5.8, figure 5.9 and figure 5.10 red lines) the broadening of the spectra started, showing an increase of absorption in the near UV and visible region. After 4h and 24h (Figure 5.8 A, B and C green lines), the UV-Vis spectra of all the samples indicates the successful polymerization of the

eumelanin-like polymers, characterized by the almost linear broad absorption band in the UV-Visible region.

5.2.4 Cyclic voltammetry measurements

To analyse the electrochemical behaviour of the material as a function of polymeric content, cyclic voltammetry (CV) was performed after different times of exposure to ammonia vapours (0h, 1h, 24h). A solution containing DAI, DAISCN, and DAISeCN (0.1 mg in total) in acetonitrile/methanol 1:1 was drop-casted onto a glassy carbon electrode (used as working electrode), then allowed to dry and exposed to ammonia vapours. The modified electrode was subsequently characterized using a three-electrode setup for CV measurements, as depicted in figure 5.11, using a platinum mesh as counter electrode and Ag/AgCl as reference electrode. The CV scans were performed over three cycles (in the following graphs the 3rd acquisition is reported), with the potential range set between 0 V and -1 V, at a scan rate of 0.01 V/s, in a 1 M Na_2SO_4 solution at pH 7.0.

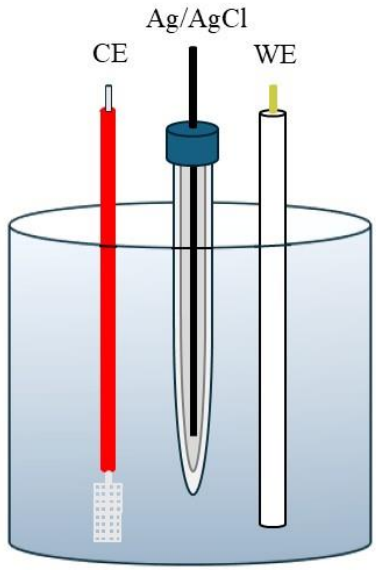

Figure 5.11: typical architecture of the electrochemical cell used for cyclic voltammetry. A glassy carbon electrode is shown on the right and used as working electrode (WE). On the left a platinum mesh is used as counter electrode (CE). As reference electrode (RE) an Ag/AgCl electrode was used and 1 M Na_2SO_4 buffer solution at pH 7.0 as electrolyte solution was used.

Figure 5.12, figure 5.13 and figure 5.14 illustrate the CV profiles of the studied derivatives, revealing, in general, an absence of well-defined oxidation and reduction peaks. This observation suggests a broad distribution of monomers or oligomers, each characterized by slightly varying redox potentials. Such diversity likely arises from the structural heterogeneity introduced during eumelanin derivative polymerization, resulting in voltammograms that represent overlapping redox events rather than distinct, sharp peaks.[33,34] This characteristic impacts the

materials' capacitance, as indicated by the CV curve areas, which reflect charge storage largely dominated by pseudocapacitive behaviour instead of discrete redox processes.

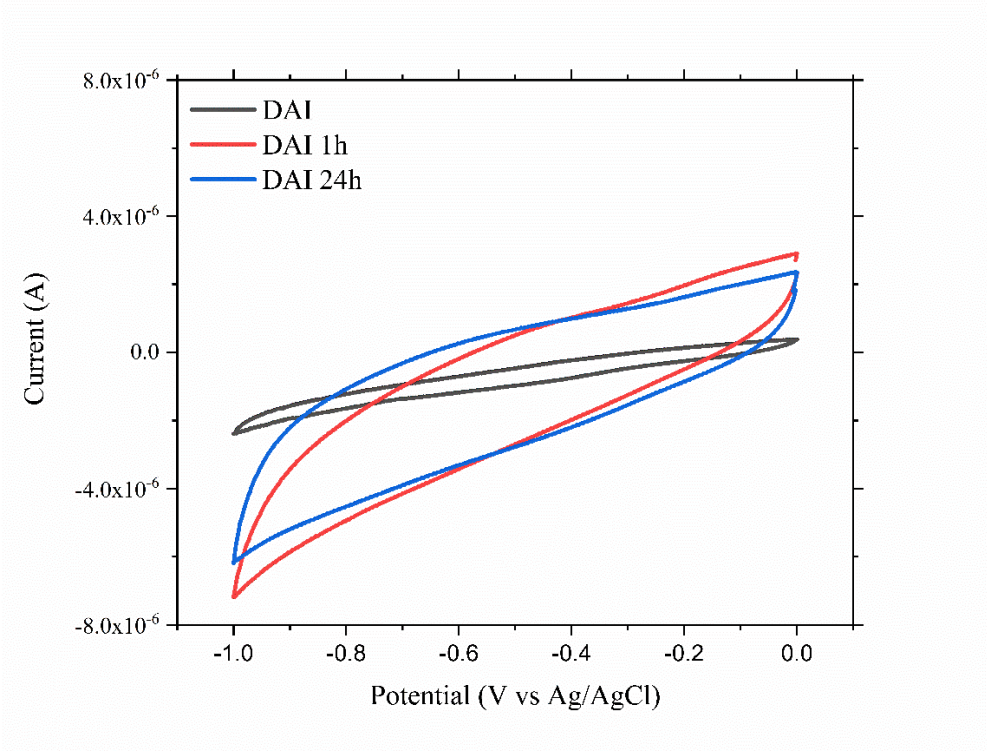

Figure 5.12: cyclic voltammetry of DAI at 0 h (black line), 1 h (red line), and 24 h (blue line) of AISSP.

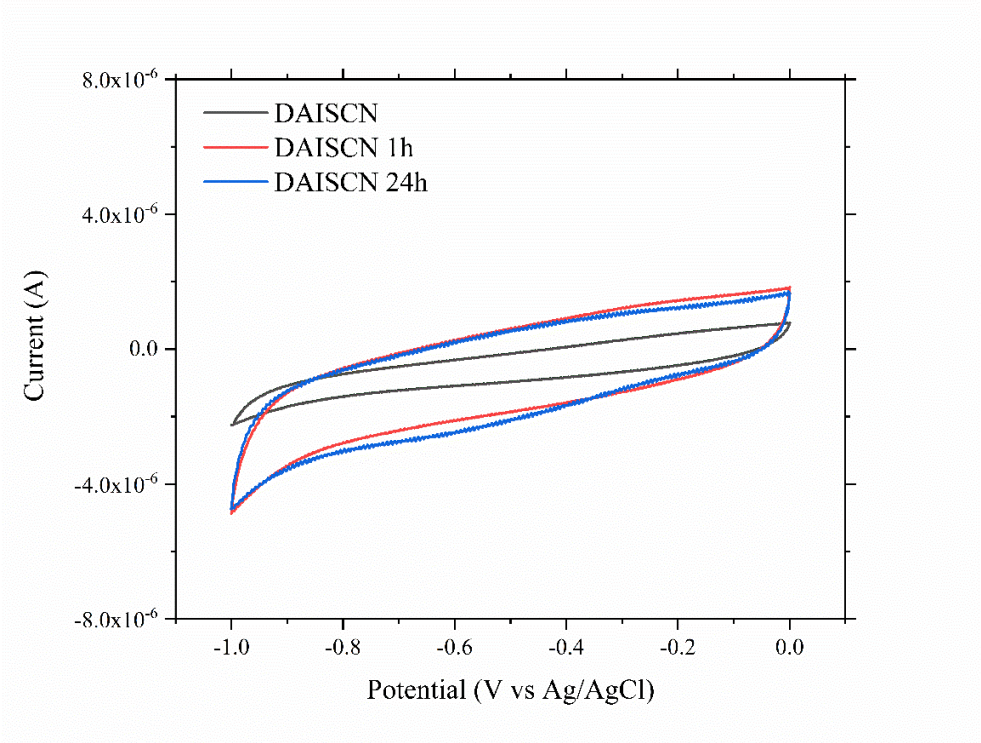

Figure 5.13: cyclic voltammetry of DAISCN at 0 h (black line), 1 h (red line), and 24 h (blue line) of AISSP.

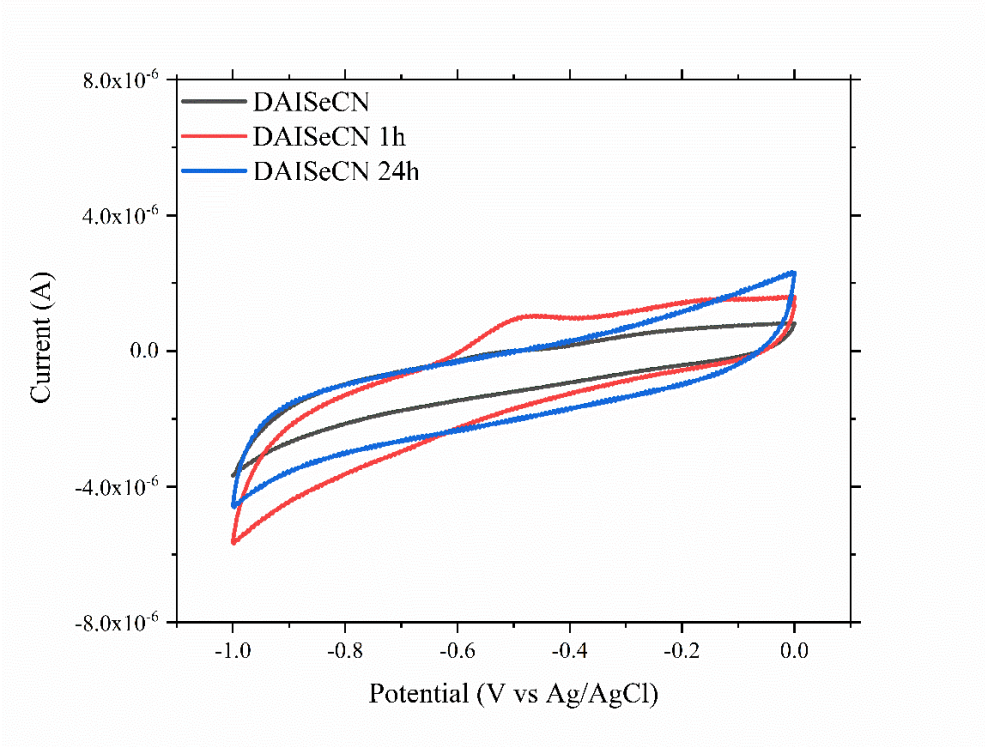

Figure 5.14: cyclic voltammetry of DAISeCN at 0 h (black line), 1 h (red line), and 24 h (blue line) of AISSP.

A fascinating case is observed in the case of DAISeCN. After 1 h of AISSP (figure 5.12), a clear peak is shown at approximately - 0.55 V. This distinct feature may indicate a more uniform oxidation process at this stage, potentially arising from the transient stabilization of specific molecular structures or intermediates facilitated by the presence of SeCN group.[34] The latter appears to enhance charge delocalization and promote uniform molecular interactions, favouring a distinct oxidation pathway. However, as polymerization progresses to 24 h, this peak

broadens and diminishes, reflecting the increasing complexity and heterogeneity within the polymer network.

A comparative analysis highlights distinct trends in current and capacitance behaviours, reflecting the influence of molecular structure on electrochemical performance. For DAI, the current shows the most significant increase over time, indicating enhanced charge transfer and conductivity as polymerization progresses. This behaviour is attributed to the efficient formation of a highly interconnected polymer network in the unmodified eumelanin structure.[35] Correspondingly, the capacitance of DAI also increases substantially. The unmodified structure appears to facilitate both charge transfer and charge storage, optimizing its electrochemical performance and underscoring the benefits of its simplicity in network formation.

In the case of DAISCN, current variations over time are less pronounced. This limitation is likely due to steric or electronic constraints introduced by the SCN group, which may hinder effective network reorganization and restrict charge transfer. Similarly, the capacitance shows minimal changes, suggesting that the steric hindrance or electronic effects imposed by the SCN group also impede the material's ability to develop an optimized polymer network for efficient charge storage.[36–38] These combined effects highlight the challenges posed by the SCN substituent in enhancing electrochemical properties. Conversely, DAISeCN exhibits the highest initial current at 0 h, reflecting the unique electronic properties of the SeCN group, which enhances charge delocalization and facilitates initial charge transfer. However, as polymerization proceeds, the current stabilizes more quickly, suggesting that the material achieves an early equilibrium in its polymer network. This rapid stabilization is mirrored in the capacitance behaviour. DAISeCN displays the highest initial capacitance, likely due to the electron-donating properties of the SeCN group, which enhance charge delocalization and improve electrochemical responsiveness.[7,39] Nevertheless, its capacitance shows

limited improvement over time, indicating that the structural complexity and heterogeneity of the polymer network increase less significantly during prolonged polymerization.

5.2.5 EPR analysis of DAI-p, DAISCN-p and DAISeCN-p

Electron paramagnetic resonance (EPR) spectroscopy is a crucial tool for investigating the structure and paramagnetic properties of functionalized eumelanin.[40,41] It reveals how modifications affect its paramagnetic centres and helps elucidate the origin of its persistent paramagnetism, offering valuable insights for designing eumelanin-based materials.

Table 5.1 summarizes the experimental EPR spectral features from Figure 5.15 for DAI, DAISCN, and DAISeCN. The g-value is 2.0029 for DAI, while for DAISCN and DAISeCN, the values are 2.0044 and 2.0043, respectively. This similarity between DAISCN and DAISeCN suggests comparable electronic effects from the thiocyano and selenocyano groups. Interestingly, the g-value for DAI aligns with the CCR species of standard eumelanin, whereas the higher values for DAISCN and DAISeCN could correspond to the SFR species, reflecting enhanced delocalization of the unpaired electron or stronger interactions with functional groups.[41] This shift suggests that in the functionalized samples, the radical species tend to reside on oxygen atoms or within the functional groups rather than being localized on carbon atoms.

	DAI-p	DAISCN-p	DAISeCN-p
g-value (unitless)	2.0029	2.0044	2.0043
ΔH_{PP} (mT)	0.3028	0.6243	0.5755
ΔY_{PP} (unitless)	1.1153	1.040	0.7825
Spin concentration 10^{15} (spin/mg)	5.64	1.91	5.92

Table 5.1

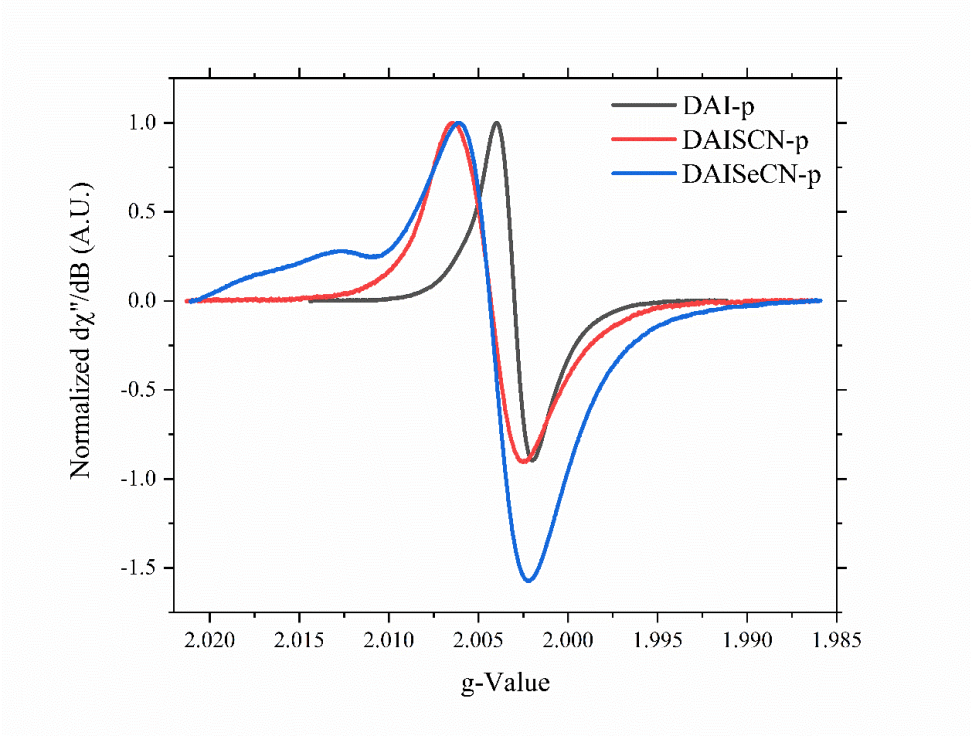

Figure 5.15: X-band solid-state EPR spectra of the 24h polymeric powder of DAI (black line), DAISCN (red line) and DAISeCN (blue line) at microwave power of 0.1 mW

The peak-to-peak linewidth (ΔH_{PP}), that reflects the magnetic environment of the radicals, increases significantly for DAISCN (0.6243 mT) and DAISeCN (0.5755 mT) compared to DAI (0.3028 mT). This broadening may be attributed to enhanced spin-spin interactions or greater inhomogeneity in the local magnetic field due to the functional groups. Additionally, the signal symmetry (ΔY_{PP}), related to the shape of the EPR peak, decreases from 1.1153 for DAI to 1.040 for DAISCN and 0.7825 for DAISeCN. This trend suggests a potential increase in structural rigidity or changes in spin dynamics introduced by the functional

groups, with the lowest ΔY_{PP} value for DAISeCN pointing to a more restricted microenvironment.

The spin concentration follows the trend: DAISeCN ≈ DAI > DAISCN. DAISCN displays a significantly lower spin concentration, possibly due to the stabilization or quenching of radical centres by the thiocyano group. However, caution is needed when interpreting these spin concentration values, as they may not quantitatively reflect the actual spin concentration in the system due to the absence of atmospheric control during the measurements. This limitation arises because of the presence of water can influence the comproportionation reaction equilibrium, leading to variations in spin concentration.[41] However, the line shape is independent of atmospheric conditions, as supported by the literature.[42]

Figure 5.16, figure 5.17 and figure 5.18 present the X-band EPR spectra of DAI-p, DAISCN-p, and DAISeCN-p recorded across a range of microwave power levels from 0.1 to 31.6 mW to evaluate spin relaxation dynamics influenced by the surrounding chemical environment. With increasing microwave power, a shoulder-like feature emerges on the positive peak side, corresponding to higher g-values (lower magnetic field). This behaviour respects eumelanin and eumelanin-inspired systems, where multiple paramagnetic species with similar g-values but differing spin-lattice relaxation rates contribute to the signal.[43,44]

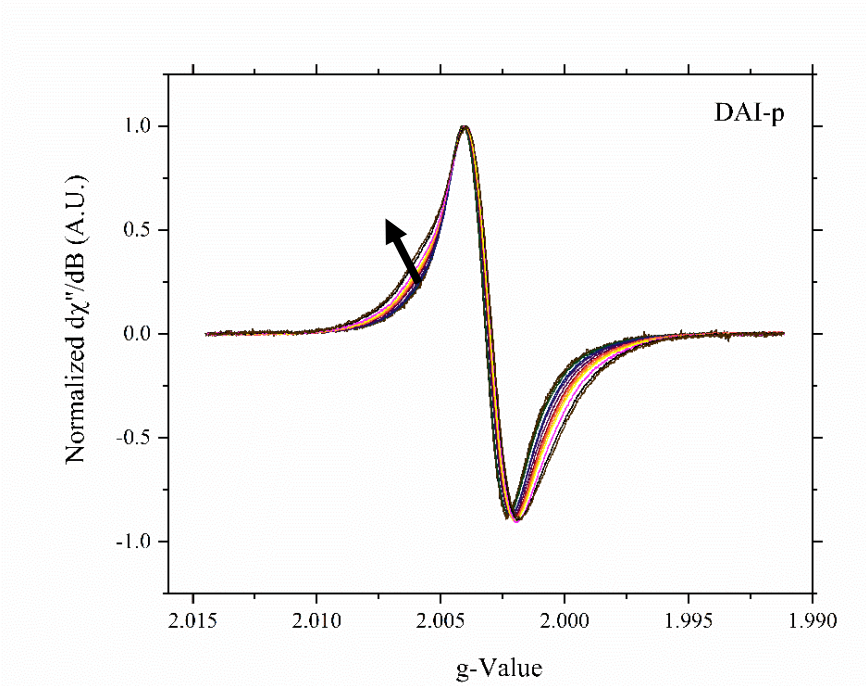

Figure 5.16: X-band EPR spectra with microwave power ranging from 0.1 to 31.6 mW for (a) DAI-p. All spectra display comparable g-values, with the arrow highlighting the emergence of a shoulder-like feature that becomes more pronounced as the microwave power increases.

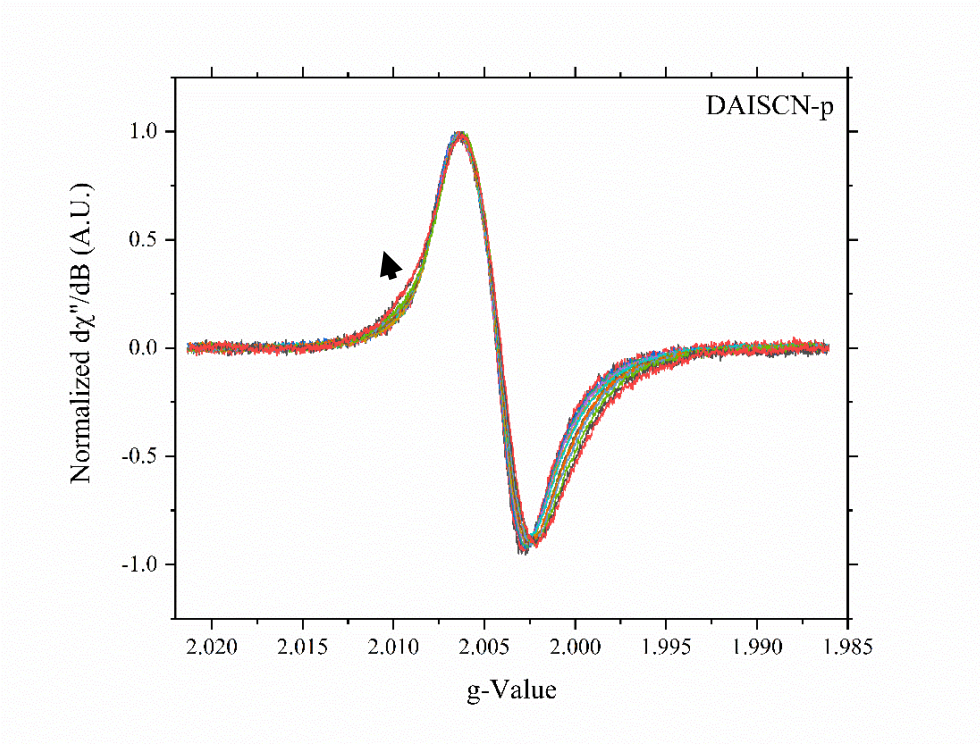

Figure 5.17: X-band EPR spectra with microwave power ranging from 0.1 to 31.6 mW for DAISCN-p. All spectra display comparable g-values, with the arrow highlighting the emergence of a shoulder-like feature that becomes more pronounced as the microwave power increases.

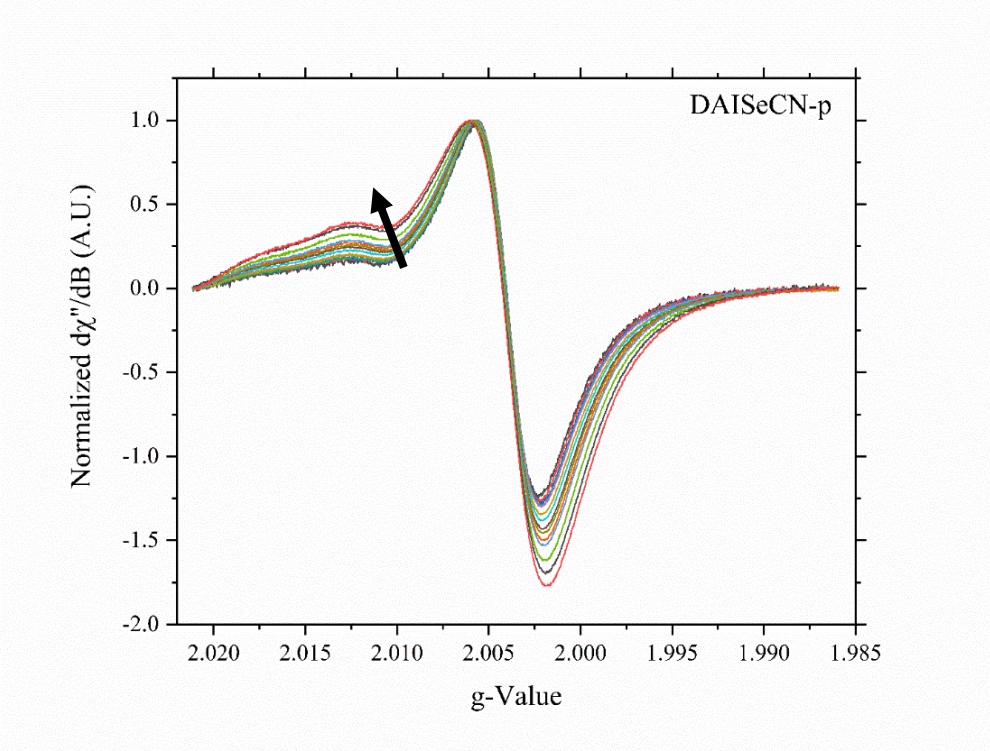

Figure 5.18: X-band EPR spectra with microwave power ranging from 0.1 to 31.6 mW for DAISeCN-p. All spectra display comparable g-values, with the arrow highlighting the emergence of a shoulder-like feature that becomes more pronounced as the microwave power increases.

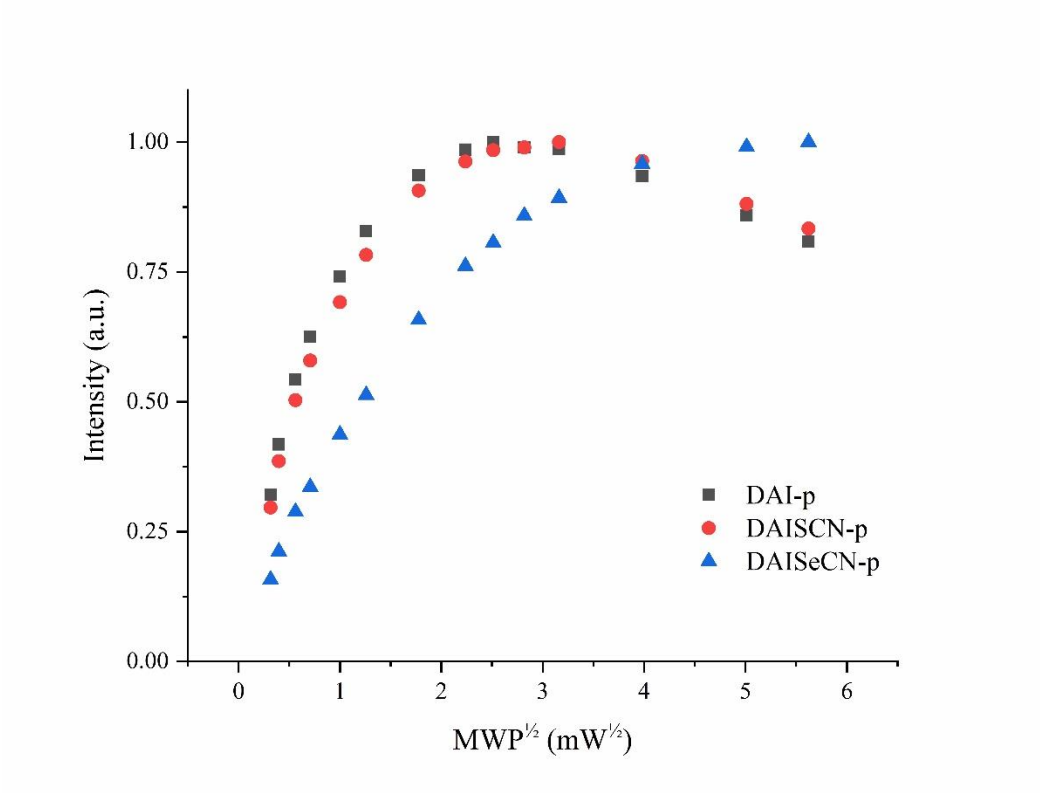

Figure 5.19: normalized signal amplitude plotted as a function of the square root of the microwave power for DAI-p, DAISCN-p, and DAISeCN-p.

Inspection of the saturation profiles highlights contrasting behaviours (figure 5.19). For DAI-p and DAISCN-p, as increasing the microwave power the signal intensity rises to a maximum before decreasing at higher microwave power levels. This behaviour is consistent with the saturation profile of homogeneous paramagnetic systems, where spin relaxation processes are relatively uniform across the sample. Indeed, such a profile suggests that these systems exhibit minimal variations in their local electronic environments, resulting in relatively

consistent spin-lattice relaxation dynamics. This uniformity likely stems from the nature of the SCN functional group, which introduces modest electronic effects while maintaining a balanced paramagnetic center distribution. In contrast, DAISeCN-p exhibits a different trend, with the signal intensity increasing with microwave power until reaching a plateau, indicative of an inhomogeneous distribution of paramagnetic centers, which points to a more complex local electronic environment.

To have a deeper understanding of these experimental observations, we are planning to combine EPR spectral simulations with density functional theory calculations to achieve a more comprehensive understanding of the samples' properties. These analyses are expected to clarify the nature of the paramagnetic centers, the influence of functional groups, and the electronic environment, offering valuable insights that complement the experimental findings.

5.2.6 Polymerization reaction of DAISCN in oxidant-free atmosphere

To investigate the activation of a unique functional group, such as the thiocyanate group on the C-3 position of 5,6-dihydroxyindole ring, and to explore the types of interactions that can be formed in a highly electron-rich environment at elevated pH levels for DAISCN, we performed a particular polymerization reaction in a specific reaction setup.

In this setup, DAISCN was exposed to a reaction environment that was *O*-deacetylating, deprotonating, and non-oxidizing at the same time. The experiment was conducted under an oxygen-free, argon-filled atmosphere, using *O*-deacetylating aqueous conditions (0.1 M phosphate buffer at approximately pH 12). The choice of conditions is key for several reasons: the argon atmosphere prevents oxidation of the product and the formation of eumelanin-derived polymers, while the highly alkaline environment promotes the de-*O*-acetylation at positions 5 and 6 of the DAISCN molecule. At that pH, after the deacetylation and considering the second pKa of 5.6-dihydroxyindole (between 12.1 and 13.1),[45,46] we should be in presence of at least one negative charge that activates the aromatic ring of the monomer.

After work-up and overnight acetylation of the reaction, we analysed the formation of reaction products. The crude was purified by silica chromatography and yielded to a yellowish product with a very low retention factor (3% mass yield, with 80% recovery of DAISCN). This suggests that, alongside the eumelanin formation typically observed from 5,6-dihydroxyindoles, thiocyanate group at this

level of pHs can participate in an orthogonal chemistry, activating the thiocyanate group and influencing the reaction's outcome.

Surprisingly, ^{1}HNMR analysis of this yellow product (from now on YA) showed the presence of only 3 singlets in the aromatic region between 9.0-6.5 p.p.m. suggesting a highly symmetric product (figure 5.28, see materials and methods). Further investigation of the nature of this compound using ^{13}CNMR, HSQC and HMBC bidimensional (figure 5.29, see materials and methods) spectra showed the lack of the proton that was present on the 2-position. On the base of this data, an important guess about the structure of YA is represented by a calix[n]arene-like structure (figure 5.20), a cyclic compound of n subunits that has been of huge interest in bioelectronics for the development of highly sensitive biosensors.[47,48]

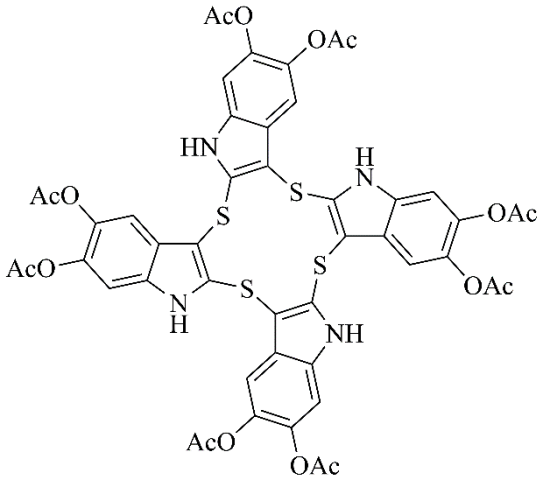

Figure 5.20: proposed calix[4]arene-like structure.

In the hypothesis of calixarene-like systems, it is not possible to conclusively attribute the structure without exact molecular mass. However, until now, mass experiments carried out with MALDI-TOF and LC/MS did not lead to any conclusive clue about the exact ionic mass of the product, thus the number of structural subunits is still to be clarified.

An important proof of the presence of soft elements in the structure of YA was given by UV-Vis spectra analysis in presence of silver salts (Figure 5.21 left). Adding silver triflate to a 0.2 mg/mL solution of YA impacted on its UV-Vis spectrum, sharply increasing UV-Vis bands at 214 nm and 256 nm (Figure 5.21 right). This suggests that silver ions chemically interact with YA via a soft-soft interaction between Ag+ ion and the sample.

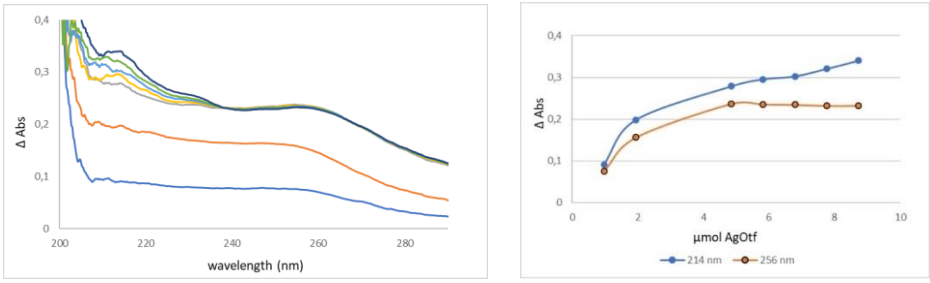

Figure 5.21: (Left) Absorption profile changes of **YA** (0.2 mg/mL) upon addition of Ag^+ (basing on a 4 subunit cyclic molecule, equiv. 0.1-0.9: 0.1 (sky blue) – 0.2 (orange) – 0.5 (gray) – 0.6 (yellow) – 0.7 (light blue) – 0.8 (green) – 0.9 (blue) in 2.0 mL methanol solution (right) Absorption intensity changes of **YA** (0.2 mg/mL) upon addition of Ag^+ at a fixed wavelength: 214 nm (blue), 256 nm (orange).

5.2.7 $SeCl_4$/DHI chalcogen-loaded melanin

A serendipitous discovery during my PhD was found by investigating another possibility of loading melanin monomers with chalcogens, by mixing 5,6-dihydroxyindole in presence of Se (IV) salts in methanol. The idea was to react electrophilic selenium species such as Se (IV) salts, with DHI to achieve an *in-situ* generation of a species that incorporated selenium atom and could be later characterized and polymerized.

In organic chemistry, one of the most studied classes of chalcogen salts are chalcogen tetrahalides, a group of stable and commercially available salts. For instance, at the close of the 19th century, it was discovered that $SeCl_4$, in the presence of $AlCl_3$, could produce chlorobenzene and diphenyl diselenide.[49] Moreover, selenium tetrahalides are frequently used selenium source, since they are known to be involved in various reactions, acting as oxidizing agents and electrophilic species that can engage interactions with different nucleophiles.[50–52]

During the addition of a solution of $SeCl_4$ to a solution of DHI (both dissolved in methanol) a fascinating phenomenon was observed. The DHI solution colour changes from a pale brown to a bloody red ($SeCl_4$ solution is transparent). Driven by curiosity, this reaction was investigated performing UV/Vis spectroscopy.

Initially, the UV-Vis spectrum of DHI showed two peaks at λ = 275 nm and 300 nm. After the addition of 0.1 equivalent of $SeCl_4$, notable changes appeared in the visible region, particularly at λ ~ 510 nm, where a broad peak emerged, and at λ ~ 275 nm, where the shoulder peak of DHI disappeared. In this case, a red-shift in the second peak near 330 nm was also noted (figure 5.22).

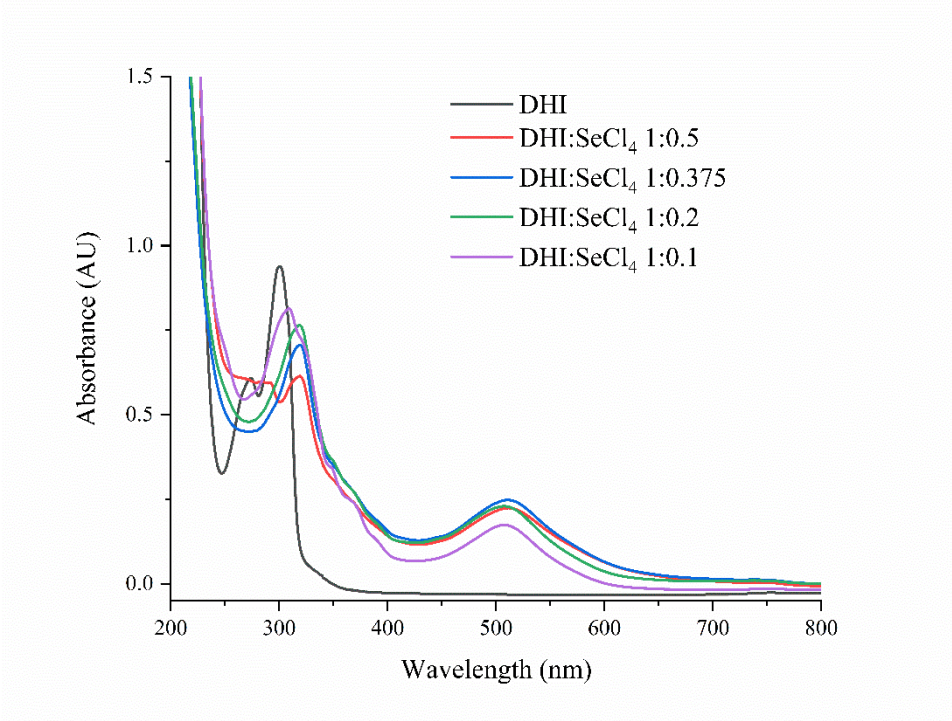

Figure 5.22: UV-Vis spectra of DHI/$SeCl_4$ solution at different molar ratio. Black, red, blue, green and purple lines represent, respectively, DHI:$SeCl_4$ 1:0.5, 1:0.375, 1:0.2 and 1:0.1.

Continuing with a further addition of $SeCl_4$, when ~ 0.4 equivalents of $SeCl_4$ were introduced, the peak at 510 nm reached a plateau, and further additions did not result in higher peak intensity but led only to a more significant red-shift around λ = 330 nm.

In order to isolate the reaction products, paving attention to the new peak at λ = 510 nm, a screening of reaction conditions was performed. For this screening we

designed a reaction protocol that involved DHI and substoichiometric quantities of $SeCl_4$, reduction, extraction and acetylation of the crude product (scheme 5.5).

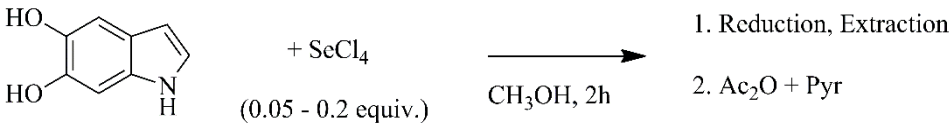

Scheme 5.5: proposed reaction for the isolation of DHI/$SeCl_4$ reaction products.

The best condition was identified to be a portion-wise protocol that involved the adding of 0.05-0.1 equivalent of $SeCl_4$ in 3 h of reaction time (Table 5.2, entry 3, figure 5.23).

Entry	time	$SeCl_4$ equiv.	Crude yield (w/w)
1	2 h	0.14	20 %
2	2 h	0.1	21 %
3	2 h	0.08	46 %
4	1 h	0.08	25 %
5	1h	0.14	29 %

Table 5.2: Explored reaction conditions. The yield was calculated on the w/w ratio.

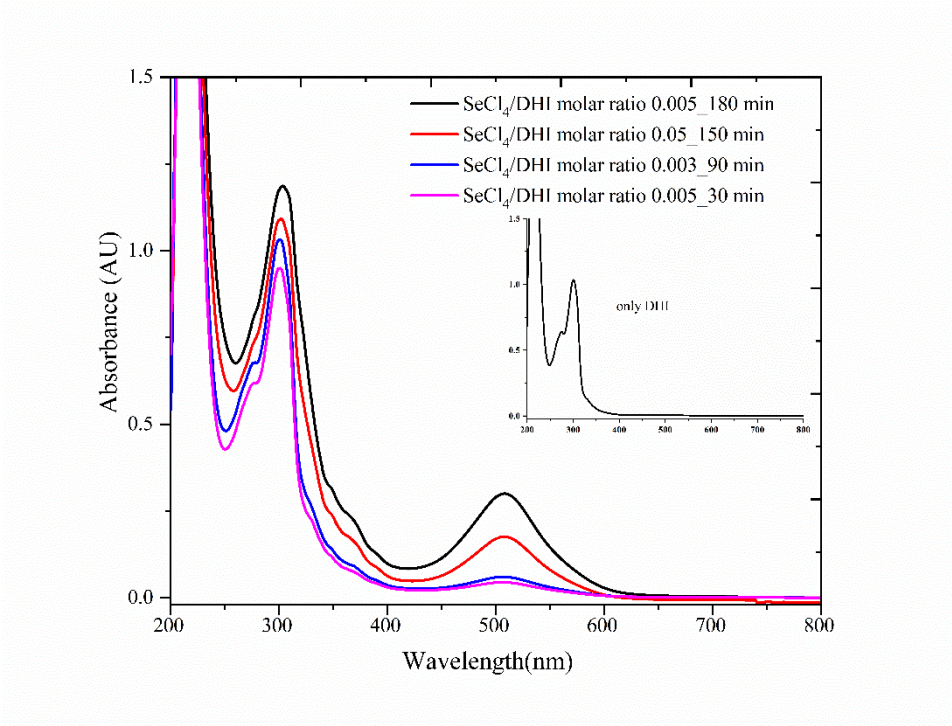

Figure 5.23: UV-Vis of the portion-wise reaction for the isolation of products.

After the optimization of reaction conditions, two main products were isolated through direct SiO_2 chromatography (figure 5.24).

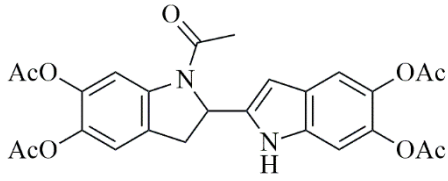

I

Figure 5.24: structure of isolated product **I.**

The first product **I**, is a reduced, N-acetylated 2-2' dimer was isolated with a 15% yield and characterized by bidimensional NMR (figure 5.30 materials and methods). A second product **II** with yield of 20 % was also isolated. The MALDI-MS data are compatible with a trimeric structure in which one of the unit is reduced, N-acetylated indolic unit. Ongoing NMR experiments will allow to clarify the connection and the structure of the compound.

Apparently, there is no evidence that selenium is incorporated inside the material and the reaction mechanism is still unclear. Although, UV-Vis band at $\lambda \sim 510$ nm and the isolation of catecholamine products suggest that Se(IV) interacts with DHI and could act a strong oxidant, activating the oxidative polymerization reaction.

Thin film fabrication for the characterization of solid-state electrical properties of DHI/$SeCl_4$ material was performed (see scheme 5.6) by spin-coating. A solution of DHI/$SeCl_4$, was dried and exposed to ammonia vapours (AISSP) to perform IV measurements.

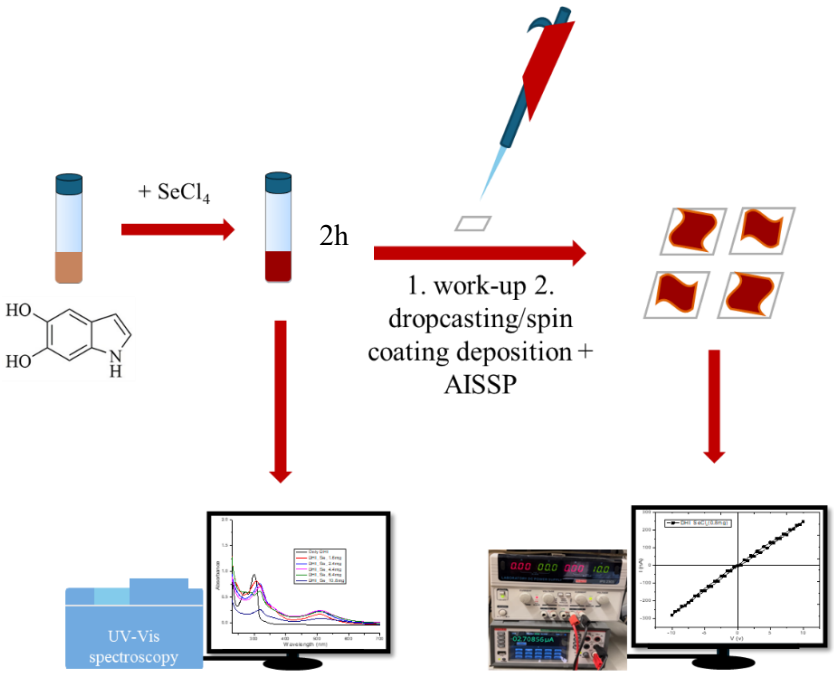

Scheme 5.6: Fabrication and characterization of DHI/$SeCl_4$ films.

Different type of work-up of samples were tested using a schematic approach. 3 different samples were deposited and studied for the I-V curves: 1) a sample with reduction and extraction (WRAE); 2) a sample without reducing agent after extraction (WORAE); 3) a sample without reduction and without extraction (WRBE).

The tested samples were characterized by a good adhesion, suitable for spin-coating deposition, optimal time stability and homogeneity before and after the AISSP treatment (figure 5.25).

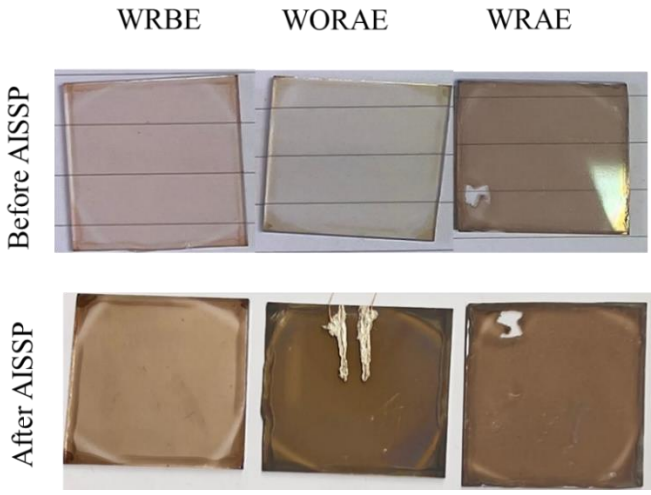

Figure 5.25: spin coated thin films of DHI/$SeCl_4$.

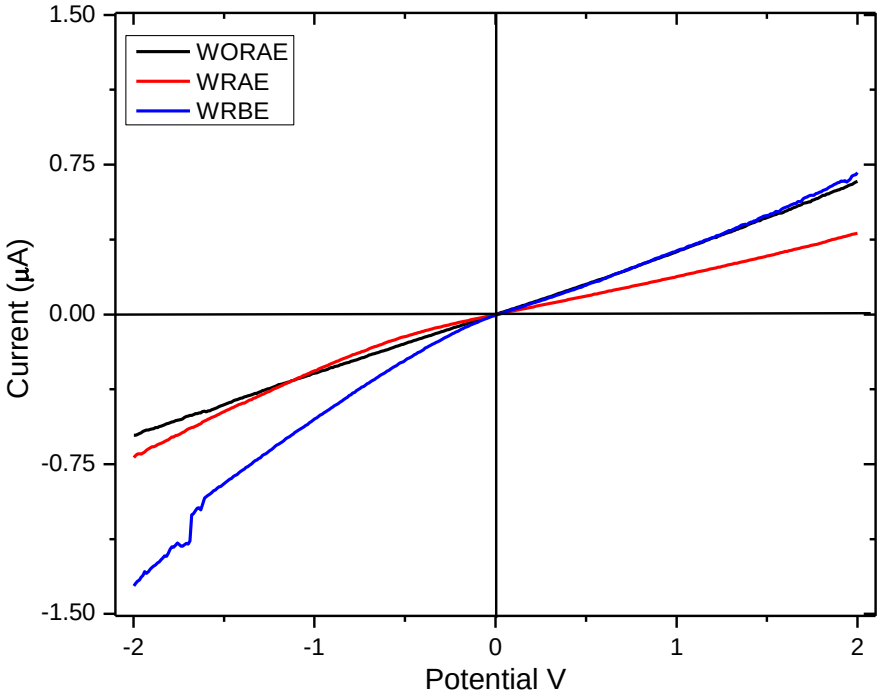

Figure 5.26: IV curve of DHI/$SeCl_4$ 1:0.08 spin-coated films treated with AISSP, WRAE (red line) WORAE (black line) and WRBE (blue line).

The I-V curves (figure 5.26 black, red and blue line) of each sample after the AISSP treatment (before ammonia the material is insulating) denote a good conductivity and high stability of the material. The I-V curves were collected using a potential range set between 2 V and -2 V, at a scan rate of 0.05 V/s.

5.3 Materials and methods

General information:

All the commercial chemical reagents used were employed without prior purification. The reactions were monitored using TLC plates, which were visualized under UV-visible light. After visualization, the plates were exposed to ammonia vapours before proceeding with carbonization (AISSP). The products obtained were separated using flash chromatography, with Merck Kieselgel 60 (63-200 mesh) silica as the stationary phase, and the purified products were characterized using NMR spectroscopy. The ^{1}H and ^{13}C NMR spectra were recorded on a ^{1}HNMR spectra were recorded with a Bruker DRX-400MHz apparatus (Bruker Corporation, Billerica, MA, USA). Chemical shifts in ppm were referenced to tetramethylsilane.

Synthesis of 5,6-dihydroxiindole, 5,6-diacetoxyindole-2-carboxylicacid, 3-thiocyanoindoles, 3-thioglycoacetoxyindoles, glycosidic diselenides were performed according to the already known protocols.[53]

UV-Vis spectra were performed using V-630 JASCO spectrophotometer, at a rate of 200 nm/min. Electrochemical tests were conducted using an Autolab PGSTAT302 potentiostat and NOVA 2.1.6 software at room temperature (~ 25 °C).

Continuous-wave X-band EPR Measurements: X-band continuous-wave (CW) spectrometer MiniScope MS300 (Magnettech, Berlin, Germany) was utilized to record EPR spectra in solid-state. For every measurement, a Frequency Counter 53181A RF monitored the microwave frequency. The acquisition of CW EPR spectra was performed with a modulation amplitude of 80 μT, microwave power of 0.1 mW with 10 passes and scan width of 6 mT. For each measurement g-Values correction against the measured value of the 2,2-diphenyl-1-picrylhydrazyl (DPPH) standard marker in g = 2.0036. All measurements were performed at room temperature (T ≈ 298 K) in a humidity atmosphere of 30-40%.

For the power saturation and evaluation of spin relaxation behaviour the microwave powers ranged between 0.10 and 31.62 mW using the same experimental conditions.

The determination of spin concentration (ρ) was calculated by comparing the signal from the sample under study to a standard model with a known number of spins and estimated using Eq. 01.[41] In Eq. 01 ARC is referred to the area under the resonance curve, CE to a spectrometer-specific constant, T to the temperature, MA is the modulation amplitude and P the applied microwave power.

$$\rho = A_{RC} \frac{C_E T}{M_A \sqrt{P}} \qquad \text{(Eq. 01)}$$

Synthesis of 3-selenocyanate-5,6-diacetoxyindole: A solution of 230 mg of DAI (1 mmol) and 216 mg potassium selenocyanate (1.5 mmol) in 10 mL of methanol were treated with 924 mg Oxone (1.5 mmol) and allowed to stir at room temperature until completion of the reaction, monitored by TCL. Potassium peroxymonosulfate is a cheap and readily accessible oxidizing reagent. It is

commonly referred to as Oxone (2KHSO5*KHSO4*K2SO4) and is a versatile oxidant for transformation of a wide range of functional groups. After completion, it was diluted with water and extracted with 3 x 15 mL of dichloromethane (DCM). DCM was then evapourated, and the residue was purified by column chromatography on silica gel (200–300 mesh, ethyl acetate/hexane).

DAISeCN: Rf = 0.40 (ethyl acetate/hexane, 3:2) amorphous solid, MALDI-TOF MS calculated for calculated for $C_{13}H_{11}N_2O_4Se$ 360.978 [M+Na]+, found 360.994; 1HNMR (400MHz,CDCl3) d(ppm): 2.39 (6H, s, OCOCH3), 7.15 (1H, s), 7.21 (1H, d, J = 2.8 Hz), 7.31 (1H, s, H-4), 9.06 (1H, s,N–H);

Solid-state X-Band Measurements: An X-band continuous-wave spectrometer MiniScope MS300 (Magnettech) coupled with an Agilent Frequency Counter 53181A RF was used to acquire microwave frequency. g Value calibration was performed using the standard 2,2-diphenyl-1-picrylhydrazyl (DPPH) with a g = 2.0036. The microwave power was increased from 0.10 to 31.62 mW.

Preparation of DAI-p/DAISCN-p/DAISeCN-p for EPR analysis: 10 mg of DAI/DAISCN/DAISeCN were dissolved into 500 uL solution of Methanol-dry/Chloroform 1:1 and drop-casted on a (2.5 cm x 2.5 cm) glass substrate. The samples were dried at room temperature for 30 minutes and consequently at 60°C for 5 minutes. After drying, the deposited films were exposed for 24 h to NH_3 vapours (AISSP). The films were then dried at 100 °C for 5 minutes, scratched and the resulting powders were stored at r.t.

Preparation of chemically-controlled DAI, DAISCN and DAISeCN thin films for electronic UV-Vis arbsorption characterization: 15 mg of DAI/DAISCN/DAISeCN were dissolved into 1 mL of Acetonitrile. The solutions were spin-coated (sequentially: 5 s at 500 rpm and 40 s at 1000 rpm) on 1.5 cm x

1.5 cm fused silica substrates. Before the spin coating procedure, the substrates were cleaned by sequential sonication in Milli-Q water (18.2 MΩ·cm^{-1}), acetone and isopropanol, followed by 20 min of UV−ozone treatment. After the deposition, the films were heated for 10 minutes at 100 °C and consequently exposed NH_3 vapours (AISSP).

Confocal images: images were acquired using a Leica DCM 3d, 3d optical surface metrology system, 50x optics.

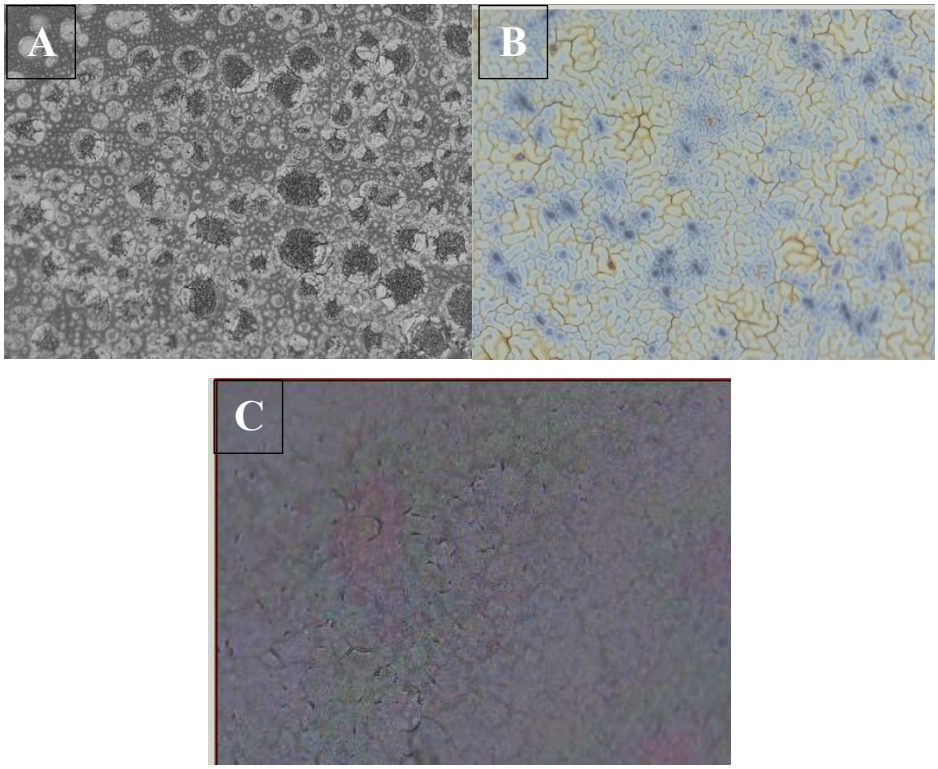

Figure 5.27: confocal images of DAI-p (A), DAISCN-p (B) and DAISeCN-p (C) after 24h AISSP.

CV measurements: the electrochemical treatments were applied and monitored using an Autolab PGSTAT302 potentiostat. For the CV treatment, the electrochemical potential was cycled between 0 V and -1 V, with a scan rate of 10 $mV \cdot s^{-1}$ for 3 cycles. The current vs voltage curves were collected after each measurement. For all measurements 1M Na_2SO_4 pH = 7.0 was used as common solvent for electrochemical characterization. 1 M Na_2SO_4 was prepared using Milli-Q water (18.2 $M\Omega \cdot cm^{-1}$). The mixture was stirred for 30 min at room temperature until total dissolution. All experiments were performed in a three-electrode cell at room temperature (23 ± 1 °C), using a glassy carbon electrode loaded with a DAI/DAISCN/DAISeCN sample film, a platinum net was the counter electrode, and $Ag/AgCl_{(aq)}$ was the reference electrode. Before the measurement the electrochemical cell was degassed for 10 minutes with Ar. The electrode was loaded by drop-cast with a 0.1 mg mass sample using 25 mg/mL solution of DAI/DAISCN/DAISeCN dissolved in CH_3OH/ CH_3OH : CH_3CN 1: 1/ CH_3OH : CH_3CN 1 : 1 respectively.

Synthesis of YA: A sample of 100 mg of 3-thiocyanate-5,6-diacetyloindole (0.35 mmol) is dissolved in acetone and conveyed, into a buffer solution consisting of 30 mL of 0.2 M tribasic sodium phosphate at pH = 12. The solution is pre-saturated with gaseous argon, which is then bubbled into the agitating solution for 15 minutes. The formation of the polymerization product and 5,6-dihydroxyindole is accompanied by a gradual change in colour. Initially yellowish, the solution turns darker and then dark green before assuming a very intense dark blue colour. After approximately ten minutes, the mixture is cautiously acidified with 3M HCl until neutral conditions are reached (pH = 7). Subsequently, a spatula of sodium dithionite (approximately 100 mg) is added as a reducing agent, along with 3M HCl, until a pH value of 4-5 is achieved. The attainment of this pH is marked by a new colour change from blue to a very intense dark yellow. The oxidation

product is extracted with ethyl acetate (3x20 mL, extracting agents H_2O/EtOAc). The organic phase is then dehydrated with anhydrous sodium sulphate, and the solvent is removed using a rotary evaporator. The crude is then acetylated with 1 mL of Ac_2O and 5 µL of Pyridine, left overnight. Post-acetylation, the residue is washed with methanol to destroy excess acetic anhydride, and the volatile reaction products are dried under vacuum using a rotary evaporator. The reaction crude is than purified twice via direct-phase chromatography (Ethyl acetate: Hexane 3 : 1 and after Acetone : Hexane 2 : 1). The reaction yields to the formation of a yellow polar product in 3 % mass yield.

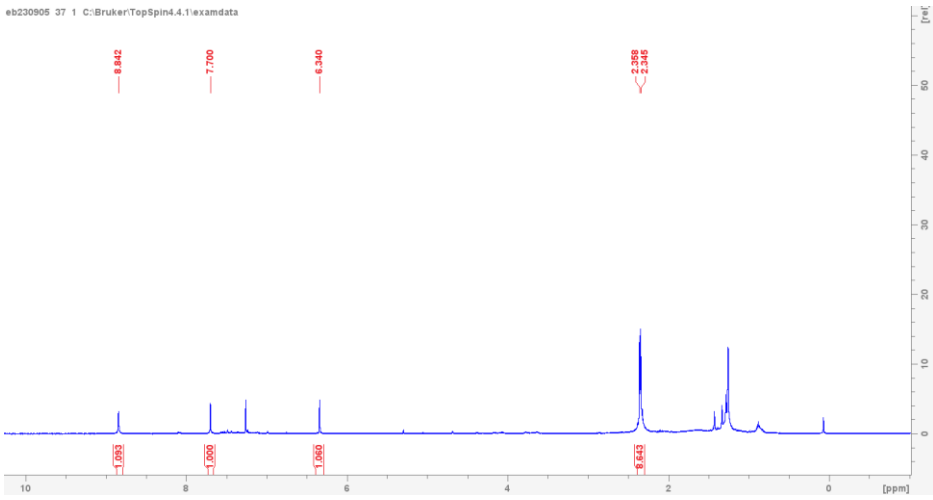

Figure 5.28: $CDCl_3$ ^{1}HNMR spectrum of YA.

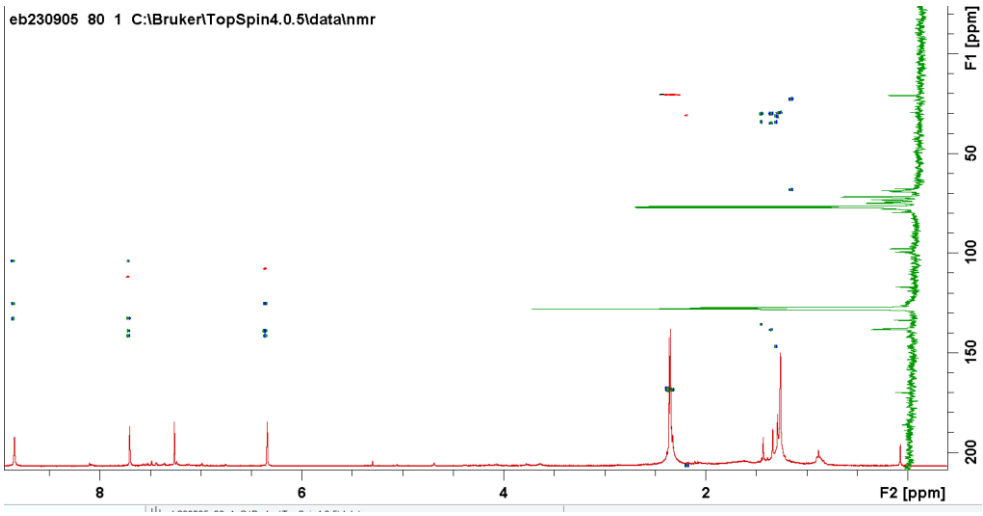

Figure 5.29: $CDCl_3$ superimposed bidimensional spectra (HSQC shown in red and HMBC shown in blue) of YA. Monodimensional ^{1}HNMR and ^{13}CNMR are shown in red (down) and green (right) respectively.

Isolation of DHI/$SeCl_4$ product C: in a 50 mL reaction flask 25 mg of DHI were dissolved into 1 mL of methanol. Then, 29.4 µL of a 0.1 mg/mL solution of SeCl4 was added into the reaction. After 2 h, the solution was treated with Na_2SO_4 and extracted with ethyl acetate. The crude product was then acetylated overnight using 0.15 mL acetic anhydride (Ac_2O) and 10 µL of pyridine (Pyr). Following the reaction was quenched with methanol and diluted with ethyl acetate. The solution was extracted, and the organic phases were combined and dried using a rotary evaporator. The crude product is purified by flash chromatography on silica gel, using mixtures of hexane/ethyl acetate.

Product I: Rf = 0.30 (ethyl acetate/hexane, 5:2) amorphous solid, MALDI-TOF MS calculated for calculated for $C_{26}H_{24}N_2O_9$ 531.14 [M+Na]+, found 530.94.

HNMR, CNMR, HMBC, HSQC spectra:

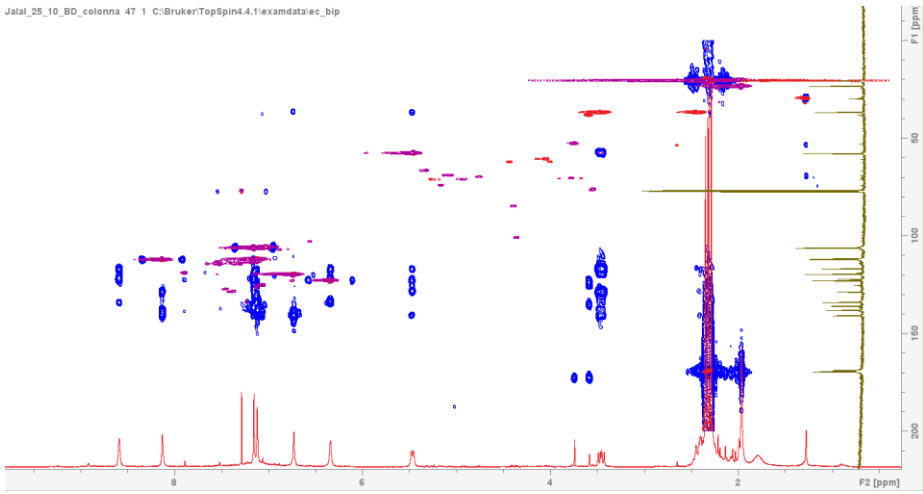

Figure 5.30: $CDCl_3$ superimposed bidimensional spectra (HSQC shown in red and HMBC shown in blue) of product C. Monodimensional ^{1}HNMR and ^{13}CNMR are shown in red (down) and yellow (right) respectively.

Product II Rf = 0.15 (ethyl acetate/hexane, 5:2) amorphous solid, MALDI-TOF MS calculated for calculated for $C_{26}H_{24}N_2O_9$ 762.18 [M+Na]+, found 763.94.

Preparation of chemically controlled DHI/SeCl4 thin films for I-V characterization: in a 50 mL reaction flask 25 mg of DHI were dissolved into 1 mL of methanol. Then, 29.4 µL of a 0.1 mg/mL solution of SeCl4 was added into the reaction. After 2 h, the solution was:

- treated with Na_2SO_4 and extracted EtOAc vs H_2O, the organic phases were collected and dried to obtain WRAE sample;

- extracted EtOAc vs H_2O, the organic phases were collected and dried to obtain WORAE sample;
- treated with Na_2SO_4 and dried to obtain WRBE sample.

All the solutions were dissolved in methanol, filtered with a 10 µm filter and spin-coated (30s at 800 rpm) on 2.5 cm x 2.5 cm fused silica substrates. Before the spin coating procedure, the substrates were cleaned by sequential sonication in distilled water, acetone and isopropanol. After the deposition, the films were heated for 10 minutes at 100 °C and consequently exposed NH_3 vapours (AISSP) for 10 minutes. After AISSP treatment the films were dried for 15 minutes at 100°C.

5.4 Conclusions

The synthesis and characterization of chalcogen-functionalized eumelanin monomers and polymers were undertaken in this work to explore the potential of these materials for electronic applications. One of the primary motivations for this research was to investigate the impact of chalcogen groups (sulphur and selenium) on the electrical conductivity of eumelanin. These groups can act as electron-withdrawing or -donating groups, thereby modulating the electronic properties of the polymer.

To explore the optical properties of these modified polymers, UV-Vis spectroscopy experiment were carried out. Eumelanin is known for its broad-spectrum light absorption capabilities. By introducing chalcogen groups, we sought to fine-tune the optical properties, such as absorption wavelength and intensity. Furthermore, the paramagnetic properties of eumelanin and its derivatives were investigated using EPR spectroscopy.

A serendipitous discovery of a new stable material DHI/$SeCl_4$ was made by adding $SeCl_4$ in presence of DHI dissolved in methanol. The reaction was characterized by a change of colour and the appearance of a new peak at $\lambda = 510$ nm. The isolation of the reaction product brought to the identification of oligomeric products, showing a catecholamine unit. The reaction strongly involved the C-2 position of the indole ring, that is known to be strongly activated in DHI monomer. We believe that selenium is not incorporated into the reaction monomer and is acting as an oxidizing agent towards DHI.

In conclusion, the synthesis and characterization of chalcogen loaded melanins represent a significant step towards developing advanced materials with tailored properties. By combining experimental and theoretical approaches, we aimed to unlock the full potential of these eumelanin-inspired polymers and contribute to the advancement of various technological fields.

5.5 References

(1) Meredith, P.; Bettinger, C. J.; Irimia-Vladu, M.; Mostert, A. B.; Schwenn, P. E. Electronic and Optoelectronic Materials and Devices Inspired by Nature. *Rep. Prog. Phys.* **2013**, *76* (3), 034501.

(2) Sheliakina, M.; Mostert, A. B.; Meredith, P. Decoupling Ionic and Electronic Currents in Melanin. *Advanced Functional Materials* **2018**, *28* (46), 1805514.

(3) Bernardus Mostert, A.; Powell, B. J.; Gentle, I. R.; Meredith, P. On the Origin of Electrical Conductivity in the Bio-Electronic Material Melanin. *Applied Physics Letters* **2012**, *100* (9), 093701.

(4) Migliaccio, L.; Manini, P.; Altamura, D.; Giannini, C.; Tassini, P.; Maglione, M. G.; Minarini, C.; Pezzella, A. Evidence of Unprecedented High Electronic Conductivity in Mammalian Pigment Based Eumelanin Thin Films After Thermal Annealing in Vacuum. *Frontiers in Chemistry* **2019**, *7*.

(5) Migliaccio, L.; Altamura, D.; Scattarella, F.; Giannini, C.; Manini, P.; Gesuele, F.; Maglione, M. G.; Tassini, P.; Pezzella, A. Impact of Eumelanin–PEDOT Blending: Increased PEDOT Crystalline Order and Packing–Conductivity Relationship in Ternary PEDOT:PSS:Eumelanin Thin Films. *Advanced Electronic Materials* **2019**, *5* (3), 1800585.

(6) Gargiulo, V.; Alfè, M.; Di Capua, R.; Rita Togna, A.; Cammisotto, V.; Fiorito, S.; Musto, A.; Navarra, A.; Parisi, S.; Pezzella, A. Supplementing π-Systems: Eumelanin and Graphene-like Integration towards Highly Conductive Materials for the Mammalian Cell Culture Bio-Interface. *Journal of Materials Chemistry B* **2015**, *3* (25), 5070–5079.

(7) Brizuela Guerra, N.; Morais Lima, J. V.; Nozella, N. L.; Boratto, M. H.; Paulin, J. V.; Graeff, C. F. de O. Electrochemical Doping Effect on the Conductivity of Melanin-Inspired Materials. *ACS Appl. Bio Mater.* **2024**, *7* (

(8) Di Capua, R.; Gargiulo, V.; Alfè, M.; De Luca, G. M.; Skála, T.; Mali, G.; Pezzella, A. Eumelanin Graphene-Like Integration: The Impact on Physical Properties and Electrical Conductivity. *Front. Chem.* **2019**, *7*.

(9) Nozella, N. L.; Lima, J. V. M.; Oliveira, R. F. de; Graeff, C. F. de O. Melanin/PEDOT:PSS Blend as Organic Mixed Ionic Electronic Conductor (OMIEC) for Sustainable Electronics. *Mater. Adv.* **2023**, *4* (20), 4732–4743.

(10) Migliaccio, L.; Aprano, S.; Iannuzzi, L.; Maglione, M. G.; Tassini, P.; Minarini, C.; Manini, P.; Pezzella, A. Eumelanin–PEDOT:PSS Complementing En Route to Mammalian-Pigment-Based Electrodes: Design and Fabrication of an ITO-Free Organic Light-Emitting Device. *Advanced Electronic Materials* **2017**, *3* (5), 1600342.

(11) Migliaccio, L.; Gesuele, F.; Manini, P.; Maglione, M. G.; Tassini, P.; Pezzella, A. Eumelanin Precursor 2-Carboxy-5,6-Dihydroxyindole (DHICA) as Doping Factor in Ternary (PEDOT:PSS/Eumelanin) Thin Films for Conductivity Enhancement. *Materials* **2020**, *13* (9), 2108.

(12) Ferraiuolo, R.; Coscia, C. C.; Maglione, M. G.; Tassini, P.; Esposito, R.; Vitiello, G.; D'Errico, G.; Pezzella, A. A Synergistic Radical Concentration Increase in Eumelanin–PEDOT:PSS Blends: Mammalian Pigment-Based Doping for Thermopower Improvement. *Mater. Adv.* **2024**, *5* (17), 6967–6973.

(13) Liu, R.; Chen, Y.; Yu, H.; Položij, M.; Guo, Y.; Sum, T. C.; Heine, T.; Jiang, D. Linkage-Engineered Donor–Acceptor Covalent Organic Frameworks for Optimal Photosynthesis of Hydrogen Peroxide from Water and Air. *Nat Catal* **2024**, *7* (2), 195–206.

(14) Wang, L.; Chen, C.; Fu, Y.; Guo, C.; Li, D.; Cheng, J.; Sun, W.; Gan, Z.; Sun, Y.; Zhou, B.; Liu, C.; Liu, D.; Li, W.; Wang, T. Donor–Acceptor Mutually Diluted Heterojunctions for Layer-by-Layer Fabrication of High-Performance Organic Solar Cells. *Nat Energy* **2024**, *9* (2), 208–218.

(15) *Donor-π-Acceptor Conjugated Copolymers for Photovoltaic Applications: Tuning the Open-Circuit Voltage by Adjusting the Donor/Acceptor Ratio | The Journal of Physical Chemistry B*.

(16) Han, J.; Fan, H.; Zhang, Q.; Hu, Q.; Russell, T. P.; Katz, H. E. Dichlorinated Dithienylethene-Based Copolymers for Air-Stable n-Type Conductivity and Thermoelectricity. *Advanced Functional Materials* **2021**, *31* (5), 2005901.

(17) Shi, H.; Liu, C.; Jiang, Q.; Xu, J. Effective Approaches to Improve the Electrical Conductivity of PEDOT:PSS: A Review. *Advanced Electronic Materials* **2015**, *1* (4), 1500017.

(18) Ahluwalia, G. K. Fundamentals of Chalcogenides in Crystalline, Amorphous, and Nanocrystalline Forms. In *Applications of Chalcogenides: S, Se, and Te*; Ahluwalia, G. K., Ed.; Springer International Publishing: Cham, 2017; pp 3–60.

(19) Kolb, S.; Oliver, G. A.; Werz, D. B. Chemistry Evolves, Terms Evolve, but Phenomena Do Not Evolve: From Chalcogen–Chalcogen Interactions to Chalcogen Bonding. *Angewandte Chemie International Edition* **2020**, *59* (50), 22306–22310.

(20) Aakeroy, C. B.; Bryce, D. L.; Desiraju, G. R.; Frontera, A.; Legon, A. C.; Nicotra, F.; Rissanen, K.; Scheiner, S.; Terraneo, G.; Metrangolo, P.; Resnati, G. Definition of the Chalcogen Bond (IUPAC Recommendations 2019). *Pure and Applied Chemistry* **2019**, *91* (11), 1889–1892.

(21) Mahmudov, K. T.; Kopylovich, M. N.; Silva, M. F. C. G. da; Pombeiro, A. J. L. Chalcogen Bonding in Synthesis, Catalysis and Design of Materials. *Dalton Trans.* **2017**, *46* (31), 10121–10138.

(22) Patra, A.; Wijsboom, Y. H.; Leitus, G.; Bendikov, M. Synthesis, Structure, and Electropolymerization of 3,4-Dimethoxytellurophene: Comparison with Selenium Analogue. *Org. Lett.* **2009**, *11* (7), 1487–1490.

(23) Li, Y.; Wu, W.; Wang, Y.; Huang, E.; Jeong, S. Y.; Woo, H. Y.; Guo, X.; Feng, K. Multi-Selenophene Incorporated Thiazole Imide-Based n-Type Polymers for High-Performance Organic Thermoelectrics. *Angewandte Chemie* **2024**, *136* (3), e202316214.

(24) Hwang, H.; Khim, D.; Yun, J.-M.; Jung, E.; Jang, S.-Y.; Jang, Y. H.; Noh, Y.-Y.; Kim, D.-Y. Quinoidal Molecules as a New Class of Ambipolar Semiconductor Originating from Amphoteric Redox Behavior. *Advanced Functional Materials* **2015**, *25* (7), 1146–1156.

(25) Ding, J.; Liu, Z.; Zhao, W.; Jin, W.; Xiang, L.; Wang, Z.; Zeng, Y.; Zou, Y.; Zhang, F.; Yi, Y.; Diao, Y.; McNeill, C. R.; Di, C.; Zhang, D.; Zhu, D. Selenium-Substituted Diketopyrrolopyrrole Polymer for High-Performance p-Type Organic Thermoelectric Materials. *Angewandte Chemie International Edition* **2019**, *58* (52), 18994–18999.

(26) Patra, A.; Bendikov, M.; Chand, S. Poly(3,4-Ethylenedioxyselenophene) and Its Derivatives: Novel Organic Electronic Materials. *Acc. Chem. Res.* **2014**, *47* (5), 1465–1474.

(27) Burrezo, P. M.; Zafra, J. L.; López Navarrete, J. T.; Casado, J. Quinoidal/Aromatic Transformations in π-Conjugated Oligomers: Vibrational Raman Studies on the Limits of Rupture for π-Bonds. *Angewandte Chemie International Edition* **2017**, *56* (9), 2250–2259.

(28) Takahashi, T.; Matsuoka, K.; Takimiya, K.; Otsubo, T.; Aso, Y. Extensive Quinoidal Oligothiophenes with Dicyanomethylene Groups at Terminal Positions as Highly Amphoteric Redox Molecules. *J. Am. Chem. Soc.* **2005**, *127* (25), 8928–8929.

(29) Yuan, D.; Guo, Y.; Zeng, Y.; Fan, Q.; Wang, J.; Yi, Y.; Zhu, X. Air-Stable n-Type Thermoelectric Materials Enabled by Organic Diradicaloids. *Angewandte Chemie International Edition* **2019**, *58* (15), 4958–4962.

(30) Pezzella, A.; Palma, A.; Iadonisi, A.; Napolitano, A.; d'Ischia, M. The First Entry to 5,6-Dihydroxy-3-Mercaptoindole, 5-Hydroxy-3-Mercaptoindole and Their 2-Carbomethoxy Derivatives by a Mild Thiocyanation/Reduction Methodology. *Tetrahedron Letters* **2007**, *48* (22), 3883–3886.

(31) Pezzella, A.; Barra, M.; Musto, A.; Navarra, A.; Alfè, M.; Manini, P.; Parisi, S.; Cassinese, A.; Criscuolo, V.; d'Ischia, M. Stem Cell-Compatible Eumelanin Biointerface Fabricated by Chemically Controlled Solid State Polymerization. *Materials Horizons* **2015**, *2* (2), 212–220.

(32) Li, J.; Liu, M.; Yang, K.; Wang, Y.; Wang, J.; Chen, Z.; Feng, K.; Wang, D.; Zhang, J.; Li, Y.; Guo, H.; Wei, Z.; Guo, X. Selenium Substitution in Bithiophene Imide Polymer Semiconductors Enables High-Performance n-Type Organic Thermoelectric. *Advanced Functional Materials* **2023**, *33* (23), 2213911.

(33) Gouda, A.; Soavi, F.; Santato, C. Eumelanin Electrodes in Buffered Aqueous Media at Different PH Values. *Electrochimica Acta* **2020**, *347*, 136250.

(34) Xu, R.; Prontera, C. T.; Di Mauro, E.; Pezzella, A.; Soavi, F.; Santato, C. An Electrochemical Study of Natural and Chemically Controlled Eumelanin. *APL Materials* **2017**, *5* (12), 126108.

(35) Cicco, S. R.; Ambrico, M.; Ambrico, P. F.; Talamo, M. M.; Cardone, A.; Ligonzo, T.; Mundo, R. D.; Giannini, C.; Sibillano, T.; Farinola, G. M.; Manini, P.; Napolitano, A.; Criscuolo, V.; d'Ischia, M. A Water-Soluble Eumelanin Polymer with Typical Polyelectrolyte Behaviour by Triethyleneglycol N-Functionalization. *J. Mater. Chem. C* **2015**, *3* (12), 2810–2816.

(36) Mishra, R.; Lim, J. M.; Son, M.; Panini, P.; Kim, D.; Sankar, J. Tuning the Electronic Nature of Mono-Bay Alkynyl–Phenyl-Substituted Perylene Bisimides: Synthesis, Structure, and Photophysical Properties. *Chemistry – A European Journal* **2014**, *20* (19), 5776–5786.

(37) Silverstein, J. S.; Casey, B. J.; Natoli, M. E.; Dair, B. J.; Kofinas, P. Rapid Modular Synthesis and Processing of Thiol–Ene Functionalized Styrene–Butadiene Block Copolymers. *Macromolecules* **2012**, *45* (7), 3161–3167.

(38) Wang, J.; Zhou, Y.; Xu, X.; Liu, P.; Dong, G. Entry to 1,2,3,4-Tetrasubstituted Arenes through Addressing the "Meta Constraint" in the Palladium/Norbornene Catalysis. *J. Am. Chem. Soc.* **2020**, *142* (6), 3050–3059.

(39) Wünsche, J.; Deng, Y.; Kumar, P.; Di Mauro, E.; Josberger, E.; Sayago, J.; Pezzella, A.; Soavi, F.; Cicoira, F.; Rolandi, M.; Santato, C. Protonic and Electronic Transport in Hydrated Thin Films of the Pigment Eumelanin. *Chem. Mater.* **2015**, *27* (2), 436–442.

(40) Mostert, A. B. Melanin, the What, the Why and the How: An Introductory Review for Materials Scientists Interested in Flexible and Versatile Polymers. *Polymers* **2021**, *13* (10), 1670.

(41) Paulin, J. V.; Graeff, C. F. O.; Mostert, A. B. Decoding Eumelanin's Spin Label Signature: A Comprehensive EPR Analysis. *Mater. Adv.* **2024**, *5* (4), 1395–1419.

(42) Paulin, J. V.; Batagin-Neto, A.; Meredith, P.; Graeff, C. F. O.; Mostert, A. B. Shedding Light on the Free Radical Nature of Sulfonated Melanins. *J. Phys. Chem. B* **2020**, *124* (46), 10365–10373.

(43) Mostert, A. B.; Hanson, G. R.; Sarna, T.; Gentle, I. R.; Powell, B. J.; Meredith, P. Hydration-Controlled X-Band EPR Spectroscopy: A Tool for Unravelling the Complexities of the Solid-State Free Radical in Eumelanin. *J. Phys. Chem. B* **2013**, *117* (17), 4965–4972.

(44) Paulin, J. V.; Batagin-Neto, A.; Graeff, C. F. O. Identification of Common Resonant Lines in the EPR Spectra of Melanins. *J. Phys. Chem. B* **2019**, *123* (6), 1248–1255.

(45) Szpoganicz, B.; Gidanian, S.; Kong, P.; Farmer, P. Metal Binding by Melanins: Studies of Colloidal Dihydroxyindole-Melanin, and Its Complexation by Cu(II) and Zn(II) Ions. *Journal of Inorganic Biochemistry* **2002**, *89* (1), 45–53.

(46) Charkoudian, L. K.; Franz, K. J. Fe(III)-Coordination Properties of Neuromelanin Components: 5,6-Dihydroxyindole and 5,6-Dihydroxyindole-2-Carboxylic Acid. *Inorg. Chem.* **2006**, *45* (9), 3657–3664.

(47) Sharma, V. S.; Vishwakarma, V. K.; Shrivastav, P. S.; Ammathnadu Sudhakar, A.; Sharma, A. S.; Shah, P. A. Calixarene Functionalized Supramolecular Liquid Crystals and Their Diverse Applications. *ACS Omega* **2022**, *7* (50), 45752–45796.

(48) Quaglio, D.; Polli, F.; Del Plato, C.; Cianfoni, G.; Tortora, C.; Mazzei, F.; Botta, B.; Calcaterra, A.; Ghirga, F. Calixarene: A Versatile Scaffold for the Development of Highly Sensitive Biosensors. *Supramolecular Chemistry* **2021**, *33* (7), 345–369.

(49) Bradt, W. E.; Green, J. Franklin. THE INTERACTION OF SELENIUM TETRACHLORIDE AND BENZENE IN THE PRESENCE OF ANHYDROUS ALUMINUM CHLORIDE. *J. Org. Chem.* **1937**, *1* (6), 540–543.

(50) Amosova, S. V.; Penzik, M. V.; Martynov, A. V.; Zhilitskaya, L. V.; Voronkov, M. G. Electrophilic Addition of Selenium and Telluriom Halides to Methyldiethynylsilane. *Russ J Gen Chem* **2009**, *79* (2), 221–227.

(51) Riley, R. F.; Flato, J.; Bengels, D. Addition of Selenium and Sulfur Tetrachlorides to Alkenes and Alkynes. *J. Org. Chem.* **1962**, *27* (7), 2651–2653.

(52) Couch, D. A.; Elmes, P. S.; Fergusson, J. E.; Greenfield, M. L.; Wilkins, C. J. Chemistry of Selenium and Tellurium Tetrahalides: Ionisation of the Chlorides and Bromides in Solution and the Constitution of Their Adducts. *J. Chem. Soc. A* **1967**, No. 0, 1813–1817.

(53) Edge, R.; D'Ischia, M.; Land, E. J.; Napolitano, A.; Navaratnam, S.; Panzella, L.; Pezzella, A.; Ramsden, C. A.; Riley, P. A. Dopaquinone Redox Exchange with Dihydroxyindole and Dihydroxyindole Carboxylic Acid. *Pigment Cell Research* **2006**, *19* (5), 443–450.